Published for SISSA by Springer

Received: *May 12, 2009*
Revised: *May 3, 2011*
Accepted: *August 24, 2011*
Published: *October 31, 2011*

JHEP10(2011)143

Generalized event shape and energy flow studies in e^+e^- annihilation at $\sqrt{s} = 91.2$-208.0 GeV

L3 Collaboration

Abstract: We present results from a study of hadronic event structure in high energy e^+e^- interactions using the L3 detector at LEP. A new class of event shape distributions are measured at and above the Z boson pole for light quark (u, d, s, c) flavours. Energy flow correlations are studied for all hadronic events. Next-to-leading-log QCD calculations and QCD models with improved leading-log approximations are compared to data and good agreement is found at the Z-pole whereas some discrepancies are observed at higher centre-of-mass energies.

Keywords: e+-e- Experiments

Dedicated to Prof. J. Allaby

doi:10.1007/JHEP10(2011)143

Contents

1 Introduction **1**

2 Event shape variables **2**
- 2.1 Inclusive event shape variables 3
- 2.2 Energy flow correlation 4

3 Data **4**
- 3.1 Event selection 4
- 3.2 Flavour tagging 6
- 3.3 Measurements 6
- 3.4 Systematic uncertainties 7

4 Results **8**
- 4.1 Inclusive event shape variables 8
- 4.2 Energy flow correlations 9

5 Summary **9**

6 The L3 collaboration **10**

1 Introduction

The hadronic final states of e^+e^- annihilation at high energy provide information about the full range of QCD [1–7] dynamics, from the short-distance production of quarks and gluons reflected in jet production, to the long-distance process of hadronization reflected in the distributions of different particles in the final state. Event-shape variables are sensitive to the distribution of gluon radiation in the final state [8, 9]. They offer a bridge between the perturbative, short-distance and the nonperturbative, long-distance, dynamics of QCD.

Event-shape variables were introduced to test QCD, which describes well their main features. Despite this success, perturbation theory cannot fully account for the exact form of event-shape variables. This is due to hadronization effects that enter as nonperturbative power corrections. The main, although not the only, effect of the hadronization process is to widen the distribution of radiation in the final state, and thus to shift the peak of the event shape distributions away from the narrow-jet limit [10, 11].

The analysis presented in the present paper is partially based on the same L3 data sample as a recent study of event-shape variables in flavour tagged events [12]. We present, for the first time, a new class of event shape variables [13] which allows a systematic study of the approach to nonperturbative dynamics using infrared safe observables, and which includes the thrust [14, 15] and jet broadening [16, 17] as special cases, as well as

JHEP10(2011)143

related [18–20] energy flow distributions. The theoretical predictions [21–23] of the event-shape variables assume massless quarks. They are therefore compared to an event sample enriched in light flavour (u, d, s, c) quarks. The energy flow distributions are presented for a data sample without flavour selection, and are compared to the predictions of several Monte Carlo event generators.

2 Event shape variables

The particle flow in hadronic e^+e^- annihilation events, with a nearly back-to-back configuration, is considered in two complementary regions Ω and $\bar{\Omega}$ as shown in figure 1. The region $\bar{\Omega}$ is defined by the cone angle δ with respect to the thrust axis of the event $\vec{n}_T$ defined as the unit vector that maximizes the value of the thrust T:

$$T = \frac{\sum |\vec{p}_i \cdot \vec{n}_T|}{\sum |p_i|} \ .$$

The 'angularity' parameter τ_a defines a new type of event shape variable [13]. It is given by

$$\begin{aligned} \tau_{a\bar{\Omega}}(a) &= \frac{1}{Q} \sum_{i \in \bar{\Omega}} \omega_i (\sin\theta_i)^a (1 - |\cos\theta_i|)^{1-a}, \\ &= \frac{1}{Q} \sum_{i \in \bar{\Omega}} p_{iT} \exp\left[-|\eta_i|(1-a)\right], \end{aligned} \tag{2.1}$$

where p_{iT} is the transverse momentum of particle i relative to the thrust axis, η_i is the corresponding pseudo-rapidity $\eta_i \equiv \ln(\cot(\theta_i/2))$ with θ_i the angle with respect to the thrust axis, ω_i is the energy of the particle i and Q $(= \sqrt{s})$ is the total centre-of-mass energy. a is any real number less than two. This variable allows to study various event shapes within the same formalism for $Q \gg \Lambda_{QCD}$. The two definitions in Equation 2.1 are equivalent for massless particles.

If the region $\bar{\Omega}$ covers the entire phase space ($\delta = 90°$), τ_a is essentially $1 - T$ for $a = 0$, while for $a = 1$, τ_a is the jet broadening variable. The scaled energy flow into Ω is denoted as

$$\varepsilon = \frac{1}{Q} \sum_{i \in \Omega} \omega_i \ . \tag{2.2}$$

The motivation for the introduction of the angularity parameter is to provide a new set of calculable infrared safe variables that may be compared with experimental measurements, The variable τ_a is infrared safe in the region $2 > a > -\infty$. However for $2 > a > 1$ small angles θ_i have a positive exponential weight in τ_a according to Equation 2.1 so that the jets contributing to a given bin of τ_a become extremely narrow. On the contrary for large negative values of a, large values of θ_i can contribute to a given bin of τ_a and the cross section within the range $\bar{\Omega}$ becomes inclusive.

In order to obtain well-defined QCD predictions at the next-to-leading logarithmic levels for τ_a, only the range $1 > a > -1$ is considered in Reference [13] and the present work.

JHEP10(2011)143

Within this range, variation of a controls the widths of the jets 1 and 2 in figure 1. They are narrowest for $a = -1$ and widest for $a = +1$. The next-to-leading order contribution to the cross section for the soft gluon, k, observed in the region Ω is due to radiation from a hard gluon, l, in the region $\bar{\Omega}$. The leading logarithmic contributions arise from radiation by the primary quarks of the e^+e^- annihilation process.

2.1 Inclusive event shape variables

The differential cross section in inclusive angularity given by $\tau_a \equiv \tau_{a\bar{\Omega}}\,|_{\delta=90^\circ}$ is

$$\frac{d\sigma(\tau_a, Q)}{d\tau_a} = \frac{1}{2\ Q^2} \sum_N |M(N)|^2 \delta(\tau_a - \tau_a(N))\,, \tag{2.3}$$

where the sum is over all final states N that contribute to the interval $d\tau_a$, and where $M(N)$ denotes the corresponding amplitude for $e^+e^- \to N$.

The resummation of large logarithms of τ_a in Laplace moment space is given by [13]:

$$\tilde{\sigma}(\nu, Q, a) = \int_0^1 d\tau_a e^{-\nu\tau_a} \frac{d\sigma(\tau_a, Q)}{d\tau_a}\ . \tag{2.4}$$

The Laplace moments probe the contributions of different event topologies to $d\sigma(\tau_a, Q)/d\tau_a$. For large values of ν, only small values of τ_a (and hence extremely two jet like events) contribute significantly to the Laplace moments due to the negative exponential weighting according to $\nu\tau_a$ in Equation 2.4. Since $\tau_0 \simeq 1-T$ and the peak in $1-T$ is at $\simeq 0.1$ at LEP energies, the corresponding peaks in the Laplace moments occur for $\nu \simeq 10$.

Logarithms of $1/\tau_a$ are transformed into logarithms of ν. The perturbative cross section is ill defined for small values of τ_a. For $\tau_a \sim \Lambda_{QCD}/Q$ nonperturbative corrections become dominant. When resummed, the next-to-leading logarithmic terms of τ_a, in the cross section in Equation 2.4 can be rewritten as the sum of a calculable perturbative term, labelled with the subscript PT, including all terms of parton transverse momenta above κ (the infrared factorization scale) and a soft term that contains all non-perturbative (NP) physics:

$$\ln\left[\frac{1}{\sigma_{\rm tot}}\tilde{\sigma}(\nu, Q, a)\right] \equiv \ln \tilde{R}_{PT}(\nu, Q, \kappa, a) + \ln \tilde{f}_{a,\rm NP}\left(\frac{\nu}{Q}, \kappa, a\right) + \mathcal{O}\left(\nu\left(\frac{\kappa}{Q}\right)^{2-a}, \nu^{\frac{2}{2-a}}\left(\frac{\kappa}{Q}\right)^2\right)\,, \tag{2.5}$$

where logarithm of the soft term can be written as an expansion in powers of ν/Q:

$$\ln \tilde{f}_{a,\rm NP}\left(\frac{\nu}{Q}, \kappa, a\right) \equiv \frac{1}{1-a}\sum_{n=1}^{\infty} \lambda_n(\kappa)\left(-\frac{\nu}{Q}\right)^n. \tag{2.6}$$

From Equation 2.6 it is clear that the only dependence on a is through an overall factor $1/(1-a)$ which leads to an approximate scaling rule between the non-perturbative shape functions for different values of a [21–23] given by rewriting it as:

$$\tilde{f}_{a,\rm NP}\left(\frac{\nu}{Q}, \kappa, a\right) = \left[\tilde{f}_{0,\rm NP}\left(\frac{\nu}{Q}, \kappa\right)\right]^{\frac{1}{(1-a)}}\ . \tag{2.7}$$

JHEP10(2011)143

2.2 Energy flow correlation

The study of energy flow into regions between energetic jets [18, 19] holds important and complementary information about the formation of final states. It reflects the flow of colour at short distances [20]. The correlations between energy flow and event shapes ("energy flow correlations") are studied here. The differential cross section giving the correlations for di-jet events (see figure 1) at fixed values of $\tau_{a\bar{\Omega}} = \tau_a(\delta)$ and ε is

$$\frac{d\bar{\sigma}(\varepsilon, \tau_a(\delta), a)}{d\varepsilon d\tau_a(\delta)} = \frac{1}{2\ Q^2} \sum_N |M(N)|^2 \delta(\varepsilon - \varepsilon(N)) \delta(\tau_a - \tau_a(N)) \,, \tag{2.8}$$

where the sum extends over final states N that contribute to the intervals $d\varepsilon$ and $d\tau_a(\delta)$ and where $M(N)$ denotes the corresponding amplitude for $e^+e^- \to N$. Taking the Laplace moment with respect to τ_a, it gives

$$\frac{d\bar{\sigma}(\varepsilon, \nu, \delta, a)}{d\varepsilon} = \int_0^1 d\tau_a(\delta) e^{-\nu\tau_a(\delta)} \frac{d\bar{\sigma}(\varepsilon, \tau_a(\delta), a)}{d\varepsilon d\tau_a(\delta)} \,. \tag{2.9}$$

The analysis presented here make use of the variables: δ, the cone angle with respect to the thrust axis, the angularity parameter τ_a, the energy flow fraction ε and the coefficient ν of the Laplace moment.

3 Data

3.1 Event selection

We have used data with an integrated luminosity of 47.97 pb^{-1} collected with the L3 detector [24–27] at LEP in 1994 at $\sqrt{s} = 91.2$ GeV and with 602.2 pb^{-1} collected during 1998-2000 at $\sqrt{s} \geq 189$ GeV as summarized in table 1.

The primary trigger for $e^+e^- \to hadrons$ events require a total energy greater than 15 GeV in the calorimeters. This trigger is in logical OR with a trigger using the barrel scintillation counters and with a charged-track trigger. The combined trigger efficiency for the selected hadronic events exceeds 99.9%.

The selection of $e^+e^- \to hadrons$ events is based on the energy measured in the electromagnetic and hadron calorimeters. Energy clusters in the calorimeters have a minimum energy of 100 MeV. The principal variables used to distinguish hadronic events from backgrounds are the cluster multiplicity and the energy imbalances. Energy clusters in the calorimeters are used to measure the total visible energy $E_{\rm vis}$, and the energy imbalances parallel and perpendicular to the beam direction: $E_\parallel = |\sum E \cos\theta_B|$ and $E_\perp = \sqrt{(\sum E \sin\theta_B \sin\phi_B)^2 + (\sum E \sin\theta_B \cos\phi_B)^2}$, respectively, where E is the energy of a cluster and θ_B and ϕ_B are its polar and azimuthal angles with respect to the beam direction. More details of the calorimetric measurements can be found in References [12] and [28]. Background processes are different for hadronic Z decays and hadronic events at high energies, resulting in different selection cuts.

We use Monte Carlo events to estimate the efficiency of the selection criteria and purity of the data sample. Monte Carlo events for the process $e^+e^- \to q\bar{q}(\gamma)$ are generated by the

JHEP10(2011)143

parton shower programs JETSET 7.4 [29] at $\sqrt{s} = 91.2$ GeV, PYTHIA [30–32] for $\sqrt{s} = 189$ GeV and KK2F [33, 34], which uses PYTHIA for hadronization, for the higher energies. The generated events are passed through the L3 detector simulation [35, 36]. The background events are simulated with appropriate event generators: PYTHIA and PHOJET [37, 38] for hadron production in two-photon interactions, KORALZ [39] for the $\tau^+\tau^-(\gamma)$ final state, BHAGENE [40, 41] for Bhabha events, KORALW [42, 43] for W-boson pair production and PYTHIA for Z-boson pair production.

The multi-hadronic final states at $\sqrt{s} = 91.2$ GeV are selected using cuts on the visible energy, $0.6 < E_{\rm vis}/\sqrt{s} < 1.4$, relative energy imbalances, $E_{\parallel}/E_{\rm vis} < 0.4$ and $E_{\perp}/E_{\rm vis} < 0.4$, and cluster multiplicity, $N_{cl} > 12$. These criteria select 1.42 million hadronic events with a selection efficiency of 97.7% and purity of 99.2%. The background due to two-photon interaction processes is negligible and that due to the $\tau^+\tau^-(\gamma)$ final state is at the level of 0.2%.

At higher centre-of-mass energies, background is mostly due to two sources: "radiative return events", where initial state radiation results in a mass of the resulting hadronic system close to the Z boson mass, and W-boson and Z-boson pair production where one or both bosons decay hadronically. Events are first selected by requiring $E_{\rm vis}/\sqrt{s} > 0.7$, $E_{\perp}/E_{\rm vis} < 0.4$, number of clusters > 12, and at least one well measured charged track. To reduce the radiative return background, events are rejected if they have a high-energy photon candidate, defined as a cluster in the electromagnetic calorimeter with at least 85% of its energy in a 15° cone and a total energy greater than $0.18\sqrt{s}$. In addition, $\sqrt{s'/s} > 0.85$ is required where $\sqrt{s'}$ is the centre-of-mass energy of a system recoiling against an unobserved photon emitted at small angle, and is estimated from the angles of the jets [12]. To reject boson-pair events where a W-boson or Z-boson decays into leptons, we remove events having an electron or muon with energy greater than 40 GeV. Fully hadronic W-boson and Z-boson pair events are reduced by

- forcing the event into a 4-jet topology using the Durham jet algorithm [44–47],
- performing a kinematic fit imposing energy and momentum conservation,
- rejecting events if all of the following criteria are met: the energy of the most energetic jet is less than $0.4\sqrt{s}$, the ratio of the energy of the most energetic jet to the least energetic jet is less than 5, the Durham jet resolution parameter $y_{34}^{D} > 0.007$, there are more than 40 clusters and more than 15 charged tracks, and $E_{\parallel} < 0.2E_{\rm vis}$.

These cuts remove 11.6% of the signal events, 98.1% of the radiative return events and 83.3% and 80.1% of W-boson and Z-boson pair events respectively. We select a total of 13.9 thousand hadronic events with an efficiency of 88.3% and with purity of 78.2% for $\sqrt{s} \geq 189$ GeV. At $\sqrt{s} \geq 189$ GeV backgrounds due to radiative return events, W-boson pairs, Z-boson pair events and two-photon interactions are 5.71%, 12.3%, 1.12% and 2.58% respectively. The remaining backgrounds are negligible. The number of selected events for each of the energy points are also summarized in table 1 together with selection efficiencies and purities. All the high energy data points between 189 and 207 GeV are combined giving high energy sample with $\langle\sqrt{s}\rangle = 197.0$ GeV.

JHEP10(2011)143

3.2 Flavour tagging

Heavy-flavour (b) events are separated from light-flavour (u, d, s, c) events using the characteristic decay properties of the b-hadrons. As a first step, the position of the interaction vertex is estimated for each machine fill by iteratively fitting all tracks measured in the detector during the fill which pass basic track quality criteria. Measurements of the decay lengths with respect to this vertex of all n tracks in the event contribute to a probability, $P^{[n]}$, which would be flat for events with quarks of zero lifetime, but peak at zero otherwise. A weighted discriminant is defined as $\mathrm{B_{Tag}} = -\log P$, where $P = P^{[n]} \sum_{j=0}^{n-1} (-\log P^{[n]})^j / j!$ and $P^{[n]} = \prod_{i=1}^{n} P_i$, where P_i is the probability that track i originates at the primary vertex [48]. A cut on this discriminant is made to distinguish light-flavour from b-flavour events. Light flavour events are selected using $0.3 < \mathrm{B_{Tag}} < 1.0$ at $\sqrt{s} = 91.2$ GeV and using $\mathrm{B_{Tag}} < 1.0$ at $\langle\sqrt{s}\rangle = 197.0$ GeV.

At $\sqrt{s} = 91.2$ GeV, 492.6 thousand light-flavour events are selected with an efficiency of $(38.84 \pm 0.10)\%$ and a purity of $(90.41 \pm 0.07)\%$. The dominant background is due to b-quark events which amount to $(9.59 \pm 0.07)\%$ of the sample. At the high centre-of-mass energy, the number of selected light-flavour events is 6895 with selection efficiency of $(75.5 \pm 0.3)\%$ and a purity of $(72.7 \pm 0.1)\%$. Here the dominant background is W-boson pair events amounting to $(17.6 \pm 0.1)\%$ while that due to b-quarks, radiative return, Z-boson pair and two-photon interactions are $(3.9 \pm 0.1)\%$, $(3.7 \pm 0.1)\%$, $(0.6 \pm 0.1)\%$ and $(1.4 \pm 0.1)\%$, respectively. Table 1 summarizes the selected number of events, efficiencies and purities at each centre-of-mass energy.

3.3 Measurements

The distributions of the inclusive event shape variables at $\sqrt{s} = 91.2$ GeV and $\langle\sqrt{s}\rangle = 197.0$ GeV are measured for the udsc-quark enriched samples for various values of the parameter a (-1, -0.75, -0.5, -0.25, 0.0, 0.25, 0.5 and 0.75) with the region Ω corresponding to $\delta = 90^\circ$. The distributions of the 'energy flow correlation' are obtained for all quark flavours at $\sqrt{s} = 91.2$ GeV and at high energies for several values of the cone angle δ (30°, 45°, 60°, 75°) and the coefficient ν (10, 25, 35, 50).

The data distributions are compared to a combination of the signal and the different background Monte Carlo distributions obtained using the same selection procedure and normalized to the integrated luminosity. For Monte Carlo events, these event shapes are calculated before (particle level) and after (detector level) detector simulation. The calculation before detector simulation takes into account all stable charged and neutral particles. The measured distributions at detector level differ from the ones at particle level because of detector effects, limited acceptance and finite resolution.

After subtracting the background events according to standard cross sections, the measured distributions are corrected for detector effects, acceptance and resolution, using a matrix unfolding method at $\sqrt{s} = 91.2$ GeV and on a bin-by-bin basis at $\langle\sqrt{s}\rangle = 197.0$ GeV. For extracting flavour-tagged distributions, the effect due to wrong flavour contamination is taken care of using a treatment similar to standard background subtraction. We also

JHEP10(2011)143

correct the data for initial- and final-state photon radiation bin-by-bin using Monte Carlo distributions at particle level with and without radiation.

Figure 2 shows the measured distributions of $dN/d\tau_a$ for $a = -1.0$, -0.5, 0.0, 0.5 at $\sqrt{s} = 91.2$ GeV for the light-flavour event sample. The same distributions for $\langle\sqrt{s}\rangle = 197$ GeV are shown in figure 3. The shaded areas show the different background contributions. The comparisons with the predictions from signal (JETSET parton shower) and background Monte Carlo programs show good agreement both at $\sqrt{s} = 91.2$ GeV and at high energy. All the following differential event shape variables are determined from the light-flavour data sample while those for 'energy flow correlations' are determined from the overall sample. Figure 4 shows the measured distributions of $dN/d\varepsilon$ for $\delta = 30°$, $45°$, $60°$, $75°$ at $\sqrt{s} = 188.6$ GeV for the overall sample. As in the previous figures, the shaded areas show the different background contributions. Again the overall agreement between data and Monte Carlo is reasonable for all values of δ.

3.4 Systematic uncertainties

The bin-by-bin systematic uncertainties in the distributions of inclusive event shape variables or for energy flow correlation parameters arise mainly from uncertainties in the estimation of detector corrections and background. The uncertainty in detector correction is estimated by several independent checks.

- The definition of reconstructed objects used to calculate the observables is changed from calorimetric clusters only to a non-linear combination of charged tracks with calorimetric clusters [28].

- The effect of different particle densities in correcting the measured distributions is estimated by using a different signal Monte Carlo program,HERWIG [49–51] instead of JETSET PS or PYTHIA.

- The acceptance is reduced by restricting the events to the central part of the detector, with improved resolution, $\cos(\theta_T) < 0.7$, where θ_T is the polar angle of the thrust axis relative to the beam direction.

The following systematic checks are made on the background estimations.

- An alternative criterion is applied to reject radiative return events based on a cut in the two dimensional plane of $E_{\parallel}/E_{\rm vis}$ and $E_{\rm vis}/\sqrt{s}$ [28].

- The estimated background from two-photon interaction is varied by $\pm 30\%$ and is simulated by using the PHOJET instead of the PYTHIA Monte Carlo program.

- The W-boson pair-production background is estimated from the KORALW Monte Carlo and subtracted from the data, while removing the cut on 4-jet events.

- The contamination from wrong-flavour events is estimated by varying the cut on the $B_{\rm Tag}$ discriminant used to tag non-b events from 1.0 to 0.9 or 1.1. An additional lower cut at 0.2 is also introduced for the high energy data.

JHEP10(2011)143

Table 2 summarizes the breakdown of different contributions of systematic uncertainty for inclusive event shape variables of the enriched light-flavour data sample. The total systematic uncertainty for the data sample at $\sqrt{s} = 91.2$ GeV is typically $3.8\% - 4.5\%$ and is primarily due to the choice of signal Monte Carlo ($\sim 3\%$) and detector correction ($\sim 2\%$). At high energies, the overall systematic uncertainty is $4.4\% - 6.4\%$. Here the contributions from detector correction, background subtraction and wrong flavour contamination are roughly equal.

Table 3 summarizes the systematic uncertainties for the energy flow correlation variables for different values δ and ν at the two centre-of-mass energies for $a = 0$. The systematic uncertainty is roughly the same for different a values at a given energy with fixed values of δ and ν. At $\sqrt{s} = 91.2$ GeV, the overall systematic uncertainty is $2.1\% - 3.7\%$. This contribution due to background correction is larger for small δ-values while that due to signal Monte Carlo is the dominant source for medium values of δ. The overall uncertainty at high energies is $3.6\% - 4.5\%$ where the largest contribution comes from background correction ($\sim 3\%$) while that for detector correction is at the level of $1.6\% - 2.3\%$.

The statistical component of the systematic uncertainty is negligible as the size of the Monte Carlo sample is more than four times and sometimes even ten times larger than the data sample. The final systematic uncertainty is taken as the sum in quadrature of all the contributions.

4 Results

4.1 Inclusive event shape variables

The corrected distributions $(1/\sigma)d\sigma/d\tau_a$ at $\sqrt{s} = 91.2$ GeV and for $\langle\sqrt{s}\rangle = 197.0$ GeV for the eight a values -1.0, -0.75, -0.5, -0.25, 0.0, 0.25, 0.5 and 0.75 are presented in tables 4–11. The first and the second moments of the distributions are also computed and quoted in the tables 4–11. Figures 5, 6, 7 and 8 show comparison of $(1/\sigma)d\sigma/d\tau_a$ for the eight a values in the form of fractional deviations from predictions of the parton shower models JETSET, ARIADNE [52] and HERWIG at $\sqrt{s} = 91.2$ GeV and $\langle\sqrt{s}\rangle = 197.0$ GeV respectively. The parameters of these models have been tuned using Z-pole data [28]. Figures 6 and 8 show the distributions from the Monte Carlo programs for two different values of a, 0.0 and 0.75. At $\sqrt{s} = 91.2$ GeV all models agree well with the data for $\tau_a \leq 0.15$, 0.3, 0.4 for $a = -1.0$, 0.0 and 0.5 respectively. At $\langle\sqrt{s}\rangle = 197.0$ GeV the same is true for $\tau_a \leq 0.07$, 0.10 and 0.20. For higher values of τ_a the models tend to underestimate the data, although the latter show large statistical fluctuations at both $\langle\sqrt{s}\rangle$ values. The levels of agreement of the different models with the data are compared in tables 12, 13 where χ^2 values and confidence levels of the model/data comparisons are shown. Among the different models, predictions from ARIADNE are the closest to the data.

The comparison between data and the scaling rule predictions of Equation 2.7 is shown for $\sqrt{s} = 91.2$ GeV for $a = -1.0$, -0.75, -0.5, -0.25, 0.25 and 0.5 in figure 5 and figure 6. Data distributions at $a = 0$ are used to determine the non-perturbative contribution of the shape function for $a = 0$. The comparison is not shown for $a = 0.75$ in order to avoid theoretical uncertainties related to the approaching $a = 1$ singularity in Equation 2.6 [53].

JHEP10(2011)143

A similar comparison at $\langle\sqrt{s}\rangle = 197.0$ GeV is shown in figure 7 and figure 8. Figure 9 shows the first moments of the distributions at $\sqrt{s} = 91.2$ GeV and $\langle\sqrt{s}\rangle = 197.0$ GeV compared with the theoretical predictions. The agreement is reasonable for $\sqrt{s} = 91.2$ GeV particularly for $a \leq 0.25$, while at $\langle\sqrt{s}\rangle = 197.0$ GeV the predictions are below the data for $a \leq 0.25$ and above the data for $a = 0.75$.

4.2 Energy flow correlations

The measured distributions for all quark flavours of the energy flow correlation for $\delta = 30°$, $45°$, $60°$ and $75°$, $\nu = 10$, 25, 35, 50 and $a = -1.0$, -0.5, 0.0 and 0.5 are given in tables 14–29 for $\sqrt{s} = 91.2$ GeV and $\langle\sqrt{s}\rangle = 197.0$ GeV. Figure 10 shows the energy flow correlation at $\sqrt{s} = 91.2$ GeV with ε for $\nu = 50$ and for different values of δ and a and a comparison with parton-shower models. The distribution gets steeper with increasing values of δ and there is an appearance of a shoulder at δ values of $30°$ and $45°$, which is reproduced by Monte Carlo models. The shoulder could be the effect of 3-jet events where the thrust axis is lined up along the direction of the most energetic jet and both of the other jets appear in the region Ω, thus contributing to ε. The energy flow correlation for various values of δ and a and $\nu = 10$ is shown in figure 11. The shoulder becomes more pronounced as a increases for $\delta = 30°$ and $45°$, while for larger δ values, the distribution is steeper for larger values of a. Monte Carlo models give a good description of this trend, while a fluctuation at $\delta = 45°$ corresponds to a phase space edge not accurately reproduced by Monte Carlo. Figure 12 shows the variation for different values of ν at four different values of a and with $\delta = 60°$.

The change in energy flow correlation with δ at $\langle\sqrt{s}\rangle = 197.0$ GeV for different values of a is shown in figure 13 for $\nu = 50$ and in figure 14 for $\nu = 10$. Figure 15 shows the variation for different values of ν and a at $\langle\sqrt{s}\rangle = 197.0$ GeV for $\delta = 60°$. Unlike the Z-pole data, there are discrepancies between the observed distributions and predictions from the parton shower models. The discrepancies increase for larger values of ε.

The possible origin of the discrepancy is further investigated to exclude an effect from background subtraction. The energy-flow correlation is determined from the corrected $dN/d\varepsilon$ distributions. This process starts from measured distributions as those shown in figure 4 together with prediction from signal and background processes. At this measured level, agreement with predictions is observed. To further check that background modeling, and in particular the dominant W-pair process, does not affect the measurement, corrected distributions are presented in figure 16 for the single highest-statistic energy point, $\sqrt{s}$ = 188.6 Gev for for $\nu = 50$, $a = -1.0$ and four different values of δ. Inspection of this figure shows a marked decrease in the level of W-pair background with increasing δ. The discrepancies observed in figure 13 do not show a similar dependency with δ, and are therefore not correlated with the level of the W-pair background.

5 Summary

We have measured for the first time recently-proposed event shape distributions at $\sqrt{s} = 91.2$ GeV and $\sqrt{s} = 189 - 207$ GeV using 650 pb^{-1} of data collected by the L3 detector

JHEP10(2011)143

at LEP. These new event shape distributions are well described by different parton shower Monte Carlo models. A next-to-leading-log approximation predicts a scaling rule for the non-perturbative component of inclusive event shapes distribution which is qualitatively observed at the Z-pole.

The Laplace moment dependence of energy flow into regions between energetic jets is studied through a set of Laplace moments at the two centre-of-mass energies by varying the inter-jet angular region. The comparison with parton shower model predictions shows agreement at $\sqrt{s} = 91.2$ GeV where the parameters of the models were tuned, whereas discrepancies are observed at $\langle\sqrt{s}\rangle = 197$ GeV for moderate or high values of ε. On the other hand, previous event shape studies [12, 28] on the same data sample, show good agreement with model predictions, tuned to Z-pole data, at both high and low energies.

Acknowledgments

We would like to thank Carola F. Berger and George Sterman for their help with the theoretical predictions.

6 The L3 collaboration

P.Achard[20], O.Adriani[17], M.Aguilar-Benitez[25], J.Alcaraz[25], G.Alemanni[23], J.Allaby[18], A.Aloisio[29], M.G.Alviggi[29], H.Anderhub[49], V.P.Andreev[6,34], F.Anselmo[8], A.Arefiev[28], T.Azemoon[3], T.Aziz[9], P.Bagnaia[39], A.Bajo[25], G.Baksay[26], L.Baksay[26], S.V.Baldew[2], S.Banerjee[9], Sw.Banerjee[4], A.Barczyk[49,47], R.Barillère[18], P.Bartalini[23], M.Basile[8], N.Batalova[46], R.Battiston[33], A.Bay[23], U.Becker[13], F.Behner[49], L.Bellucci[17], R.Berbeco[3], J.Berdugo[25], P.Berges[13], B.Bertucci[33], B.L.Betev[49], M.Biasini[33], M.Biglietti[29], A.Biland[49], J.J.Blaising[4], S.C.Blyth[35], G.J.Bobbink[2], A.Böhm[1], L.Boldizsar[12], B.Borgia[39], S.Bottai[17], D.Bourilkov[49], M.Bourquin[20], S.Braccini[20], J.G.Branson[41], F.Brochu[4], J.D.Burger[13], W.J.Burger[33], X.D.Cai[13], M.Capell[13], G.Cara Romeo[8], G.Carlino[29], A.Cartacci[17], J.Casaus[25],F.Cavallari[39],N.Cavallo[36],C.Cecchi[33],M.Cerrada[25],M.Chamizo[20],Y.H.Chang[44], M.Chemarin[24], A.Chen[44], G.Chen[7], G.M.Chen[7], H.F.Chen[22], H.S.Chen[7], G.Chiefari[29], L.Cifarelli[40], F.Cindolo[8], I.Clare[13], R.Clare[38], G.Coignet[4], N.Colino[25], S.Costantini[39], B.de la Cruz[25], S.Cucciarelli[33], R.de Asmundis[29], P.Déglon[20], J.Debreczeni[12], A.Degré[4], K.Dehmelt[26], K.Deiters[47], D.della Volpe[29], E.Delmeire[20], P.Denes[37], F.DeNotaristefani[39], A.De Salvo[49], M.Diemoz[39], M.Dierckxsens[2], C.Dionisi[39], M.Dittmar[49], A.Doria[29], M.T.Dova[10,♯], D.Duchesneau[4], M.Duda[1], B.Echenard[20], A.Eline[18], A.El Hage[1], H.El Mamouni[24], A.Engler[35], F.J.Eppling[13], P.Extermann[20], M.A.Falagan[25], S.Falciano[39], A.Favara[32], J.Fay[24], O.Fedin[34], M.Felcini[49], T.Ferguson[35], H.Fesefeldt[1], E.Fiandrini[33], J.H.Field[20], F.Filthaut[31], P.H.Fisher[13], W.Fisher[37], G.Forconi[13], K.Freudenreich[49], C.Furetta[27],Yu.Galaktionov[28,13],S.N.Ganguli[9],P.Garcia-Abia[25],M.Gataullin[32],S.Gentile[39], S.Giagu[39], Z.F.Gong[22], G.Grenier[24], O.Grimm[49], M.W.Gruenewald[16], V.K.Gupta[37], A.Gurtu[9],L.J.Gutay[46],D.Haas[5],D.Hatzifotiadou[8],T.Hebbeker[1],A.Hervé[18],J.Hirschfelder[35], H.Hofer[49], M.Hohlmann[26], G.Holzner[49], S.R.Hou[44], B.N.Jin[7], P.Jindal[14], L.W.Jones[3], P.de Jong[2], I.Josa-Mutuberría[25], M.Kaur[14], M.N.Kienzle-Focacci[20], J.K.Kim[43], J.Kirkby[18],

JHEP10(2011)143

W.Kittel[31], A.Klimentov[13,28], A.C.König[31], M.Kopal[46], V.Koutsenko[13,28], M.Kräber[49], R.W.Kraemer[35], A.Krüger[48], A.Kunin[13], P.Ladron de Guevara[25], I.Laktineh[24], G.Landi[17], M.Lebeau[18], A.Lebedev[13], P.Lebrun[24], P.Lecomte[49], P.Lecoq[18], P.Le Coultre[49], J.M.Le Goff[18], R.Leiste[48], M.Levtchenko[27], P.Levtchenko[34], C.Li[22], S.Likhoded[48], C.H.Lin[44], W.T.Lin[44], F.L.Linde[2], L.Lista[29], Z.A.Liu[7], W.Lohmann[48], E.Longo[39], Y.S.Lu[7], C.Luci[39], L.Luminari[39], W.Lustermann[49], W.G.Ma[22], L.Malgeri[18], A.Malinin[28], C.Maña[25], J.Mans[37], J.P.Martin[24], F.Marzano[39], K.Mazumdar[9], R.R.McNeil[6], S.Mele[18,29], L.Merola[29], M.Meschini[17], W.J.Metzger[31], A.Mihul[11], H.Milcent[18], G.Mirabelli[39], J.Mnich[1], G.B.Mohanty[9], G.S.Muanza[24], A.J.M.Muijs[2], M.Musy[39], S.Nagy[15], S.Natale[20], M.Napolitano[29], F.Nessi-Tedaldi[49], H.Newman[32], A.Nisati[39], T.Novak[31], H.Nowak[48], R.Ofierzynski[49], G.Organtini[39], I.Pal[46], C.Palomares[25], P.Paolucci[29], R.Paramatti[39], G.Passaleva[17], S.Patricelli[29], T.Paul[10], M.Pauluzzi[33], C.Paus[13], F.Pauss[49], M.Pedace[39], S.Pensotti[27], D.Perret-Gallix[4], D.Piccolo[29], F.Pierella[8], M.Pieri[41], M.Pioppi[33], P.A.Piroué[37], E.Pistolesi[27], V.Plyaskin[28], M.Pohl[20], V.Pojidaev[17], J.Pothier[18], D.Prokofiev[34], G.Rahal-Callot[49], M.A.Rahaman[9], P.Raics[15], N.Raja[9], R.Ramelli[49], P.G.Rancoita[27], R.Ranieri[17], A.Raspereza[48], P.Razis[30], S.Rembeczki[26], D.Ren[49], M.Rescigno[39], S.Reucroft[10], S.Riemann[48], K.Riles[3], B.P.Roe[3], L.Romero[25], A.Rosca[48], C.Rosemann[1], C.Rosenbleck[1], S.Rosier-Lees[4], S.Roth[1], J.A.Rubio[18], G.Ruggiero[17], H.Rykaczewski[49], A.Sakharov[49], S.Saremi[6], S.Sarkar[39], J.Salicio[18], E.Sanchez[25], C.Schäfer[18], V.Schegelsky[34], H.Schopper[21], D.J.Schotanus[31], C.Sciacca[29], L.Servoli[33], S.Shevchenko[32], N.Shivarov[42], V.Shoutko[13], E.Shumilov[28], A.Shvorob[32], D.Son[43], C.Souga[24], P.Spillantini[17], M.Steuer[13], D.P.Stickland[37], B.Stoyanov[42], A.Straessner[20], K.Sudhakar[9], G.Sultanov[42], L.Z.Sun[22], S.Sushkov[1], H.Suter[49], J.D.Swain[10], Z.Szillasi[26,¶], X.W.Tang[7], P.Tarjan[15], L.Tauscher[5], L.Taylor[10], B.Tellili[24], D.Teyssier[24], C.Timmermans[31], Samuel C.C.Ting[13], S.M.Ting[13], S.C.Tonwar[9], J.Tóth[12], C.Tully[37], K.L.Tung[7], J.Ulbricht[49], E.Valente[39], R.T.Van de Walle[31], R.Vasquez[46], G.Vesztergombi[12], I.Vetlitsky[28], G.Viertel[49], M.Vivargent[4], S.Vlachos[5], I.Vodopianov[26], H.Vogel[35], H.Vogt[48], I.Vorobiev[35,28], A.A.Vorobyov[34], M.Wadhwa[5], Q.Wang[31], X.L.Wang[22], Z.M.Wang[22], M.Weber[18], S.Wynhoff[37,†], L.Xia[32], Z.Z.Xu[22], J.Yamamoto[3], B.Z.Yang[22], C.G.Yang[7], H.J.Yang[3], M.Yang[7], S.C.Yeh[45], An.Zalite[34], Yu.Zalite[34], Z.P.Zhang[22], J.Zhao[22], G.Y.Zhu[7], R.Y.Zhu[32], H.L.Zhuang[7], A.Zichichi[8,18,19], B.Zimmermann[49], M.Zöller[1].

1 III. Physikalisches Institut, RWTH, D-52056 Aachen, Germany[§]
2 National Institute for High Energy Physics, NIKHEF, and University of Amsterdam, NL-1009 DB Amsterdam, The Netherlands
3 University of Michigan, Ann Arbor, MI 48109, USA
4 Laboratoire d'Annecy-le-Vieux de Physique des Particules, LAPP,IN2P3-CNRS, BP 110, F-74941 Annecy-le-Vieux CEDEX, France
5 Institute of Physics, University of Basel, CH-4056 Basel, Switzerland
6 Louisiana State University, Baton Rouge, LA 70803, USA
7 Institute of High Energy Physics, IHEP, 100039 Beijing, China[△]
8 University of Bologna and INFN-Sezione di Bologna, I-40126 Bologna, Italy
9 Tata Institute of Fundamental Research, Mumbai (Bombay) 400 005, India
10 Northeastern University, Boston, MA 02115, USA

JHEP10(2011)143

11 Institute of Atomic Physics and University of Bucharest, R-76900 Bucharest, Romania
12 Central Research Institute for Physics of the Hungarian Academy of Sciences, H-1525 Budapest 114, Hungary‡
13 Massachusetts Institute of Technology, Cambridge, MA 02139, USA
14 Panjab University, Chandigarh 160 014, India
15 KLTE-ATOMKI, H-4010 Debrecen, Hungary¶
16 UCD School of Physics, University College Dublin, Belfield, Dublin 4, Ireland
17 INFN Sezione di Firenze and University of Florence, I-50125 Florence, Italy
18 European Laboratory for Particle Physics, CERN, CH-1211 Geneva 23, Switzerland
19 World Laboratory, FBLJA Project, CH-1211 Geneva 23, Switzerland
20 University of Geneva, CH-1211 Geneva 4, Switzerland
21 University of Hamburg, D-22761 Hamburg, Germany
22 Chinese University of Science and Technology, USTC, Hefei, Anhui 230 029, China△
23 University of Lausanne, CH-1015 Lausanne, Switzerland
24 Institut de Physique Nucléaire de Lyon, IN2P3-CNRS,Université Claude Bernard, F-69622 Villeurbanne, France
25 Centro de Investigaciones Energéticas, Medioambientales y Tecnológicas, CIEMAT, E-28040 Madrid, Spain♭
26 Florida Institute of Technology, Melbourne, FL 32901, USA
27 INFN-Sezione di Milano, I-20133 Milan, Italy
28 Institute of Theoretical and Experimental Physics, ITEP, Moscow, Russia
29 INFN-Sezione di Napoli and University of Naples, I-80125 Naples, Italy
30 Department of Physics, University of Cyprus, Nicosia, Cyprus
31 Radboud University and NIKHEF, NL-6525 ED Nijmegen, The Netherlands
32 California Institute of Technology, Pasadena, CA 91125, USA
33 INFN-Sezione di Perugia and Università Degli Studi di Perugia, I-06100 Perugia, Italy
34 Nuclear Physics Institute, St. Petersburg, Russia
35 Carnegie Mellon University, Pittsburgh, PA 15213, USA
36 INFN-Sezione di Napoli and University of Potenza, I-85100 Potenza, Italy
37 Princeton University, Princeton, NJ 08544, USA
38 University of Californa, Riverside, CA 92521, USA
39 INFN-Sezione di Roma and University of Rome, "La Sapienza", I-00185 Rome, Italy
40 University and INFN, Salerno, I-84100 Salerno, Italy
41 University of California, San Diego, CA 92093, USA
42 Bulgarian Academy of Sciences, Central Lab. of Mechatronics and Instrumentation, BU-1113 Sofia, Bulgaria
43 The Center for High Energy Physics, Kyungpook National University, 702-701 Taegu, Republic of Korea
44 National Central University, Chung-Li, Taiwan, China
45 Department of Physics, National Tsing Hua University, Taiwan, China
46 Purdue University, West Lafayette, IN 47907, USA
47 Paul Scherrer Institut, PSI, CH-5232 Villigen, Switzerland

JHEP10(2011)143

48 DESY, D-15738 Zeuthen, Germany
49 Eidgenössische Technische Hochschule, ETH Zürich, CH-8093 Zürich, Switzerland
§ Supported by the German Bundesministerium für Bildung, Wissenschaft, Forschung und Technologie.
‡ Supported by the Hungarian OTKA fund under contract numbers T019181, F023259 and T037350.
¶ Also supported by the Hungarian OTKA fund under contract number T026178.
♭ Supported also by the Comisión Interministerial de Ciencia y Tecnología.
♯ Also supported by CONICET and Universidad Nacional de La Plata, CC 67, 1900 La Plata, Argentina.
△ Supported by the National Natural Science Foundation of China.
† Deceased.

References

[1] H. Fritzsch, M. Gell-Mann and H. Leutwyler, *Advantages of the color octet gluon picture*, *Phys. Lett.* **B 47** (1973) 365 [SPIRES].

[2] S. Weinberg, *Nonabelian gauge theories of the strong interactions*, *Phys. Rev. Lett.* **31** (1973) 494 [SPIRES].

[3] D.J. Gross and F. Wilczek, *Ultraviolet behavior of non-abelian gauge theories*, *Phys. Rev. Lett.* **30** (1973) 1343 [SPIRES].

[4] D.J. Gross and F. Wilczek, *Asymptotically free gauge theories. 1*, *Phys. Rev.* **D 8** (1973) 3633 [SPIRES].

[5] H.D. Politzer, *Reliable perturbative results for strong interactions?*, *Phys. Rev. Lett.* **30** (1973) 1346 [SPIRES].

[6] R.K. Ellis, W.J. Stirling and B.R. Webber, *QCD and collider physics*, Cambridge University Press, Cambridge U.K. (1996).

[7] G. Dissertori, I, Knowles and M. Schmelling, *Quantum chormodynamics*, Clarendon Press, Oxford Science Publication, Oxford U.K. (2003).

[8] E. Farhi, *A QCD test for jets*, *Phys. Rev. Lett.* **39** (1977) 1587 [SPIRES]

[9] A. De Rujula, J.R. Ellis, E.G. Floratos and M.K. Gaillard, *QCD predictions for hadronic final states in e^+e^- annihilation*, *Nucl. Phys.* **B 138** (1978) 387 [SPIRES].

[10] Y.L. Dokshitzer and B.R. Webber, *Power corrections to event shape distributions*, *Phys. Lett.* **B 404** (1997) 321 [hep-ph/9704298] [SPIRES].

[11] G.P. Korchemsky and G.F. Sterman, *Nonperturbative corrections in resummed cross-sections*, *Nucl. Phys.* **B 437** (1995) 415 [hep-ph/9411211] [SPIRES].

[12] L3 collaboration, P. Achard et al., *PMC Physics* **A 2008** (2008) 2.

[13] C.F. Berger, T. Kucs and G.F. Sterman, *Event shape/energy flow correlations*, *Phys. Rev.* **D 68** (2003) 014012 [hep-ph/0303051] [SPIRES].

[14] S. Brandt et al., *The principal axis of jets. An attempt to analyze high-energy collisions as two-body processes*, *Phys. Lett.* **12** (1964) 57.

JHEP10(2011)143

[15] E. Farhi, *A QCD test for jets*, *Phys. Rev. Lett.* **39** (1977) 1587 [SPIRES].

[16] S. Catani et al., *Jet broadening measures in e^+e^- annihilation*, *Phys. Lett.* **B 295** (1992) 269.

[17] Y.L. Dokshitzer, A. Lucenti, G. Marchesini and G.P. Salam, *On the QCD analysis of jet broadening*, *JHEP* **01** (1998) 011 [hep-ph/9801324] [SPIRES].

[18] Yu.L. Dokshitzer, V.A. Khoze, S.I. Troian, *Coherence and physics of QCD jets, in perturbative quantum chromodynamics*, A.H. Mueller ed., World Scientific, Singapore (1989).

[19] J.R. Ellis, V.A. Khoze and W.J. Stirling, *Hadronic antenna patterns to distinguish production mechanisms for large E(T) jets*, *Z. Phys.* **C 75** (1997) 287 [hep-ph/9608486] [SPIRES].

[20] C.F. Berger, T. Kucs and G.F. Sterman, *Energy flow in interjet radiation*, *Phys. Rev.* **D 65** (2002) 094031 [hep-ph/0110004] [SPIRES].

[21] C.F. Berger and G.F. Sterman, *Scaling rule for nonperturbative radiation in a class of event shapes*, *JHEP* **09** (2003) 058 [hep-ph/0307394] [SPIRES].

[22] C.F. Berger, *Soft gluon exponentiation and resummation*, hep-ph/0305076 [SPIRES].

[23] C.F. Berger and L. Magnea, *Scaling of power corrections for angularities from dressed gluon exponentiation*, *Phys. Rev.* **D 70** (2004) 094010 [hep-ph/0407024] [SPIRES].

[24] L3 collaboration, *The construction of the L3 experiment*, *Nucl. Instrum. Meth.* **A 289** (1990) 35 [SPIRES].

[25] M. Chemarin et al., *Test beam results for an upgraded forward tagger of the L3 Experiment at LEP-2*, *Nucl. Instrum. Meth.* **A 349** (1994) 345 [SPIRES].

[26] I.C. Brock et al., *Luminosity measurement in the L3 detector at LEP*, *Nucl. Instrum. Meth.* **A 381** (1996) 236 [SPIRES].

[27] H. Anderhub et al., *Experience with the L3 vertex drift chamber at LEP*, *Nucl. Instrum. Meth.* **A 515** (2003) 31 [SPIRES].

[28] L3 collaboration, P. Achard et al., *Studies of hadronic event structure in e^+e^- annihilation from 30-GeV to 209-GeV with the L3 detector*, *Phys. Rept.* **399** (2004) 71 [hep-ex/0406049] [SPIRES].

[29] T. Sjöstrand, *High-energy physics event generation with PYTHIA 5.7 and JETSET 7.4*, *Comput. Phys. Commun.* **82** (1994) 74 [SPIRES].

[30] Pythia, Pythia 5.7 Monte Carlo Program. QCD parton shower and fragmentation process are taken from Jetset 7.4.

[31] T. Sjöstrand, *Pythia 5.7 and jetset 7.4 physics and manual*, CERN-TH-7112/93 (1993).

[32] T. Sjöstrand, *High-energy physics event generation with PYTHIA 5.7 and JETSET 7.4*, *Comput. Phys. Commun.* **82** (1994) 74 [SPIRES].

[33] S. Jadach, B.F.L. Ward and Z. Wąs, KK2f *4.14 Monte Carlo Program*, *Comp. Phys. Comm.* **130** (2000) 260.

[34] S. Jadach, B.F.L. Ward and Z. Was, *Coherent exclusive exponentiation for precision Monte Carlo calculations*, *Phys. Rev.* **D 63** (2001) 113009 [hep-ph/0006359] [SPIRES].

[35] R. Brun et al., *GEANT 3*, CERN DD/EE/84-1 (1983);

[36] H. Fesefeldt, *The GHEISHA program*, RWTH Aachen Report PITHA 85/02 (1985).

[37] R. Engel, Phojet *Monte Carlo Program*, *Z. Phys.* **C 66** (1995) 1459.

JHEP10(2011)143

[38] R. Engel, J. Ranft and S. Roesler, *Hard diffraction in hadron hadron interactions and in photoproduction*, *Phys. Rev.* **D 52** (1995) 1459 [hep-ph/9502319] [SPIRES].

[39] S. Jadach, B. F. L. Ward and Z. Wąs, KoralZ *Monte Carlo Program*, *Comp. Phys. Comm.* **79** (1994) 503.

[40] J.H. Field, *New calculations of cross-sections and charge asymmetries for lepton pair production and wide angle Bhabha scattering in e^+e^- collisions near the Z peak*, *Phys. Lett.* **B 323** (1994) 432 [SPIRES].

[41] J.H. Field and T. Riemann, *BHAGENE3, a Monte Carlo event generator for lepton pair production and wide-angle Bhabha scattering in e+e- collisions near the Z peak*, *Comp. Phys. Comm.* **94** (1996) 53

[42] M. Skrzypek et al., *Monte Carlo program KORALW 1.02 for W-pair production at LEP2/NLC energies with Yennie-Frautschi-Suura exponentiation*, *Comp. Phys. Comm.* **94** (1996) 216.

[43] M. Skrzypek, S. Jadach, M. Martinez, W. Placzek and Z. Was, *Initial state QED corrections to W pair production at LEP- 2/NLC: Monte Carlo versus semianalytical approach*, *Phys. Lett.* **B 372** (1996) 289 [SPIRES].

[44] Yu.L. Dokshitzer, talk at the *Workshop on Jets* at LEP and HERA (1990).

[45] N. Brown and W.J. Stirling, *Rutherford Preprint*, RAL-91-049 (1991).

[46] S. Catani, Y.L. Dokshitzer, M. Olsson, G. Turnock and B.R. Webber, *New clustering algorithm for multi-jet cross-sections in e^+e^- annihilation*, *Phys. Lett.* **B 269** (1991) 432 [SPIRES].

[47] S. Bethke, Z. Kunszt, D.E. Soper and W.J. Stirling, *New jet cluster algorithms: Next-to-leading order QCD and hadronization corrections*, *Nucl. Phys.* **B 370** (1992) 310 [SPIRES].

[48] L3 collaboration, M. Acciarri et al., *Search for the standard model Higgs boson in e^+e^- interactions at* $161\,GeV \leq \sqrt{s} \leq 172\,GeV$, *Phys. Lett.* **B 411** (1997) 373 [SPIRES].

[49] G. Marchesini and B.R. Webber, *Monte Carlo simulation of general hard processes with coherent QCD radiation*, *Nucl. Phys.* **B 310** (1988) 461 [SPIRES].

[50] I.G. Knowles, *Spin correlations in parton-parton scattering*, *Nucl. Phys.* **B 310** (1988) 571 [SPIRES].

[51] G. Marchesini et al., *HERWIG 5.1 - a Monte Carlo event generator for simulating hadron emission reactions with interfering gluons*, *Comp. Phys. Comm.* **67** (1992) 465.

[52] L. Lönnblad, *ARIADNE version 4: A Program for simulation of QCD cascades implementing the color dipole model*, *Comput. Phys. Commun.* **71** (1992) 15 [SPIRES].

[53] C.F. Berger, private communication.

JHEP10(2011)143

$\sqrt{s}$ (GeV)	Integrated Luminosity (pb^{-1})	All events			udsc events		
		Efficiency (%)	Purity (%)	# events	Efficiency (%)	Purity (%)	# events
91.2	48.0	97.69±0.15	99.24±0.01	1420489	38.84±0.10	90.41±0.07	492555
188.6	175.1	87.72±0.62	80.92±0.25	4473	74.14±0.67	73.26±0.66	2179
191.6	29.4	87.77±0.62	80.11±0.26	720	76.24±0.68	74.83±0.67	363
195.5	83.4	88.42±0.63	78.60±0.27	1884	75.85±0.67	75.70±0.67	977
199.5	81.2	88.51±0.62	77.54±0.25	1835	76.56±0.67	73.22±0.64	927
201.7	36.5	89.02±0.63	76.98±0.25	817	75.68±0.67	71.80±0.63	403
205.1	70.5	88.78±0.64	75.57±0.22	1496	76.08±0.68	72.89±0.66	738
206.5	126.2	88.97±0.63	75.18±0.22	2688	76.25±0.68	69.67±0.62	1308

Table 1. Summary of integrated luminosity, selection efficiency, purity and yield at different centre-of-mass energies.

$\sqrt{s}$ (GeV)		Value of the parameter a							
		−1.0	−0.75	−0.50	−0.25	0.0	0.25	0.50	0.75
91.2	Detector	1.3	1.4	1.5	1.6	1.8	1.9	2.1	2.1
	Frag. Model	3.0	3.2	3.3	3.6	3.4	3.0	2.1	3.3
	Background	1.4	1.3	1.2	1.0	1.2	1.2	1.2	1.0
	Wrong Flavour	1.0	1.0	1.0	1.0	1.0	0.9	0.9	0.9
	Total	4.1	4.1	4.3	4.5	4.5	4.1	3.8	4.4
197.0	Detector	2.1	2.1	2.2	3.1	4.1	3.3	4.7	3.9
	Frag. Model	1.4	1.2	1.0	0.9	0.8	1.1	1.1	0.7
	Background	1.8	2.0	2.1	2.3	2.5	2.7	3.3	3.1
	Wrong Flavour	2.8	2.7	3.3	2.4	2.3	2.5	2.6	2.1
	Total	4.9	4.4	5.1	4.5	5.7	5.3	6.4	5.5

Table 2. Percentage bin-averaged systematic uncertainties due to different sources for the event shape τ_a distributions at the two centre-of-mass energies.

JHEP10(2011)143

$\sqrt{s}$ (GeV)	δ		Value of the parameter ν			
			10	25	35	50
91.2	30°	Detector	1.3	1.5	1.6	1.7
		Frag. Model	1.1	1.3	1.4	1.6
		Background	1.5	1.6	1.6	1.7
		Total	2.5	2.7	2.9	3.2
	45°	Detector	1.1	1.3	1.5	1.7
		Frag. Model	2.6	2.6	2.6	2.6
		Background	1.1	1.2	1.2	1.3
		Total	3.2	3.4	3.6	3.8
	60°	Detector	1.0	1.5	1.7	2.1
		Frag. Model	2.4	2.3	2.2	2.0
		Background	1.2	1.3	1.3	1.5
		Total	3.0	3.2	3.4	3.7
	75°	Detector	1.0	1.5	1.7	2.1
		Frag. Model	1.6	1.2	0.9	1.2
		Background	0.9	1.1	1.2	1.5
		Total	2.1	2.3	2.6	3.1
197.0	30°	Detector	2.1	2.1	2.1	2.2
		Frag. Model	1.5	1.5	1.5	1.5
		Background	2.8	2.8	2.9	2.9
		Total	4.1	4.2	4.3	4.4
	45°	Detector	1.5	1.5	1.5	1.6
		Frag. Model	1.2	0.9	0.8	0.8
		Background	2.9	3.0	3.2	3.3
		Total	3.8	3.8	4.0	4.1
	60°	Detector	2.0	2.1	2.1	2.3
		Frag. Model	1.8	1.7	1.6	1.5
		Background	2.7	2.9	3.0	3.2
		Total	4.1	4.2	4.3	4.5
	75°	Detector	1.6	1.7	1.9	2.1
		Frag. Model	1.9	1.8	1.8	1.7
		Background	2.1	2.4	2.5	2.8
		Total	3.6	3.7	3.9	4.2

Table 3. Percentage bin-averaged systematic uncertainties due to different sources for the energy flow correlation for $a = 0.0$.

JHEP10(2011)143

$\sqrt{s}$ = 91.2 GeV		$\langle\sqrt{s}\rangle$ = 197.0 GeV	
τ_a	$(1/\sigma)\cdot(\mathrm{d}\sigma/\mathrm{d}\tau_a)$	τ_a	$(1/\sigma)\cdot(\mathrm{d}\sigma/\mathrm{d}\tau_a)$
0.0000–0.0100	19.319±0.074±0.661	0.0000–0.0076	31.686±1.515±1.304
0.0100–0.0200	30.001±0.099±1.498	0.0076–0.0152	29.809±1.302±1.349
0.0200–0.0300	15.606±0.070±0.416	0.0152–0.0228	15.306±0.851±0.607
0.0300–0.0400	8.923±0.053±0.365	0.0228–0.0304	9.504±0.684±0.368
0.0400–0.0500	5.911±0.045±0.155	0.0304–0.0380	6.892±0.587±0.702
0.0500–0.0600	4.272±0.039±0.161	0.0380–0.0456	6.036±0.541±0.175
0.0600–0.0700	3.294±0.034±0.063	0.0456–0.0532	4.274±0.481±0.377
0.0700–0.0800	2.509±0.030±0.073	0.0532–0.0608	3.273±0.443±0.382
0.0800–0.0900	1.856±0.026±0.069	0.0608–0.0684	2.717±0.431±0.448
0.0900–0.1000	1.653±0.025±0.051	0.0684–0.0760	1.725±0.347±0.422
0.1000–0.1100	1.324±0.023±0.052	0.0760–0.0836	2.841±0.444±0.319
0.1100–0.1200	1.097±0.021±0.050	0.0836–0.0912	2.311±0.460±0.475
0.1200–0.1300	0.954±0.020±0.055	0.0912–0.0988	1.570±0.418±0.387
0.1300–0.1400	0.752±0.017±0.034	0.0988–0.1064	2.415±0.518±0.829
0.1400–0.1500	0.633±0.016±0.045	0.1064–0.1140	0.968±0.371±0.340
0.1500–0.1600	0.535±0.015±0.060	0.1140–0.1216	1.355±0.454±0.197
0.1600–0.1700	0.391±0.013±0.051	0.1216–0.1292	1.285±0.436±0.368
0.1700–0.1800	0.335±0.011±0.050	0.1292–0.1368	1.599±0.493±0.701
0.1800–0.1900	0.210±0.009±0.041	0.1368–0.1444	2.035±0.609±0.753
0.1900–0.2000	0.150±0.009±0.039	0.1444–0.1520	0.927±0.409±0.276
0.2000–0.2100	0.112±0.007±0.029	0.1520–0.1596	0.000±0.085±0.000
0.2100–0.2200	0.070±0.006±0.026	0.1596–0.1672	0.776±0.346±0.393
0.2200–0.2300	0.047±0.005±0.022	0.1672–0.1748	1.276±0.429±0.439
0.2300–0.2400	0.018±0.003±0.008	0.1748–0.1824	0.725±0.511±0.430
0.2400–0.2500	0.027±0.006±0.011	0.1824–0.1900	0.276±0.272±0.238
First Moment	0.0338±0.0001±0.0008		0.0350±0.0014±0.0018
Second Moment	0.0024±0.0001±0.0001		0.0029±0.0002±0.0003

Table 4. Differential distribution for event shape τ_a at $\sqrt{s} = 91.2$ GeV and $\langle\sqrt{s}\rangle = 197.0$ GeV for $a = -1.0$. Some of these data points are compared with theoretical predictions in figures 5 and 7. The first uncertainty is statistical and the second is systematic.

JHEP10(2011)143

$\sqrt{s}$ = 91.2 GeV		$\langle\sqrt{s}\rangle$ = 197.0 GeV	
τ_a	$(1/\sigma)\cdot(\mathrm{d}\sigma/\mathrm{d}\tau_a)$	τ_a	$(1/\sigma)\cdot(\mathrm{d}\sigma/\mathrm{d}\tau_a)$
0.0000–0.0112	15.377±0.061±0.647	0.0000–0.0088	26.502±1.289±1.077
0.0112–0.0224	27.150±0.089±1.388	0.0088–0.0176	25.133±1.122±0.895
0.0224–0.0336	14.369±0.064±0.361	0.0176–0.0264	13.305±0.729±0.566
0.0336–0.0448	8.226±0.049±0.308	0.0264–0.0352	9.042±0.613±0.259
0.0448–0.0560	5.511±0.041±0.140	0.0352–0.0440	6.396±0.518±0.470
0.0560–0.0672	4.001±0.035±0.115	0.0440–0.0528	4.782±0.452±0.251
0.0672–0.0784	2.984±0.032±0.100	0.0528–0.0616	3.950±0.427±0.209
0.0784–0.0896	2.349±0.027±0.066	0.0616–0.0704	2.994±0.388±0.284
0.0896–0.1008	1.758±0.024±0.049	0.0704–0.0792	2.319±0.363±0.281
0.1008–0.1120	1.465±0.022±0.048	0.0792–0.0880	1.834±0.340±0.350
0.1120–0.1232	1.242±0.021±0.038	0.0880–0.0968	2.275±0.385±0.282
0.1232–0.1344	1.028±0.019±0.034	0.0968–0.1056	1.719±0.371±0.555
0.1344–0.1456	0.832±0.017±0.032	0.1056–0.1144	2.103±0.440±0.421
0.1456–0.1568	0.707±0.016±0.029	0.1144–0.1232	1.356±0.398±0.506
0.1568–0.1680	0.543±0.014±0.036	0.1232–0.1320	0.797±0.368±0.421
0.1680–0.1792	0.494±0.013±0.049	0.1320–0.1408	0.987±0.362±0.285
0.1792–0.1904	0.379±0.012±0.039	0.1408–0.1496	1.389±0.397±0.343
0.1904–0.2016	0.292±0.009±0.048	0.1496–0.1584	1.519±0.563±0.351
0.2016–0.2128	0.201±0.009±0.035	0.1584–0.1672	1.534±0.507±0.399
0.2128–0.2240	0.141±0.008±0.036	0.1672–0.1760	0.259±0.303±0.368
0.2240–0.2352	0.114±0.007±0.027	0.1760–0.1848	0.221±0.212±0.226
0.2352–0.2464	0.058±0.005±0.023	0.1848–0.1936	1.264±0.520±0.752
0.2464–0.2576	0.035±0.004±0.011	0.1936–0.2024	0.650±0.276±0.157
0.2576–0.2688	0.025±0.003±0.007	0.2024–0.2112	0.763±0.445±0.475
0.2688–0.2800	0.007±0.002±0.003	0.2112–0.2200	0.544±0.264±0.177
First Moment	0.0388±0.0001±0.0009		0.0412±0.0017±0.0019
Second Moment	0.0031±0.0001±0.0002		0.0040±0.0003±0.0004

Table 5. Differential distribution for event shape τ_a at $\sqrt{s} = 91.2$ GeV and $\langle\sqrt{s}\rangle = 197.0$ GeV for $a = -0.75$. Some of these data points are compared with theoretical predictions in figures 5 and 7. The first uncertainty is statistical and the second is systematic.

JHEP10(2011)143

$\sqrt{s}$ = 91.2 GeV		$\langle\sqrt{s}\rangle$ = 197.0 GeV	
τ_a	$(1/\sigma)\cdot(\mathrm{d}\sigma/\mathrm{d}\tau_a)$	τ_a	$(1/\sigma)\cdot(\mathrm{d}\sigma/\mathrm{d}\tau_a)$
0.0000–0.0128	11.755±0.049±0.638	0.0000–0.0100	21.363±1.083±0.886
0.0128–0.0256	24.076±0.078±1.273	0.0100–0.0200	22.582±1.013±1.008
0.0256–0.0384	12.958±0.056±0.285	0.0200–0.0300	11.901±0.659±0.395
0.0384–0.0512	7.486±0.044±0.281	0.0300–0.0400	8.106±0.535±0.620
0.0512–0.0640	5.040±0.037±0.112	0.0400–0.0500	6.076±0.476±0.188
0.0640–0.0768	3.675±0.032±0.107	0.0500–0.0600	4.536±0.406±0.364
0.0768–0.0896	2.691±0.028±0.091	0.0600–0.0700	3.724±0.385±0.266
0.0896–0.1024	2.123±0.024±0.078	0.0700–0.0800	2.718±0.346±0.362
0.1024–0.1152	1.620±0.022±0.023	0.0800–0.0900	2.105±0.316±0.246
0.1152–0.1280	1.324±0.020±0.049	0.0900–0.1000	1.679±0.305±0.503
0.1280–0.1408	1.106±0.018±0.037	0.1000–0.1100	2.163±0.351±0.359
0.1408–0.1536	0.910±0.017±0.026	0.1100–0.1200	1.432±0.299±0.410
0.1536–0.1664	0.765±0.015±0.029	0.1200–0.1300	1.624±0.368±0.294
0.1664–0.1792	0.616±0.014±0.030	0.1300–0.1400	1.794±0.400±0.330
0.1792–0.1920	0.487±0.012±0.034	0.1400–0.1500	0.789±0.320±0.301
0.1920–0.2048	0.398±0.011±0.031	0.1500–0.1600	0.844±0.313±0.373
0.2048–0.2176	0.361±0.010±0.046	0.1600–0.1700	0.848±0.317±0.268
0.2176–0.2304	0.249±0.008±0.044	0.1700–0.1800	1.519±0.477±0.381
0.2304–0.2432	0.168±0.007±0.033	0.1800–0.1900	0.573±0.402±0.397
0.2432–0.2560	0.131±0.007±0.030	0.1900–0.2000	0.690±0.302±0.157
0.2560–0.2688	0.100±0.006±0.023	0.2000–0.2100	0.182±0.230±0.263
0.2688–0.2816	0.043±0.004±0.020	0.2100–0.2200	1.021±0.482±0.525
0.2816–0.2944	0.024±0.003±0.007	0.2200–0.2300	0.422±0.240±0.234
0.2944–0.3072	0.016±0.003±0.009	0.2300–0.2400	0.744±0.349±0.322
0.3072–0.3200	0.004±0.002±0.002	0.2400–0.2500	0.565±0.307±0.162
First Moment	0.0453±0.0001±0.0010		0.0473±0.0019±0.0023
Second Moment	0.0041±0.0001±0.0002		0.0051±0.0004±0.0005

Table 6. Differential distribution for event shape τ_a at $\sqrt{s} = 91.2$ GeV and $\langle\sqrt{s}\rangle = 197.0$ GeV for $a = -0.5$. Some of these data points are compared with theoretical predictions in figures 5 and 7. The first uncertainty is statistical and the second is systematic.

JHEP10(2011)143

$\sqrt{s}$ = 91.2 GeV		$\langle\sqrt{s}\rangle$ = 197.0 GeV	
τ_a	$(1/\sigma)\cdot(\mathrm{d}\sigma/\mathrm{d}\tau_a)$	τ_a	$(1/\sigma)\cdot(\mathrm{d}\sigma/\mathrm{d}\tau_a)$
0.0000–0.0140	7.569±0.036±0.706	0.0000–0.0116	16.247±0.879±0.653
0.0140–0.0280	21.504±0.070±1.232	0.0116–0.0232	19.985±0.898±0.837
0.0280–0.0420	12.626±0.053±0.186	0.0232–0.0348	10.633±0.594±0.303
0.0420–0.0560	7.543±0.042±0.270	0.0348–0.0464	7.272±0.467±0.308
0.0560–0.0700	5.039±0.035±0.095	0.0464–0.0580	5.966±0.432±0.216
0.0700–0.0840	3.636±0.031±0.140	0.0580–0.0696	3.668±0.340±0.291
0.0840–0.0980	2.759±0.026±0.056	0.0696–0.0812	3.722±0.361±0.237
0.0980–0.1120	2.103±0.024±0.104	0.0812–0.0928	2.414±0.297±0.201
0.1120–0.1260	1.649±0.021±0.047	0.0928–0.1044	1.735±0.271±0.092
0.1260–0.1400	1.364±0.019±0.023	0.1044–0.1160	2.130±0.295±0.214
0.1400–0.1540	1.081±0.017±0.043	0.1160–0.1276	1.791±0.308±0.140
0.1540–0.1680	0.954±0.016±0.018	0.1276–0.1392	1.120±0.269±0.212
0.1680–0.1820	0.739±0.014±0.023	0.1392–0.1508	1.307±0.319±0.228
0.1820–0.1960	0.648±0.014±0.030	0.1508–0.1624	1.225±0.303±0.212
0.1960–0.2100	0.506±0.012±0.031	0.1624–0.1740	0.901±0.307±0.288
0.2100–0.2240	0.418±0.011±0.024	0.1740–0.1856	0.922±0.317±0.270
0.2240–0.2380	0.369±0.010±0.031	0.1856–0.1972	0.553±0.285±0.413
0.2380–0.2520	0.300±0.009±0.036	0.1972–0.2088	0.799±0.350±0.351
0.2520–0.2660	0.200±0.007±0.041	0.2088–0.2204	1.196±0.438±0.347
0.2660–0.2800	0.160±0.007±0.034	0.2204–0.2320	0.237±0.190±0.088
0.2800–0.2940	0.115±0.006±0.023	0.2320–0.2436	0.290±0.237±0.268
0.2940–0.3080	0.076±0.005±0.019	0.2436–0.2552	0.514±0.381±0.258
0.3080–0.3220	0.030±0.003±0.014	0.2552–0.2668	0.567±0.249±0.442
0.3220–0.3360	0.034±0.005±0.014	0.2668–0.2784	0.363±0.267±0.396
0.3360–0.3500	0.007±0.002±0.006	0.2784–0.2900	0.651±0.348±0.306
First Moment	0.0540±0.0001±0.0011		0.0552±0.0023±0.0022
Second Moment	0.0056±0.0001±0.0003		0.0068±0.0006±0.0005

Table 7. Differential distribution for event shape τ_a at $\sqrt{s} = 91.2$ GeV and $\langle\sqrt{s}\rangle = 197.0$ GeV for $a = -0.25$. Some of these data points are compared with theoretical predictions in figures 5 and 7. The first uncertainty is statistical and the second is systematic.

JHEP10(2011)143

$\sqrt{s}$ = 91.2 GeV		$\langle\sqrt{s}\rangle$ = 197.0 GeV	
τ_a	$(1/\sigma)\cdot(\mathrm{d}\sigma/\mathrm{d}\tau_a)$	τ_a	$(1/\sigma)\cdot(\mathrm{d}\sigma/\mathrm{d}\tau_a)$
0.0000–0.0160	4.263±0.024±0.684	0.0000–0.0136	11.298±0.670±0.440
0.0160–0.0320	18.067±0.059±1.029	0.0136–0.0272	16.603±0.786±0.560
0.0320–0.0480	11.735±0.048±0.132	0.0272–0.0408	10.044±0.531±0.383
0.0480–0.0640	7.183±0.038±0.210	0.0408–0.0544	6.401±0.406±0.404
0.0640–0.0800	4.800±0.032±0.088	0.0544–0.0680	5.660±0.381±0.263
0.0800–0.0960	3.503±0.028±0.095	0.0680–0.0816	3.243±0.300±0.376
0.0960–0.1120	2.630±0.025±0.044	0.0816–0.0952	3.328±0.301±0.365
0.1120–0.1280	2.074±0.022±0.064	0.0952–0.1088	2.315±0.275±0.355
0.1280–0.1440	1.544±0.019±0.081	0.1088–0.1224	1.664±0.240±0.172
0.1440–0.1600	1.287±0.018±0.035	0.1224–0.1360	1.803±0.253±0.264
0.1600–0.1760	1.104±0.016±0.035	0.1360–0.1496	1.593±0.253±0.399
0.1760–0.1920	0.829±0.014±0.041	0.1496–0.1632	1.371±0.267±0.225
0.1920–0.2080	0.751±0.014±0.015	0.1632–0.1768	0.877±0.243±0.229
0.2080–0.2240	0.604±0.013±0.023	0.1768–0.1904	0.841±0.245±0.215
0.2240–0.2400	0.496±0.011±0.023	0.1904–0.2040	1.306±0.277±0.550
0.2400–0.2560	0.402±0.010±0.029	0.2040–0.2176	0.791±0.250±0.418
0.2560–0.2720	0.312±0.009±0.029	0.2176–0.2312	0.314±0.255±0.497
0.2720–0.2880	0.318±0.009±0.042	0.2312–0.2448	0.667±0.319±0.218
0.2880–0.3040	0.202±0.007±0.030	0.2448–0.2584	0.838±0.327±0.218
0.3040–0.3200	0.144±0.006±0.032	0.2584–0.2720	0.202±0.167±0.090
0.3200–0.3360	0.121±0.005±0.025	0.2720–0.2856	0.658±0.304±0.253
0.3360–0.3520	0.066±0.004±0.015	0.2856–0.2992	0.554±0.272±0.328
0.3520–0.3680	0.031±0.003±0.011	0.2992–0.3128	0.162±0.183±0.156
0.3680–0.3840	0.027±0.004±0.014	0.3128–0.3264	0.705±0.314±0.202
0.3840–0.4000	0.009±0.002±0.005	0.3264–0.3400	0.293±0.225±0.154
First Moment	0.0659±0.0001±0.0011		0.0678±0.0026±0.0029
Second Moment	0.0080±0.0001±0.0003		0.0098±0.0008±0.0009

Table 8. Differential distribution for event shape τ_a at $\sqrt{s} = 91.2$ GeV and $\langle\sqrt{s}\rangle = 197.0$ GeV for $a = 0.0$. Some of these data points are compared with theoretical predictions in figures 6 and 8. The first uncertainty is statistical and the second is systematic.

JHEP10(2011)143

$\sqrt{s}$ = 91.2 GeV		$\langle\sqrt{s}\rangle$ = 197.0 GeV	
τ_a	$(1/\sigma)\cdot(\mathrm{d}\sigma/\mathrm{d}\tau_a)$	τ_a	$(1/\sigma)\cdot(\mathrm{d}\sigma/\mathrm{d}\tau_a)$
0.0000–0.0180	1.521±0.012±0.521	0.0000–0.0152	6.025±0.444±0.426
0.0180–0.0360	13.544±0.047±0.646	0.0152–0.0304	14.911±0.736±0.617
0.0360–0.0540	11.383±0.045±0.215	0.0304–0.0456	9.359±0.504±0.162
0.0540–0.0720	7.177±0.036±0.126	0.0456–0.0608	6.187±0.384±0.541
0.0720–0.0900	4.886±0.031±0.121	0.0608–0.0760	5.057±0.340±0.246
0.0900–0.1080	3.588±0.027±0.071	0.0760–0.0912	3.991±0.299±0.218
0.1080–0.1260	2.653±0.023±0.089	0.0912–0.1064	2.710±0.261±0.180
0.1260–0.1440	2.149±0.021±0.039	0.1064–0.1216	2.731±0.261±0.248
0.1440–0.1620	1.673±0.019±0.051	0.1216–0.1368	1.961±0.233±0.187
0.1620–0.1800	1.279±0.016±0.069	0.1368–0.1520	1.323±0.206±0.204
0.1800–0.1980	1.113±0.016±0.025	0.1520–0.1672	1.355±0.207±0.169
0.1980–0.2160	0.918±0.014±0.034	0.1672–0.1824	1.549±0.245±0.294
0.2160–0.2340	0.712±0.012±0.030	0.1824–0.1976	1.215±0.234±0.200
0.2340–0.2520	0.631±0.012±0.026	0.1976–0.2128	1.043±0.245±0.243
0.2520–0.2700	0.513±0.011±0.022	0.2128–0.2280	0.491±0.191±0.179
0.2700–0.2880	0.440±0.010±0.022	0.2280–0.2432	1.160±0.257±0.364
0.2880–0.3060	0.349±0.009±0.024	0.2432–0.2584	0.754±0.247±0.226
0.3060–0.3240	0.279±0.008±0.027	0.2584–0.2736	0.520±0.218±0.226
0.3240–0.3420	0.263±0.008±0.034	0.2736–0.2888	0.572±0.261±0.204
0.3420–0.3600	0.170±0.006±0.030	0.2888–0.3040	0.894±0.274±0.186
0.3600–0.3780	0.128±0.005±0.027	0.3040–0.3192	0.219±0.134±0.094
0.3780–0.3960	0.086±0.004±0.018	0.3192–0.3344	0.464±0.250±0.214
0.3960–0.4140	0.048±0.003±0.014	0.3344–0.3496	0.176±0.200±0.153
0.4140–0.4320	0.025±0.003±0.017	0.3496–0.3648	0.347±0.217±0.137
0.4320–0.4500	0.028±0.005±0.012	0.3648–0.3800	0.779±0.341±0.356
First Moment	0.0828±0.0001±0.0012		0.0841±0.0030±0.0040
Second Moment	0.0119±0.0001±0.0004		0.0140±0.0011±0.0016

Table 9. Differential distribution for event shape τ_a at $\sqrt{s} = 91.2$ GeV and $\langle\sqrt{s}\rangle = 197.0$ GeV for $a = 0.25$. Some of these data points are compared with theoretical predictions in figures 6 and 8. The first uncertainty is statistical and the second is systematic.

JHEP10(2011)143

$\sqrt{s}$ = 91.2 GeV		$\langle\sqrt{s}\rangle$ = 197.0 GeV	
τ_a	$(1/\sigma)\cdot(\mathrm{d}\sigma/\mathrm{d}\tau_a)$	τ_a	$(1/\sigma)\cdot(\mathrm{d}\sigma/\mathrm{d}\tau_a)$
0.0000–0.0216	0.392±0.005±0.177	0.0000–0.0176	1.986±0.222±0.268
0.0216–0.0432	8.134±0.031±0.361	0.0176–0.0352	11.976±0.639±0.654
0.0432–0.0648	10.226±0.040±0.371	0.0352–0.0528	8.037±0.465±0.392
0.0648–0.0864	6.697±0.032±0.122	0.0528–0.0704	6.339±0.376±0.325
0.0864–0.1080	4.703±0.027±0.072	0.0704–0.0880	5.069±0.319±0.336
0.1080–0.1296	3.390±0.024±0.120	0.0880–0.1056	3.489±0.268±0.311
0.1296–0.1512	2.584±0.021±0.064	0.1056–0.1232	3.239±0.248±0.162
0.1512–0.1728	2.074±0.019±0.042	0.1232–0.1408	2.430±0.227±0.105
0.1728–0.1944	1.622±0.017±0.035	0.1408–0.1584	2.182±0.221±0.204
0.1944–0.2160	1.272±0.019±0.054	0.1584–0.1760	1.646±0.200±0.146
0.2160–0.2376	0.995±0.013±0.041	0.1760–0.1936	1.382±0.196±0.145
0.2376–0.2592	0.900±0.013±0.026	0.1936–0.2112	1.087±0.182±0.109
0.2592–0.2808	0.703±0.011±0.028	0.2112–0.2288	1.250±0.199±0.148
0.2808–0.3024	0.569±0.010±0.036	0.2288–0.2464	1.092±0.213±0.086
0.3024–0.3240	0.474±0.009±0.016	0.2464–0.2640	0.900±0.210±0.205
0.3240–0.3456	0.408±0.009±0.016	0.2640–0.2816	0.643±0.185±0.201
0.3456–0.3672	0.326±0.008±0.020	0.2816–0.2992	1.061±0.242±0.253
0.3672–0.3888	0.251±0.007±0.028	0.2992–0.3168	0.595±0.195±0.119
0.3888–0.4104	0.216±0.006±0.027	0.3168–0.3344	0.322±0.181±0.213
0.4104–0.4320	0.153±0.005±0.026	0.3344–0.3520	0.389±0.193±0.219
0.4320–0.4536	0.090±0.004±0.023	0.3520–0.3696	0.666±0.254±0.183
0.4536–0.4752	0.059±0.003±0.016	0.3696–0.3872	0.201±0.158±0.116
0.4752–0.4968	0.031±0.002±0.013	0.3872–0.4048	0.221±0.255±0.158
0.4968–0.5184	0.015±0.002±0.005	0.4048–0.4224	0.346±0.199±0.166
0.5184–0.5400	0.015±0.003±0.007	0.4224–0.4400	0.272±0.177±0.295
First Moment	0.1078±0.0002±0.0015		0.1042±0.0033±0.0060
Second Moment	0.0187±0.0001±0.0006		0.0193±0.0013±0.0025

Table 10. Differential distribution for event shape τ_a at $\sqrt{s} = 91.2$ GeV and $\langle\sqrt{s}\rangle = 197.0$ GeV for $a = 0.5$. Some of these data points are compared with theoretical predictions in figures 6 and 8. The first uncertainty is statistical and the second is systematic.

JHEP10(2011)143

$\sqrt{s}$ = 91.2 GeV		$\langle\sqrt{s}\rangle$ = 197.0 GeV	
τ_a	$(1/\sigma)\cdot(\mathrm{d}\sigma/\mathrm{d}\tau_a)$	τ_a	$(1/\sigma)\cdot(\mathrm{d}\sigma/\mathrm{d}\tau_a)$
0.0000–0.0256	0.068±0.002±0.025	0.0000–0.0208	0.528±0.101±0.201
0.0256–0.0512	2.447±0.013±0.522	0.0208–0.0416	6.395±0.430±0.346
0.0512–0.0768	8.014±0.030±0.405	0.0416–0.0624	7.320±0.439±0.265
0.0768–0.1024	6.694±0.029±0.118	0.0624–0.0832	5.717±0.356±0.271
0.1024–0.1280	4.830±0.025±0.061	0.0832–0.1040	4.097±0.277±0.178
0.1280–0.1536	3.564±0.022±0.068	0.1040–0.1248	4.294±0.270±0.315
0.1536–0.1792	2.719±0.020±0.080	0.1248–0.1456	2.864±0.220±0.176
0.1792–0.2048	2.153±0.018±0.068	0.1456–0.1664	2.643±0.208±0.192
0.2048–0.2304	1.735±0.016±0.051	0.1664–0.1872	2.026±0.183±0.102
0.2304–0.2560	1.402±0.014±0.035	0.1872–0.2080	1.902±0.195±0.162
0.2560–0.2816	1.107±0.013±0.049	0.2080–0.2288	1.421±0.171±0.168
0.2816–0.3072	0.883±0.012±0.025	0.2288–0.2496	1.394±0.174±0.041
0.3072–0.3328	0.749±0.010±0.024	0.2496–0.2704	0.871±0.148±0.131
0.3328–0.3584	0.618±0.010±0.028	0.2704–0.2912	0.945±0.168±0.170
0.3584–0.3840	0.501±0.009±0.028	0.2912–0.3120	0.938±0.166±0.046
0.3840–0.4096	0.399±0.008±0.011	0.3120–0.3328	0.903±0.194±0.087
0.4096–0.4352	0.357±0.008±0.012	0.3328–0.3536	0.576±0.173±0.268
0.4352–0.4608	0.269±0.006±0.021	0.3536–0.3744	0.926±0.198±0.162
0.4608–0.4864	0.200±0.006±0.022	0.3744–0.3952	0.573±0.190±0.208
0.4864–0.5120	0.162±0.005±0.020	0.3952–0.4160	0.247±0.130±0.150
0.5120–0.5376	0.092±0.004±0.022	0.4160–0.4368	0.650±0.211±0.180
0.5376–0.5632	0.046±0.002±0.014	0.4368–0.4576	0.136±0.157±0.167
0.5632–0.5888	0.031±0.002±0.011	0.4576–0.4784	0.405±0.196±0.305
0.5888–0.6144	0.011±0.001±0.006	0.4784–0.4992	0.192±0.094±0.189
0.6144–0.6400	0.014±0.002±0.007	0.4992–0.5200	0.115±0.091±0.084
First Moment	0.1474±0.0002±0.0016		0.1384±0.0034±0.0047
Second Moment	0.0319±0.0001±0.0008		0.0310±0.0016±0.0023

Table 11. Differential distribution for event shape τ_a at $\sqrt{s} = 91.2$ GeV and $\langle\sqrt{s}\rangle = 197.0$ GeV for $a = 0.75$. Some of these data points are compared with theoretical predictions in figures 6 and 8. The first uncertainty is statistical and the second is systematic.

JHEP10(2011)143

a-value	Jetset		Herwig		Ariadne	
	χ^2/d.o.f.	C.L.	χ^2/d.o.f.	C.L.	χ^2/d.o.f.	C.L.
-1.00	34.2/25	0.104	54.9/25	0.0005	32.0/25	0.158
-0.75	25.3/25	0.446	45.8/25	0.007	27.2/25	0.346
-0.50	17.4/25	0.867	39.2/25	0.035	21.1/25	0.687
-0.25	16.6/25	0.896	35.7/25	0.076	21.9/25	0.642
0.0	11.7/25	0.989	38.2/25	0.044	23.2/25	0.566
0.25	10.2/25	0.996	37.3/25	0.054	20.5/25	0.720
0.50	13.7/25	0.967	37.3/25	0.054	22.9/25	0.583
0.75	19.1/25	0.792	34.0/25	0.108	30.9/25	0.192

Table 12. Goodness of agreement between data and different parton shower models in terms of χ^2 per degree of freedom and confidence level at $\sqrt{s} = 91.2$ GeV.

a-value	Jetset		Herwig		Ariadne	
	χ^2/d.o.f.	C.L.	χ^2/d.o.f.	C.L.	χ^2/d.o.f.	C.L.
-1.00	61.8/25	0.0001	60.2/25	0.0001	49.7/25	0.002
-0.75	39.3/25	0.034	30.3/25	0.213	27.0/25	0.356
-0.50	34.4/25	0.100	28.4/25	0.290	24.8/25	0.474
-0.25	34.3/25	0.102	30.7/25	0.191	26.5/25	0.381
0.0	35.0/25	0.088	31.7/25	0.167	27.2/25	0.346
0.25	29.9/25	0.228	31.8/25	0.164	26.6/25	0.376
0.50	23.5/25	0.548	33.6/25	0.117	23.9/25	0.525
0.75	32.1/25	0.155	30.3/25	0.213	24.7/25	0.479

Table 13. Goodness of agreement between data and different parton shower models in terms of χ^2 per degree of freedom and confidence level at $\langle\sqrt{s}\rangle = 197.0$ GeV.

JHEP10(2011)143

ε	$(1/\sigma)\cdot(\mathrm{d}\sigma/\mathrm{d}\varepsilon)$			
	$(\nu=10)$	$(\nu=25)$	$(\nu=35)$	$(\nu=50)$
	$\sqrt{s}=91.2$ GeV			
0.025	6.294±0.009±0.190	6.177±0.009±0.187	6.101±0.009±0.186	5.990±0.009±0.183
0.075	5.555±0.009±0.079	5.406±0.009±0.078	5.311±0.008±0.077	5.172±0.008±0.076
0.125	2.634±0.006±0.074	2.532±0.006±0.073	2.466±0.006±0.072	2.373±0.006±0.071
0.175	1.555±0.005±0.027	1.472±0.005±0.026	1.420±0.004±0.026	1.346±0.004±0.025
0.225	0.929±0.004±0.010	0.867±0.004±0.011	0.827±0.003±0.011	0.773±0.003±0.011
0.275	0.558±0.003±0.012	0.516±0.003±0.012	0.490±0.003±0.012	0.454±0.002±0.011
0.325	0.364±0.002±0.010	0.335±0.002±0.010	0.318±0.002±0.009	0.294±0.002±0.009
0.375	0.278±0.002±0.007	0.258±0.002±0.006	0.245±0.002±0.006	0.227±0.002±0.005
0.425	0.240±0.002±0.005	0.225±0.002±0.004	0.215±0.002±0.004	0.201±0.002±0.004
0.475	0.222±0.002±0.006	0.211±0.002±0.006	0.203±0.002±0.006	0.192±0.002±0.006
0.525	0.231±0.002±0.006	0.221±0.002±0.006	0.215±0.002±0.006	0.206±0.002±0.006
0.575	0.248±0.002±0.006	0.240±0.002±0.006	0.235±0.002±0.006	0.227±0.002±0.007
0.625	0.228±0.002±0.009	0.222±0.002±0.009	0.218±0.002±0.009	0.212±0.002±0.008
0.675	0.117±0.001±0.014	0.113±0.001±0.013	0.111±0.001±0.013	0.107±0.001±0.012
0.725	0.040±0.001±0.009	0.038±0.001±0.009	0.037±0.000±0.008	0.036±0.001±0.008
0.775	0.019±0.000±0.006	0.018±0.000±0.005	0.017±0.000±0.005	0.017±0.000±0.005
0.825	0.011±0.000±0.003	0.010±0.000±0.003	0.010±0.000±0.003	0.010±0.000±0.003
0.875	0.008±0.000±0.002	0.008±0.000±0.002	0.008±0.000±0.002	0.008±0.000±0.002
0.925	0.004±0.000±0.002	0.003±0.000±0.002	0.003±0.000±0.002	0.003±0.000±0.001
	$\langle\sqrt{s}\rangle=197.0$ GeV			
0.020	9.460±0.148±0.379	9.335±0.146±0.375	9.254±0.145±0.373	9.135±0.143±0.369
0.060	4.824±0.103±0.169	4.716±0.101±0.168	4.647±0.100±0.167	4.547±0.097±0.166
0.100	2.611±0.080±0.128	2.534±0.077±0.121	2.484±0.076±0.117	2.413±0.074±0.112
0.140	1.855±0.072±0.055	1.780±0.069±0.053	1.733±0.067±0.051	1.665±0.065±0.048
0.180	1.296±0.066±0.033	1.220±0.062±0.030	1.173±0.060±0.029	1.106±0.056±0.027
0.220	0.881±0.056±0.030	0.816±0.052±0.028	0.776±0.049±0.027	0.721±0.046±0.026
0.260	0.528±0.047±0.048	0.485±0.043±0.045	0.458±0.041±0.043	0.421±0.037±0.040
0.300	0.403±0.043±0.042	0.369±0.040±0.038	0.348±0.037±0.036	0.319±0.034±0.032
0.340	0.300±0.040±0.022	0.274±0.036±0.020	0.259±0.034±0.019	0.238±0.031±0.017
0.380	0.250±0.039±0.049	0.230±0.035±0.045	0.217±0.033±0.043	0.200±0.031±0.040
0.420	0.232±0.035±0.025	0.218±0.033±0.023	0.209±0.032±0.023	0.197±0.030±0.022
0.460	0.256±0.039±0.022	0.242±0.037±0.021	0.234±0.036±0.020	0.222±0.034±0.019
0.500	0.198±0.034±0.042	0.190±0.032±0.038	0.185±0.031±0.036	0.177±0.030±0.033
0.540	0.341±0.046±0.030	0.331±0.045±0.030	0.325±0.044±0.031	0.316±0.043±0.031
0.580	0.265±0.046±0.061	0.259±0.045±0.058	0.255±0.044±0.056	0.249±0.043±0.053
0.620	0.395±0.062±0.085	0.387±0.061±0.082	0.382±0.060±0.080	0.374±0.059±0.078
0.660	0.229±0.044±0.036	0.223±0.043±0.034	0.220±0.043±0.033	0.214±0.042±0.031
0.700	0.098±0.023±0.033	0.095±0.022±0.031	0.092±0.022±0.030	0.089±0.021±0.028
0.740	0.046±0.013±0.048	0.044±0.013±0.044	0.043±0.012±0.042	0.041±0.012±0.040
0.780	0.024±0.008±0.034	0.022±0.008±0.032	0.021±0.007±0.031	0.020±0.007±0.029

Table 14. Differential distribution for the energy flow correlation for $a=-1.0$ and $\delta=30°$.

JHEP10(2011)143

ε	$(1/\sigma)\cdot(\mathrm{d}\sigma/\mathrm{d}\varepsilon)$			
	$(\nu=10)$	$(\nu=25)$	$(\nu=35)$	$(\nu=50)$
	$\sqrt{s}=91.2$ GeV			
0.025	6.160±0.009±0.180	5.872±0.009±0.174	5.690±0.008±0.170	5.432±0.008±0.164
0.075	5.407±0.009±0.078	5.055±0.008±0.076	4.838±0.008±0.074	4.536±0.007±0.073
0.125	2.534±0.006±0.073	2.301±0.005±0.070	2.161±0.005±0.068	1.970±0.005±0.065
0.175	1.478±0.005±0.026	1.298±0.004±0.024	1.193±0.004±0.023	1.053±0.003±0.022
0.225	0.874±0.004±0.010	0.744±0.003±0.010	0.670±0.003±0.010	0.575±0.002±0.010
0.275	0.522±0.003±0.012	0.438±0.002±0.011	0.391±0.002±0.010	0.330±0.002±0.009
0.325	0.341±0.002±0.010	0.286±0.002±0.008	0.254±0.002±0.008	0.215±0.001±0.007
0.375	0.262±0.002±0.006	0.222±0.002±0.005	0.199±0.002±0.004	0.170±0.001±0.004
0.425	0.230±0.002±0.005	0.198±0.002±0.004	0.180±0.002±0.004	0.157±0.001±0.003
0.475	0.215±0.002±0.006	0.191±0.002±0.006	0.177±0.002±0.006	0.158±0.001±0.006
0.525	0.221±0.002±0.006	0.201±0.002±0.006	0.189±0.002±0.006	0.172±0.001±0.005
0.575	0.241±0.002±0.006	0.223±0.002±0.006	0.213±0.002±0.006	0.198±0.002±0.006
0.625	0.222±0.002±0.009	0.208±0.002±0.008	0.200±0.002±0.008	0.188±0.002±0.007
0.675	0.114±0.001±0.013	0.106±0.001±0.012	0.101±0.001±0.011	0.095±0.001±0.010
0.725	0.038±0.001±0.008	0.035±0.001±0.008	0.033±0.001±0.007	0.030±0.001±0.007
0.775	0.019±0.000±0.005	0.017±0.000±0.005	0.016±0.000±0.004	0.015±0.000±0.004
0.825	0.011±0.000±0.003	0.010±0.000±0.003	0.009±0.000±0.003	0.008±0.000±0.002
0.875	0.008±0.000±0.002	0.007±0.000±0.002	0.007±0.000±0.001	0.006±0.000±0.001
	$\langle\sqrt{s}\rangle=197.0$ GeV			
0.020	9.336±0.146±0.394	9.027±0.141±0.384	8.831±0.138±0.378	8.552±0.134±0.369
0.060	4.705±0.101±0.166	4.453±0.096±0.163	4.297±0.092±0.161	4.081±0.088±0.158
0.100	2.531±0.077±0.115	2.351±0.072±0.103	2.242±0.069±0.096	2.092±0.064±0.086
0.140	1.791±0.070±0.059	1.621±0.063±0.053	1.519±0.059±0.049	1.380±0.054±0.044
0.180	1.226±0.063±0.036	1.068±0.054±0.030	0.976±0.050±0.026	0.855±0.044±0.022
0.220	0.807±0.052±0.025	0.683±0.044±0.023	0.613±0.039±0.021	0.524±0.034±0.019
0.260	0.496±0.044±0.044	0.411±0.037±0.038	0.364±0.032±0.035	0.305±0.027±0.031
0.300	0.409±0.044±0.028	0.336±0.036±0.024	0.297±0.031±0.021	0.247±0.026±0.018
0.340	0.292±0.038±0.023	0.242±0.031±0.019	0.214±0.027±0.017	0.180±0.023±0.014
0.380	0.222±0.035±0.052	0.187±0.029±0.043	0.168±0.026±0.038	0.143±0.022±0.032
0.420	0.242±0.037±0.028	0.211±0.032±0.023	0.193±0.029±0.021	0.170±0.025±0.018
0.460	0.224±0.035±0.024	0.201±0.031±0.020	0.187±0.029±0.018	0.168±0.026±0.015
0.500	0.230±0.037±0.037	0.210±0.034±0.031	0.198±0.032±0.027	0.182±0.029±0.023
0.540	0.340±0.046±0.038	0.320±0.043±0.038	0.307±0.042±0.038	0.290±0.039±0.037
0.580	0.247±0.044±0.066	0.234±0.042±0.060	0.226±0.041±0.057	0.215±0.039±0.053
0.620	0.355±0.058±0.069	0.338±0.056±0.063	0.328±0.056±0.060	0.314±0.053±0.056
0.660	0.213±0.041±0.040	0.201±0.039±0.035	0.194±0.038±0.032	0.185±0.036±0.028
0.700	0.081±0.021±0.048	0.074±0.019±0.043	0.070±0.018±0.040	0.065±0.017±0.037
0.740	0.044±0.012±0.041	0.040±0.011±0.035	0.037±0.011±0.032	0.034±0.010±0.028
0.780	0.023±0.008±0.038	0.020±0.007±0.033	0.019±0.007±0.031	0.016±0.006±0.027

Table 15. Differential distribution for energy flow correlation for $a=-0.5$ and $\delta=30^\circ$.

JHEP10(2011)143

ε	$(1/\sigma)\cdot(\mathrm{d}\sigma/\mathrm{d}\varepsilon)$			
	$(\nu=10)$	$(\nu=25)$	$(\nu=35)$	$(\nu=50)$
	$\sqrt{s}=91.2$ GeV			
0.025	5.810±0.009±0.171	5.101±0.008±0.154	4.690±0.007±0.144	4.149±0.006±0.132
0.075	5.015±0.008±0.077	4.209±0.007±0.074	3.763±0.006±0.072	3.201±0.005±0.070
0.125	2.287±0.005±0.069	1.793±0.004±0.062	1.533±0.004±0.058	1.223±0.003±0.052
0.175	1.299±0.004±0.023	0.948±0.003±0.019	0.773±0.003±0.018	0.575±0.002±0.017
0.225	0.754±0.003±0.009	0.519±0.002±0.009	0.408±0.002±0.009	0.287±0.001±0.009
0.275	0.448±0.002±0.011	0.301±0.002±0.008	0.233±0.001±0.007	0.161±0.001±0.006
0.325	0.294±0.002±0.008	0.198±0.001±0.006	0.154±0.001±0.005	0.107±0.001±0.004
0.375	0.229±0.002±0.005	0.159±0.001±0.003	0.126±0.001±0.002	0.090±0.001±0.002
0.425	0.203±0.002±0.004	0.148±0.001±0.003	0.120±0.001±0.003	0.090±0.001±0.002
0.475	0.192±0.002±0.005	0.147±0.001±0.005	0.125±0.001±0.004	0.098±0.001±0.004
0.525	0.204±0.002±0.007	0.165±0.001±0.006	0.144±0.001±0.006	0.119±0.001±0.005
0.575	0.225±0.002±0.006	0.190±0.002±0.005	0.171±0.002±0.005	0.147±0.001±0.005
0.625	0.206±0.002±0.008	0.177±0.002±0.006	0.161±0.002±0.005	0.141±0.001±0.004
0.675	0.107±0.001±0.012	0.090±0.001±0.010	0.081±0.001±0.009	0.070±0.001±0.008
0.725	0.036±0.001±0.008	0.029±0.000±0.006	0.025±0.000±0.006	0.021±0.000±0.005
0.775	0.017±0.000±0.005	0.014±0.000±0.004	0.012±0.000±0.004	0.010±0.000±0.003
0.825	0.010±0.000±0.003	0.008±0.000±0.002	0.007±0.000±0.002	0.006±0.000±0.002
0.875	0.007±0.000±0.002	0.006±0.000±0.001	0.005±0.000±0.001	0.005±0.000±0.001
	$\langle\sqrt{s}\rangle=197.0$ GeV			
0.020	8.940±0.140±0.364	8.152±0.129±0.338	7.687±0.122±0.323	7.066±0.113±0.303
0.060	4.425±0.095±0.153	3.840±0.083±0.145	3.513±0.077±0.140	3.093±0.069±0.131
0.100	2.337±0.072±0.094	1.935±0.060±0.072	1.716±0.054±0.062	1.445±0.046±0.051
0.140	1.614±0.063±0.048	1.256±0.049±0.037	1.070±0.042±0.032	0.847±0.034±0.026
0.180	1.072±0.054±0.030	0.771±0.039±0.020	0.625±0.032±0.017	0.462±0.024±0.014
0.220	0.696±0.045±0.019	0.479±0.031±0.016	0.378±0.024±0.014	0.270±0.018±0.012
0.260	0.410±0.037±0.031	0.274±0.025±0.023	0.212±0.019±0.020	0.147±0.014±0.015
0.300	0.333±0.035±0.027	0.220±0.023±0.018	0.170±0.018±0.014	0.117±0.012±0.011
0.340	0.255±0.033±0.024	0.171±0.022±0.015	0.133±0.017±0.012	0.094±0.012±0.008
0.380	0.181±0.028±0.050	0.128±0.020±0.036	0.103±0.016±0.029	0.075±0.012±0.022
0.420	0.203±0.031±0.016	0.152±0.023±0.012	0.126±0.019±0.011	0.098±0.015±0.009
0.460	0.237±0.034±0.017	0.186±0.027±0.010	0.159±0.023±0.009	0.128±0.019±0.007
0.500	0.214±0.032±0.038	0.178±0.027±0.026	0.159±0.024±0.021	0.137±0.021±0.016
0.540	0.303±0.043±0.045	0.262±0.037±0.041	0.239±0.034±0.039	0.210±0.030±0.035
0.580	0.256±0.044±0.057	0.229±0.041±0.047	0.214±0.039±0.042	0.193±0.036±0.036
0.620	0.332±0.056±0.074	0.296±0.051±0.063	0.275±0.049±0.058	0.249±0.046±0.053
0.660	0.219±0.042±0.022	0.194±0.038±0.017	0.180±0.036±0.014	0.163±0.034±0.012
0.700	0.086±0.021±0.029	0.071±0.018±0.023	0.064±0.016±0.020	0.054±0.014±0.016
0.740	0.045±0.012±0.041	0.037±0.010±0.031	0.033±0.009±0.025	0.028±0.008±0.019
0.780	0.021±0.007±0.031	0.016±0.006±0.024	0.014±0.005±0.020	0.011±0.004±0.016

Table 16. Differential distribution for energy flow correlation for $a = 0.0$ and $\delta = 30°$.

JHEP10(2011)143

ε	$(1/\sigma)\cdot(\mathrm{d}\sigma/\mathrm{d}\varepsilon)$			
	$(\nu = 10)$	$(\nu = 25)$	$(\nu = 35)$	$(\nu = 50)$
	$\sqrt{s} = 91.2$ GeV			
0.025	4.848±0.007±0.146	3.313±0.005±0.112	2.606±0.004±0.098	1.852±0.003±0.084
0.075	3.997±0.006±0.073	2.461±0.004±0.066	1.819±0.003±0.062	1.188±0.002±0.054
0.125	1.709±0.004±0.058	0.895±0.002±0.042	0.596±0.002±0.034	0.334±0.001±0.024
0.175	0.921±0.003±0.019	0.415±0.001±0.014	0.251±0.001±0.011	0.122±0.000±0.008
0.225	0.519±0.002±0.008	0.212±0.001±0.007	0.120±0.001±0.005	0.054±0.000±0.004
0.275	0.307±0.002±0.008	0.122±0.001±0.004	0.068±0.000±0.003	0.030±0.000±0.002
0.325	0.206±0.001±0.006	0.084±0.001±0.003	0.048±0.000±0.002	0.022±0.000±0.001
0.375	0.166±0.001±0.003	0.074±0.001±0.001	0.045±0.000±0.000	0.022±0.000±0.000
0.425	0.151±0.001±0.003	0.074±0.001±0.001	0.048±0.000±0.001	0.026±0.000±0.001
0.475	0.150±0.001±0.006	0.084±0.001±0.004	0.058±0.001±0.003	0.035±0.000±0.003
0.525	0.166±0.001±0.005	0.102±0.001±0.004	0.076±0.001±0.003	0.051±0.000±0.002
0.575	0.190±0.002±0.005	0.128±0.001±0.004	0.101±0.001±0.004	0.073±0.001±0.003
0.625	0.176±0.002±0.007	0.124±0.001±0.004	0.100±0.001±0.003	0.074±0.001±0.002
0.675	0.090±0.001±0.010	0.061±0.001±0.007	0.049±0.001±0.005	0.035±0.001±0.004
0.725	0.030±0.001±0.006	0.019±0.000±0.004	0.014±0.000±0.003	0.009±0.000±0.002
0.775	0.015±0.000±0.004	0.009±0.000±0.003	0.007±0.000±0.002	0.005±0.000±0.001
0.825	0.008±0.000±0.002	0.005±0.000±0.002	0.004±0.000±0.001	0.003±0.000±0.001
	$\langle\sqrt{s}\rangle = 197.0$ GeV			
0.020	7.857±0.124±0.343	6.004±0.098±0.284	5.089±0.085±0.255	4.036±0.070±0.220
0.060	3.642±0.080±0.152	2.464±0.056±0.121	1.940±0.046±0.104	1.389±0.035±0.084
0.100	1.824±0.057±0.080	1.089±0.035±0.047	0.790±0.027±0.035	0.502±0.018±0.024
0.140	1.191±0.047±0.033	0.614±0.025±0.017	0.405±0.017±0.013	0.223±0.010±0.009
0.180	0.754±0.038±0.020	0.338±0.017±0.012	0.205±0.011±0.010	0.102±0.006±0.007
0.220	0.482±0.031±0.015	0.203±0.013±0.010	0.119±0.008±0.007	0.058±0.005±0.005
0.260	0.279±0.025±0.027	0.111±0.010±0.013	0.064±0.006±0.008	0.030±0.003±0.004
0.300	0.227±0.024±0.014	0.093±0.010±0.006	0.054±0.006±0.004	0.026±0.003±0.002
0.340	0.169±0.022±0.016	0.074±0.010±0.006	0.046±0.007±0.004	0.025±0.004±0.003
0.380	0.137±0.021±0.035	0.065±0.010±0.016	0.041±0.007±0.012	0.022±0.004±0.007
0.420	0.162±0.024±0.016	0.088±0.013±0.009	0.061±0.009±0.006	0.038±0.006±0.004
0.460	0.190±0.029±0.017	0.112±0.017±0.009	0.081±0.013±0.007	0.051±0.008±0.004
0.500	0.186±0.027±0.023	0.127±0.019±0.011	0.102±0.016±0.009	0.076±0.012±0.008
0.540	0.260±0.036±0.041	0.190±0.026±0.032	0.157±0.022±0.028	0.121±0.018±0.022
0.580	0.241±0.041±0.046	0.184±0.033±0.031	0.157±0.029±0.026	0.125±0.025±0.021
0.620	0.307±0.051±0.047	0.237±0.043±0.038	0.203±0.039±0.034	0.165±0.034±0.030
0.660	0.194±0.037±0.021	0.146±0.030±0.014	0.124±0.026±0.011	0.101±0.023±0.009
0.700	0.089±0.021±0.019	0.063±0.014±0.013	0.051±0.012±0.010	0.040±0.010±0.007
0.740	0.037±0.011±0.032	0.025±0.008±0.017	0.019±0.006±0.012	0.014±0.005±0.007
0.780	0.016±0.006±0.032	0.009±0.004±0.018	0.007±0.003±0.013	0.004±0.002±0.008

Table 17. Differential distribution for energy flow correlation for $a = 0.5$ and $\delta = 30°$.

JHEP10(2011)143

ε	$(1/\sigma)\cdot(\mathrm{d}\sigma/\mathrm{d}\varepsilon)$			
	$(\nu=10)$	$(\nu=25)$	$(\nu=35)$	$(\nu=50)$
	$\sqrt{s}=91.2$ GeV			
0.020	12.112±0.015±0.334	11.516±0.014±0.320	11.147±0.013±0.310	10.631±0.013±0.298
0.060	5.231±0.009±0.238	4.809±0.008±0.229	4.560±0.008±0.224	4.224±0.008±0.216
0.100	2.296±0.006±0.048	2.050±0.006±0.046	1.909±0.005±0.045	1.724±0.005±0.044
0.140	1.340±0.005±0.027	1.168±0.004±0.023	1.071±0.004±0.021	0.946±0.004±0.018
0.180	0.840±0.004±0.020	0.708±0.003±0.017	0.635±0.003±0.015	0.543±0.003±0.013
0.220	0.539±0.003±0.009	0.437±0.003±0.009	0.381±0.002±0.009	0.313±0.002±0.009
0.260	0.349±0.002±0.012	0.271±0.002±0.011	0.230±0.002±0.010	0.182±0.001±0.009
0.300	0.213±0.002±0.017	0.162±0.001±0.014	0.136±0.001±0.012	0.105±0.001±0.010
0.340	0.145±0.002±0.012	0.109±0.001±0.009	0.091±0.001±0.008	0.070±0.001±0.006
0.380	0.101±0.001±0.007	0.077±0.001±0.005	0.064±0.001±0.005	0.049±0.001±0.004
0.420	0.081±0.001±0.005	0.063±0.001±0.004	0.053±0.001±0.003	0.042±0.001±0.002
0.460	0.068±0.001±0.005	0.055±0.001±0.004	0.048±0.001±0.003	0.039±0.001±0.002
0.500	0.057±0.001±0.006	0.046±0.001±0.004	0.041±0.001±0.004	0.034±0.001±0.003
0.540	0.052±0.001±0.003	0.044±0.001±0.002	0.040±0.001±0.002	0.034±0.001±0.002
0.580	0.047±0.001±0.004	0.041±0.001±0.003	0.038±0.001±0.003	0.034±0.001±0.002
0.620	0.033±0.001±0.006	0.030±0.001±0.005	0.028±0.001±0.005	0.026±0.001±0.004
0.660	0.014±0.001±0.002	0.013±0.001±0.002	0.012±0.000±0.002	0.011±0.001±0.002
0.700	0.004±0.000±0.001	0.003±0.000±0.001	0.003±0.000±0.001	0.003±0.000±0.001
	$\langle\sqrt{s}\rangle=197.0$ GeV			
0.0175	15.049±0.197±0.504	14.427±0.189±0.491	14.047±0.184±0.483	13.519±0.178±0.471
0.0525	4.067±0.103±0.172	3.759±0.095±0.159	3.581±0.090±0.151	3.346±0.084±0.141
0.0875	2.153±0.079±0.077	1.952±0.071±0.068	1.838±0.067±0.063	1.691±0.062±0.056
0.1225	1.392±0.069±0.070	1.246±0.061±0.060	1.163±0.057±0.055	1.056±0.052±0.048
0.1575	1.085±0.068±0.051	0.938±0.059±0.047	0.857±0.054±0.046	0.753±0.048±0.043
0.1925	0.746±0.064±0.041	0.616±0.053±0.035	0.546±0.047±0.032	0.459±0.040±0.029
0.2275	0.619±0.064±0.019	0.490±0.050±0.019	0.421±0.043±0.019	0.339±0.035±0.018
0.2625	0.348±0.046±0.028	0.267±0.035±0.021	0.226±0.030±0.018	0.178±0.024±0.015
0.2975	0.298±0.046±0.022	0.221±0.035±0.016	0.183±0.030±0.014	0.140±0.023±0.013
0.3325	0.243±0.043±0.061	0.184±0.033±0.047	0.154±0.027±0.040	0.119±0.021±0.032
0.3675	0.154±0.032±0.045	0.118±0.024±0.031	0.100±0.021±0.025	0.079±0.017±0.018
0.4025	0.115±0.028±0.046	0.088±0.022±0.035	0.074±0.019±0.029	0.058±0.016±0.023
0.4375	0.123±0.028±0.050	0.101±0.023±0.036	0.089±0.020±0.029	0.074±0.017±0.022
0.4725	0.118±0.031±0.010	0.095±0.027±0.006	0.082±0.024±0.006	0.067±0.020±0.006
0.5075	0.063±0.024±0.057	0.054±0.021±0.046	0.049±0.019±0.040	0.042±0.016±0.033
0.5425	0.100±0.026±0.039	0.085±0.023±0.034	0.077±0.021±0.032	0.067±0.019±0.028
0.5775	0.065±0.024±0.038	0.058±0.021±0.032	0.054±0.020±0.028	0.048±0.018±0.024
0.6125	0.089±0.029±0.050	0.081±0.027±0.042	0.077±0.026±0.038	0.071±0.024±0.033
0.6475	0.080±0.022±0.018	0.075±0.021±0.013	0.072±0.021±0.011	0.068±0.020±0.009
0.6825	0.030±0.010±0.017	0.028±0.009±0.013	0.027±0.009±0.011	0.025±0.008±0.009

Table 18. Differential distribution for energy flow correlation for $a=-1.0$ and $\delta=45°$.

JHEP10(2011)143

ε	$(1/\sigma)\cdot(\mathrm{d}\sigma/\mathrm{d}\varepsilon)$			
	$(\nu=10)$	$(\nu=25)$	$(\nu=35)$	$(\nu=50)$
	$\sqrt{s}=91.2$ GeV			
0.020	11.659±0.014±0.314	10.520±0.013±0.282	9.855±0.012±0.264	8.973±0.011±0.242
0.060	4.939±0.009±0.230	4.203±0.007±0.214	3.802±0.007±0.204	3.302±0.006±0.190
0.100	2.129±0.006±0.046	1.719±0.005±0.043	1.506±0.004±0.041	1.252±0.004±0.038
0.140	1.225±0.005±0.024	0.945±0.004±0.017	0.804±0.003±0.014	0.641±0.003±0.011
0.180	0.753±0.004±0.018	0.547±0.003±0.013	0.447±0.002±0.011	0.336±0.002±0.008
0.220	0.475±0.003±0.009	0.322±0.002±0.008	0.251±0.002±0.008	0.177±0.001±0.007
0.260	0.301±0.002±0.011	0.192±0.001±0.009	0.144±0.001±0.008	0.096±0.001±0.007
0.300	0.183±0.002±0.015	0.113±0.001±0.010	0.083±0.001±0.008	0.054±0.001±0.006
0.340	0.125±0.001±0.010	0.076±0.001±0.006	0.056±0.001±0.005	0.036±0.000±0.003
0.380	0.088±0.001±0.006	0.055±0.001±0.004	0.040±0.001±0.003	0.026±0.000±0.002
0.420	0.071±0.001±0.004	0.046±0.001±0.002	0.035±0.001±0.002	0.024±0.000±0.001
0.460	0.060±0.001±0.004	0.042±0.001±0.002	0.033±0.001±0.002	0.023±0.000±0.001
0.500	0.052±0.001±0.005	0.037±0.001±0.003	0.030±0.001±0.002	0.022±0.000±0.002
0.540	0.048±0.001±0.003	0.036±0.001±0.002	0.030±0.001±0.001	0.023±0.000±0.001
0.580	0.044±0.001±0.004	0.036±0.001±0.003	0.031±0.001±0.002	0.025±0.001±0.002
0.620	0.031±0.001±0.005	0.027±0.001±0.004	0.024±0.001±0.004	0.021±0.001±0.003
0.660	0.013±0.001±0.002	0.011±0.000±0.002	0.010±0.000±0.002	0.009±0.000±0.001
0.700	0.004±0.000±0.001	0.003±0.000±0.001	0.003±0.000±0.001	0.002±0.000±0.000
	$\langle\sqrt{s}\rangle=197.0$ GeV			
0.0175	14.606±0.191±0.500	13.463±0.177±0.474	12.804±0.170±0.460	11.933±0.160±0.441
0.0525	3.842±0.097±0.158	3.335±0.084±0.137	3.063±0.078±0.126	2.726±0.070±0.112
0.0875	2.024±0.074±0.065	1.693±0.062±0.052	1.523±0.056±0.045	1.318±0.049±0.038
0.1225	1.304±0.063±0.063	1.056±0.051±0.048	0.929±0.046±0.040	0.779±0.039±0.031
0.1575	0.990±0.062±0.046	0.753±0.047±0.039	0.637±0.040±0.035	0.505±0.033±0.031
0.1925	0.678±0.058±0.031	0.473±0.040±0.026	0.379±0.033±0.023	0.277±0.025±0.019
0.2275	0.517±0.053±0.022	0.341±0.035±0.018	0.262±0.027±0.015	0.181±0.019±0.013
0.2625	0.308±0.041±0.021	0.194±0.026±0.016	0.146±0.020±0.014	0.098±0.014±0.011
0.2975	0.262±0.042±0.015	0.158±0.026±0.011	0.116±0.019±0.009	0.074±0.013±0.007
0.3325	0.212±0.038±0.052	0.133±0.024±0.031	0.099±0.018±0.023	0.066±0.012±0.016
0.3675	0.124±0.029±0.045	0.080±0.020±0.026	0.061±0.015±0.019	0.043±0.011±0.012
0.4025	0.097±0.024±0.036	0.062±0.016±0.022	0.047±0.012±0.017	0.032±0.009±0.012
0.4375	0.125±0.029±0.030	0.090±0.021±0.017	0.073±0.017±0.013	0.054±0.013±0.008
0.4725	0.104±0.025±0.019	0.074±0.019±0.011	0.061±0.016±0.008	0.046±0.013±0.006
0.5075	0.053±0.018±0.037	0.041±0.014±0.025	0.035±0.012±0.019	0.028±0.010±0.014
0.5425	0.103±0.026±0.027	0.081±0.021±0.021	0.070±0.018±0.019	0.057±0.015±0.015
0.5775	0.059±0.022±0.042	0.048±0.019±0.031	0.043±0.017±0.027	0.036±0.015±0.021
0.6125	0.090±0.029±0.052	0.078±0.026±0.040	0.072±0.025±0.034	0.064±0.023±0.028
0.6475	0.074±0.023±0.017	0.067±0.021±0.010	0.062±0.020±0.007	0.057±0.019±0.005
0.6825	0.029±0.009±0.018	0.024±0.008±0.012	0.023±0.008±0.009	0.020±0.007±0.006

Table 19. Differential distribution for energy flow correlation for $a=-0.5$ and $\delta=45°$.

JHEP10(2011)143

ε	$(1/\sigma)\cdot(\mathrm{d}\sigma/\mathrm{d}\varepsilon)$			
	$(\nu=10)$	$(\nu=25)$	$(\nu=35)$	$(\nu=50)$
	$\sqrt{s}=91.2$ GeV			
0.020	10.662±0.013±0.274	8.539±0.010±0.216	7.439±0.009±0.189	6.122±0.008±0.162
0.060	4.350±0.008±0.215	3.141±0.006±0.184	2.581±0.005±0.165	1.967±0.004±0.142
0.100	1.810±0.005±0.041	1.184±0.003±0.036	0.917±0.003±0.032	0.645±0.002±0.027
0.140	1.012±0.004±0.018	0.605±0.002±0.010	0.443±0.002±0.008	0.286±0.001±0.006
0.180	0.602±0.003±0.014	0.323±0.002±0.008	0.220±0.001±0.006	0.128±0.001±0.005
0.220	0.368±0.002±0.007	0.176±0.001±0.006	0.111±0.001±0.005	0.059±0.000±0.004
0.260	0.229±0.002±0.009	0.100±0.001±0.006	0.060±0.000±0.004	0.029±0.000±0.003
0.300	0.139±0.001±0.011	0.059±0.001±0.006	0.034±0.000±0.004	0.016±0.000±0.002
0.340	0.095±0.001±0.007	0.040±0.000±0.003	0.023±0.000±0.002	0.011±0.000±0.001
0.380	0.067±0.001±0.005	0.029±0.000±0.002	0.017±0.000±0.001	0.008±0.000±0.001
0.420	0.056±0.001±0.003	0.026±0.000±0.001	0.017±0.000±0.001	0.009±0.000±0.000
0.460	0.049±0.001±0.003	0.026±0.000±0.001	0.017±0.000±0.001	0.010±0.000±0.000
0.500	0.043±0.001±0.004	0.024±0.000±0.002	0.017±0.000±0.001	0.010±0.000±0.001
0.540	0.041±0.001±0.002	0.025±0.001±0.001	0.018±0.000±0.001	0.012±0.000±0.000
0.580	0.039±0.001±0.003	0.027±0.001±0.002	0.021±0.000±0.001	0.015±0.000±0.001
0.620	0.028±0.001±0.005	0.021±0.001±0.003	0.018±0.001±0.003	0.014±0.000±0.002
0.660	0.012±0.000±0.002	0.009±0.000±0.001	0.008±0.000±0.001	0.006±0.000±0.001
	$\langle\sqrt{s}\rangle=197.0$ GeV			
0.0175	13.628±0.179±0.473	11.513±0.154±0.423	10.412±0.142±0.398	9.070±0.127±0.368
0.0525	3.458±0.087±0.135	2.625±0.068±0.107	2.236±0.059±0.094	1.800±0.049±0.079
0.0875	1.780±0.065±0.060	1.260±0.047±0.038	1.032±0.040±0.031	0.787±0.032±0.025
0.1225	1.101±0.054±0.039	0.727±0.036±0.022	0.567±0.029±0.016	0.402±0.021±0.010
0.1575	0.796±0.050±0.037	0.470±0.030±0.024	0.342±0.023±0.018	0.221±0.015±0.012
0.1925	0.515±0.044±0.039	0.267±0.023±0.020	0.179±0.016±0.014	0.104±0.010±0.009
0.2275	0.404±0.040±0.019	0.188±0.019±0.013	0.118±0.012±0.011	0.062±0.007±0.007
0.2625	0.231±0.031±0.019	0.102±0.014±0.011	0.063±0.009±0.008	0.033±0.005±0.005
0.2975	0.173±0.029±0.020	0.071±0.013±0.010	0.042±0.008±0.007	0.020±0.004±0.005
0.3325	0.164±0.030±0.046	0.072±0.013±0.021	0.043±0.008±0.013	0.022±0.005±0.007
0.3675	0.096±0.023±0.034	0.046±0.011±0.013	0.030±0.007±0.008	0.017±0.004±0.004
0.4025	0.080±0.019±0.027	0.039±0.010±0.013	0.026±0.007±0.008	0.015±0.004±0.005
0.4375	0.114±0.025±0.024	0.066±0.014±0.013	0.047±0.010±0.009	0.029±0.007±0.006
0.4725	0.092±0.022±0.012	0.053±0.013±0.005	0.038±0.010±0.004	0.024±0.007±0.004
0.5075	0.056±0.020±0.027	0.037±0.013±0.014	0.029±0.011±0.010	0.021±0.008±0.006
0.5425	0.085±0.023±0.023	0.056±0.016±0.015	0.044±0.013±0.012	0.032±0.010±0.008
0.5775	0.061±0.021±0.036	0.044±0.016±0.023	0.036±0.013±0.018	0.028±0.010±0.013
0.6125	0.085±0.024±0.023	0.066±0.020±0.013	0.057±0.018±0.010	0.046±0.015±0.008
0.6475	0.070±0.018±0.018	0.057±0.016±0.008	0.050±0.014±0.006	0.043±0.013±0.005
0.6825	0.032±0.009±0.013	0.026±0.007±0.006	0.023±0.007±0.004	0.019±0.006±0.003

Table 20. Differential distribution for energy flow correlation for $a=0.0$ and $\delta=45°$.

JHEP10(2011)143

ε	$(1/\sigma)\cdot(\mathrm{d}\sigma/\mathrm{d}\varepsilon)$			
	$(\nu=10)$	$(\nu=25)$	$(\nu=35)$	$(\nu=50)$
	$\sqrt{s}=91.2$ GeV			
0.020	8.425±0.010±0.213	4.982±0.006±0.133	3.625±0.005±0.110	2.333±0.003±0.090
0.060	3.178±0.006±0.185	1.559±0.003±0.123	1.025±0.002±0.095	0.579±0.001±0.066
0.100	1.231±0.004±0.036	0.497±0.002±0.023	0.290±0.001±0.017	0.138±0.001±0.011
0.140	0.651±0.003±0.010	0.220±0.001±0.005	0.114±0.001±0.004	0.046±0.000±0.002
0.180	0.367±0.002±0.008	0.102±0.001±0.003	0.047±0.000±0.002	0.016±0.000±0.001
0.220	0.216±0.001±0.006	0.051±0.000±0.003	0.021±0.000±0.002	0.006±0.000±0.001
0.260	0.131±0.001±0.006	0.028±0.000±0.003	0.011±0.000±0.001	0.003±0.000±0.001
0.300	0.080±0.001±0.007	0.016±0.000±0.002	0.006±0.000±0.001	0.002±0.000±0.000
0.340	0.056±0.001±0.004	0.012±0.000±0.001	0.005±0.000±0.000	0.001±0.000±0.000
0.380	0.041±0.001±0.002	0.010±0.000±0.001	0.004±0.000±0.000	0.001±0.000±0.000
0.420	0.036±0.001±0.002	0.010±0.000±0.000	0.004±0.000±0.000	0.001±0.000±0.000
0.460	0.033±0.001±0.002	0.010±0.000±0.000	0.005±0.000±0.000	0.002±0.000±0.000
0.500	0.030±0.001±0.003	0.011±0.000±0.001	0.006±0.000±0.000	0.003±0.000±0.000
0.540	0.029±0.001±0.002	0.012±0.000±0.000	0.007±0.000±0.000	0.003±0.000±0.000
0.580	0.030±0.001±0.003	0.015±0.000±0.001	0.010±0.000±0.000	0.005±0.000±0.001
0.620	0.023±0.001±0.003	0.013±0.000±0.002	0.009±0.000±0.001	0.006±0.000±0.001
0.660	0.010±0.000±0.002	0.006±0.000±0.001	0.004±0.000±0.001	0.003±0.000±0.000
0.700	0.003±0.000±0.001	0.002±0.000±0.000	0.001±0.000±0.000	0.001±0.000±0.000
	$\langle\sqrt{s}\rangle=197.0$ GeV			
0.0175	11.382±0.153±0.384	7.729±0.110±0.323	6.175±0.092±0.292	4.557±0.072±0.254
0.0525	2.633±0.067±0.114	1.467±0.041±0.071	1.049±0.031±0.055	0.666±0.021±0.039
0.0875	1.271±0.047±0.040	0.615±0.025±0.022	0.404±0.018±0.016	0.227±0.011±0.011
0.1225	0.760±0.038±0.021	0.312±0.017±0.006	0.182±0.010±0.003	0.087±0.006±0.002
0.1575	0.512±0.032±0.022	0.173±0.012±0.008	0.091±0.007±0.004	0.037±0.003±0.002
0.1925	0.325±0.027±0.021	0.088±0.008±0.007	0.040±0.004±0.004	0.014±0.002±0.002
0.2275	0.229±0.024±0.011	0.054±0.006±0.004	0.024±0.003±0.003	0.008±0.001±0.001
0.2625	0.144±0.018±0.014	0.034±0.005±0.005	0.015±0.003±0.003	0.005±0.001±0.001
0.2975	0.121±0.019±0.011	0.025±0.004±0.004	0.010±0.002±0.002	0.003±0.001±0.001
0.3325	0.084±0.015±0.018	0.021±0.004±0.005	0.010±0.002±0.002	0.004±0.001±0.001
0.3675	0.051±0.011±0.021	0.016±0.004±0.003	0.008±0.002±0.001	0.004±0.001±0.000
0.4025	0.054±0.014±0.015	0.016±0.005±0.004	0.008±0.003±0.002	0.003±0.001±0.001
0.4375	0.087±0.019±0.019	0.033±0.007±0.007	0.018±0.004±0.004	0.009±0.002±0.002
0.4725	0.059±0.015±0.009	0.023±0.007±0.005	0.014±0.005±0.004	0.008±0.003±0.002
0.5075	0.052±0.016±0.016	0.026±0.008±0.007	0.018±0.006±0.005	0.011±0.004±0.003
0.5425	0.072±0.019±0.014	0.038±0.010±0.007	0.026±0.007±0.005	0.016±0.005±0.003
0.5775	0.058±0.018±0.015	0.034±0.011±0.007	0.025±0.009±0.005	0.016±0.006±0.004
0.6125	0.067±0.024±0.026	0.040±0.016±0.015	0.031±0.013±0.012	0.022±0.010±0.009
0.6475	0.058±0.016±0.009	0.040±0.012±0.005	0.032±0.010±0.005	0.024±0.008±0.005
0.6825	0.023±0.007±0.010	0.015±0.005±0.003	0.011±0.004±0.002	0.008±0.003±0.001

Table 21. Differential distribution for energy flow correlation for $a=0.5$ and $\delta=45°$.

JHEP10(2011)143

ε	$(1/\sigma)\cdot(\mathrm{d}\sigma/\mathrm{d}\varepsilon)$			
	$(\nu=10)$	$(\nu=25)$	$(\nu=35)$	$(\nu=50)$
	$\sqrt{s}=91.2$ GeV			
0.0125	21.114±0.024±0.510	19.113±0.022±0.477	17.963±0.021±0.458	16.454±0.019±0.434
0.0375	7.236±0.013±0.293	6.110±0.011±0.270	5.520±0.010±0.255	4.802±0.009±0.233
0.0625	2.689±0.008±0.100	2.126±0.007±0.089	1.852±0.006±0.082	1.535±0.005±0.074
0.0875	1.520±0.006±0.027	1.163±0.005±0.023	0.995±0.004±0.021	0.807±0.004±0.019
0.1125	0.972±0.005±0.017	0.719±0.004±0.016	0.603±0.003±0.015	0.477±0.003±0.014
0.1375	0.659±0.004±0.012	0.471±0.003±0.010	0.387±0.003±0.009	0.298±0.002±0.008
0.1625	0.452±0.003±0.011	0.311±0.002±0.007	0.249±0.002±0.006	0.185±0.002±0.004
0.1875	0.317±0.003±0.017	0.207±0.002±0.011	0.161±0.002±0.009	0.115±0.001±0.007
0.2125	0.219±0.002±0.014	0.135±0.001±0.009	0.101±0.001±0.007	0.069±0.001±0.005
0.2375	0.142±0.002±0.015	0.083±0.001±0.009	0.060±0.001±0.007	0.039±0.001±0.005
0.2625	0.086±0.001±0.013	0.048±0.001±0.008	0.034±0.001±0.006	0.021±0.000±0.004
0.2875	0.053±0.001±0.011	0.029±0.001±0.006	0.020±0.000±0.004	0.012±0.000±0.003
0.3125	0.027±0.001±0.007	0.014±0.000±0.004	0.010±0.000±0.003	0.006±0.000±0.002
0.3375	0.017±0.001±0.004	0.009±0.000±0.002	0.006±0.000±0.001	0.004±0.000±0.001
0.3625	0.010±0.001±0.003	0.005±0.000±0.001	0.004±0.000±0.001	0.002±0.000±0.001
	$\langle\sqrt{s}\rangle=197.0$ GeV			
0.010	27.964±0.355±0.953	25.731±0.328±0.893	24.460±0.314±0.857	22.789±0.295±0.810
0.030	6.021±0.164±0.352	5.036±0.136±0.316	4.548±0.124±0.294	3.973±0.110±0.265
0.050	2.749±0.118±0.089	2.243±0.095±0.081	2.003±0.085±0.076	1.726±0.074±0.068
0.070	1.864±0.099±0.053	1.469±0.077±0.052	1.290±0.068±0.049	1.090±0.058±0.043
0.090	1.189±0.081±0.055	0.923±0.062±0.042	0.807±0.055±0.040	0.681±0.047±0.038
0.110	0.929±0.079±0.083	0.694±0.057±0.051	0.592±0.048±0.042	0.483±0.040±0.033
0.130	0.797±0.077±0.037	0.595±0.057±0.017	0.504±0.049±0.014	0.405±0.040±0.011
0.150	0.727±0.077±0.049	0.508±0.055±0.044	0.415±0.046±0.040	0.318±0.036±0.034
0.170	0.474±0.071±0.060	0.327±0.048±0.041	0.265±0.039±0.033	0.201±0.030±0.025
0.190	0.448±0.069±0.061	0.304±0.047±0.029	0.240±0.037±0.020	0.173±0.028±0.013
0.210	0.395±0.069±0.031	0.256±0.045±0.017	0.197±0.036±0.013	0.137±0.026±0.009
0.230	0.346±0.066±0.039	0.204±0.042±0.022	0.149±0.033±0.017	0.097±0.023±0.013
0.250	0.208±0.045±0.035	0.127±0.029±0.021	0.095±0.022±0.017	0.064±0.015±0.012
0.270	0.146±0.031±0.042	0.084±0.019±0.022	0.059±0.014±0.016	0.037±0.009±0.010
0.290	0.069±0.020±0.036	0.041±0.012±0.021	0.030±0.009±0.015	0.019±0.006±0.010
0.310	0.047±0.014±0.032	0.030±0.009±0.018	0.023±0.008±0.014	0.017±0.006±0.009
0.330	0.025±0.009±0.018	0.014±0.005±0.009	0.010±0.004±0.006	0.006±0.002±0.003
0.350	0.012±0.006±0.031	0.006±0.003±0.018	0.004±0.002±0.013	0.002±0.001±0.008
0.370	0.009±0.006±0.033	0.006±0.004±0.018	0.004±0.003±0.013	0.003±0.002±0.008
0.390	0.010±0.006±0.018	0.007±0.004±0.010	0.005±0.003±0.007	0.004±0.002±0.005

Table 22. Differential distribution for energy flow correlation for $a=-1.0$ and $\delta=60°$.

JHEP10(2011)143

ε	$(1/\sigma)\cdot(\mathrm{d}\sigma/\mathrm{d}\varepsilon)$			
	$(\nu=10)$	$(\nu=25)$	$(\nu=35)$	$(\nu=50)$
	$\sqrt{s}=91.2$ GeV			
0.0125	20.006±0.023±0.474	16.901±0.020±0.412	15.254±0.018±0.382	13.229±0.016±0.346
0.0375	6.648±0.012±0.281	5.080±0.010±0.243	4.343±0.008±0.220	3.515±0.007±0.189
0.0625	2.407±0.007±0.091	1.675±0.005±0.075	1.361±0.004±0.067	1.031±0.004±0.058
0.0875	1.339±0.006±0.023	0.888±0.004±0.019	0.703±0.003±0.017	0.515±0.004±0.015
0.1125	0.844±0.004±0.016	0.532±0.003±0.013	0.410±0.002±0.012	0.289±0.002±0.010
0.1375	0.564±0.004±0.010	0.336±0.002±0.007	0.251±0.002±0.006	0.169±0.001±0.005
0.1625	0.381±0.003±0.010	0.214±0.002±0.005	0.153±0.001±0.004	0.098±0.001±0.003
0.1875	0.263±0.002±0.014	0.136±0.001±0.008	0.093±0.001±0.006	0.056±0.001±0.004
0.2125	0.178±0.002±0.012	0.085±0.001±0.006	0.055±0.001±0.004	0.031±0.000±0.002
0.2375	0.114±0.001±0.013	0.050±0.001±0.006	0.031±0.000±0.004	0.016±0.000±0.002
0.2625	0.069±0.001±0.010	0.028±0.001±0.005	0.017±0.000±0.003	0.008±0.000±0.002
0.2875	0.044±0.001±0.010	0.018±0.000±0.004	0.011±0.000±0.003	0.005±0.000±0.001
0.3125	0.021±0.001±0.005	0.008±0.000±0.002	0.005±0.000±0.001	0.002±0.000±0.001
0.3375	0.013±0.001±0.003	0.005±0.000±0.001	0.003±0.000±0.001	0.001±0.000±0.000
0.3625	0.007±0.000±0.002	0.003±0.000±0.001	0.002±0.000±0.000	0.001±0.000±0.000
	$\langle\sqrt{s}\rangle=197.0$ GeV			
0.010	26.789±0.340±0.871	23.432±0.302±0.784	21.651±0.283±0.739	19.435±0.259±0.684
0.030	5.543±0.150±0.330	4.253±0.116±0.274	3.678±0.103±0.244	3.044±0.088±0.209
0.050	2.511±0.105±0.080	1.863±0.079±0.063	1.585±0.069±0.052	1.286±0.057±0.041
0.070	1.692±0.088±0.070	1.198±0.063±0.055	0.997±0.053±0.047	0.787±0.044±0.038
0.090	1.096±0.073±0.053	0.762±0.052±0.032	0.631±0.044±0.027	0.497±0.036±0.024
0.110	0.827±0.067±0.067	0.548±0.044±0.035	0.440±0.036±0.027	0.333±0.028±0.021
0.130	0.658±0.064±0.042	0.428±0.042±0.019	0.336±0.033±0.013	0.243±0.025±0.009
0.150	0.625±0.068±0.051	0.359±0.041±0.039	0.263±0.031±0.031	0.176±0.022±0.023
0.170	0.409±0.057±0.061	0.236±0.033±0.030	0.175±0.025±0.021	0.118±0.018±0.013
0.190	0.344±0.055±0.048	0.186±0.031±0.015	0.129±0.023±0.010	0.079±0.015±0.007
0.210	0.338±0.060±0.030	0.175±0.031±0.017	0.118±0.022±0.013	0.068±0.013±0.009
0.230	0.249±0.049±0.028	0.114±0.024±0.014	0.072±0.016±0.011	0.040±0.010±0.008
0.250	0.156±0.034±0.033	0.073±0.016±0.015	0.046±0.010±0.010	0.025±0.006±0.005
0.270	0.129±0.026±0.022	0.054±0.012±0.009	0.032±0.007±0.006	0.015±0.004±0.004
0.290	0.062±0.019±0.032	0.027±0.009±0.014	0.017±0.006±0.009	0.009±0.003±0.006
0.310	0.042±0.012±0.027	0.022±0.007±0.012	0.015±0.005±0.008	0.010±0.004±0.005
0.330	0.020±0.007±0.017	0.008±0.003±0.007	0.005±0.002±0.004	0.002±0.001±0.002
0.350	0.008±0.004±0.024	0.003±0.002±0.010	0.002±0.001±0.006	0.001±0.000±0.000
0.370	0.007±0.005±0.026	0.003±0.002±0.010	0.002±0.002±0.006	0.001±0.001±0.003
0.390	0.008±0.005±0.018	0.004±0.003±0.008	0.003±0.002±0.005	0.002±0.001±0.003

Table 23. Differential distribution for energy flow correlation for $a=-0.5$ and $\delta=60°$.

JHEP10(2011)143

ε	$(1/\sigma)\cdot(\mathrm{d}\sigma/\mathrm{d}\varepsilon)$			
	$(\nu=10)$	$(\nu=25)$	$(\nu=35)$	$(\nu=50)$
	$\sqrt{s}=91.2$ GeV			
0.0125	17.835±0.020±0.405	13.051±0.015±0.305	10.832±0.013±0.267	8.386±0.011±0.230
0.0375	5.647±0.012±0.259	3.585±0.007±0.199	2.767±0.006±0.168	1.959±0.004±0.132
0.0625	1.959±0.006±0.081	1.087±0.004±0.059	0.780±0.003±0.049	0.502±0.002±0.038
0.0875	1.065±0.006±0.019	0.547±0.003±0.014	0.376±0.002±0.012	0.229±0.001±0.010
0.1125	0.655±0.005±0.013	0.311±0.002±0.010	0.204±0.001±0.008	0.117±0.001±0.006
0.1375	0.426±0.004±0.008	0.184±0.001±0.005	0.114±0.001±0.004	0.060±0.001±0.003
0.1625	0.280±0.002±0.007	0.109±0.001±0.003	0.064±0.001±0.002	0.031±0.000±0.001
0.1875	0.188±0.003±0.010	0.065±0.001±0.004	0.036±0.000±0.003	0.016±0.000±0.001
0.2125	0.124±0.001±0.008	0.038±0.000±0.003	0.019±0.000±0.002	0.008±0.000±0.001
0.2375	0.078±0.001±0.009	0.021±0.000±0.003	0.010±0.000±0.002	0.004±0.000±0.001
0.2625	0.046±0.002±0.007	0.012±0.000±0.002	0.005±0.000±0.001	0.002±0.000±0.001
0.2875	0.029±0.002±0.006	0.007±0.000±0.002	0.003±0.000±0.001	
0.3125	0.014±0.000±0.003	0.004±0.000±0.001	0.002±0.000±0.000	
0.3375	0.009±0.000±0.002	0.002±0.000±0.001	0.001±0.000±0.000	
	$\langle\sqrt{s}\rangle=197.0$ GeV			
0.010	24.599±0.315±0.853	19.497±0.259±0.723	17.081±0.234±0.664	14.320±0.205±0.592
0.030	4.782±0.129±0.288	3.163±0.090±0.211	2.537±0.075±0.178	1.910±0.060±0.143
0.050	2.135±0.089±0.067	1.352±0.060±0.041	1.060±0.049±0.033	0.774±0.038±0.027
0.070	1.406±0.073±0.056	0.834±0.046±0.033	0.633±0.036±0.024	0.444±0.028±0.015
0.090	0.868±0.058±0.034	0.498±0.035±0.020	0.370±0.027±0.017	0.249±0.019±0.014
0.110	0.635±0.051±0.052	0.335±0.028±0.021	0.238±0.021±0.015	0.152±0.014±0.010
0.130	0.518±0.050±0.027	0.256±0.026±0.010	0.173±0.018±0.007	0.103±0.012±0.006
0.150	0.479±0.051±0.046	0.200±0.024±0.025	0.125±0.016±0.017	0.068±0.010±0.010
0.170	0.322±0.044±0.039	0.137±0.019±0.014	0.086±0.013±0.009	0.046±0.008±0.006
0.190	0.255±0.039±0.027	0.094±0.015±0.006	0.052±0.009±0.003	0.023±0.005±0.002
0.210	0.220±0.040±0.038	0.076±0.014±0.012	0.040±0.008±0.007	0.017±0.004±0.004
0.230	0.160±0.034±0.032	0.048±0.011±0.012	0.024±0.006±0.007	0.010±0.003±0.003
0.250	0.111±0.025±0.026	0.035±0.008±0.008	0.019±0.005±0.005	0.008±0.002±0.002
0.270	0.092±0.019±0.014	0.024±0.005±0.003	0.010±0.002±0.002	0.003±0.001±0.001
0.290	0.038±0.012±0.024	0.010±0.003±0.008	0.005±0.002±0.005	0.002±0.001±0.003
0.310	0.034±0.009±0.019	0.013±0.004±0.007	0.008±0.003±0.004	0.004±0.002±0.002
0.330	0.014±0.005±0.011	0.003±0.001±0.003	0.001±0.001±0.001	
0.350	0.005±0.003±0.019	0.001±0.001±0.005	0.001±0.000±0.000	
0.370	0.006±0.004±0.017	0.002±0.002±0.005	0.001±0.001±0.002	
0.390	0.006±0.004±0.012	0.002±0.001±0.004	0.001±0.001±0.002	

Table 24. Differential distribution for energy flow correlation for $a=0.0$ and $\delta=60°$.

JHEP10(2011)143

ε	$(1/\sigma)\cdot(\mathrm{d}\sigma/\mathrm{d}\varepsilon)$			
	$(\nu = 10)$	$(\nu = 25)$	$(\nu = 35)$	$(\nu = 50)$
	$\sqrt{s} = 91.2$ GeV			
0.0125	13.601±0.016±0.304	7.169±0.009±0.194	4.919±0.007±0.161	2.939±0.004±0.129
0.0375	3.966±0.008±0.213	1.698±0.004±0.124	1.052±0.002±0.089	0.558±0.001±0.057
0.0625	1.276±0.004±0.064	0.439±0.002±0.034	0.241±0.001±0.024	0.108±0.001±0.014
0.0875	0.664±0.003±0.015	0.199±0.001±0.008	0.101±0.001±0.006	0.040±0.000±0.003
0.1125	0.391±0.002±0.010	0.102±0.001±0.005	0.047±0.000±0.003	0.017±0.000±0.002
0.1375	0.245±0.002±0.005	0.054±0.000±0.002	0.023±0.000±0.001	0.007±0.000±0.001
0.1625	0.155±0.001±0.004	0.029±0.000±0.001	0.011±0.000±0.001	0.003±0.000±0.000
0.1875	0.100±0.001±0.006	0.016±0.000±0.001	0.005±0.000±0.001	0.001±0.000±0.000
0.2125	0.064±0.001±0.004	0.009±0.000±0.001	0.003±0.000±0.000	
0.2375	0.039±0.001±0.004	0.005±0.000±0.001	0.001±0.000±0.000	
0.2625	0.023±0.000±0.004	0.002±0.000±0.000	0.001±0.000±0.000	
0.2875	0.015±0.000±0.003	0.002±0.000±0.000		
0.3125	0.008±0.000±0.002	0.001±0.000±0.000		
0.3375	0.005±0.000±0.001			
0.3625	0.003±0.000±0.001			
	$\langle\sqrt{s}\rangle = 197.0$ GeV			
0.010	19.714±0.258±0.562	12.340±0.176±0.437	9.498±0.143±0.385	6.723±0.110±0.326
0.030	3.494±0.097±0.211	1.697±0.053±0.122	1.151±0.039±0.092	0.692±0.026±0.064
0.050	1.514±0.064±0.044	0.679±0.033±0.022	0.440±0.023±0.018	0.248±0.014±0.014
0.070	0.941±0.049±0.030	0.376±0.023±0.013	0.229±0.015±0.009	0.120±0.009±0.006
0.090	0.573±0.038±0.023	0.212±0.016±0.009	0.122±0.010±0.006	0.058±0.005±0.003
0.110	0.405±0.032±0.025	0.130±0.012±0.011	0.069±0.007±0.007	0.029±0.003±0.004
0.130	0.319±0.031±0.018	0.089±0.010±0.005	0.043±0.005±0.003	0.016±0.002±0.001
0.150	0.273±0.030±0.028	0.060±0.008±0.007	0.026±0.004±0.003	0.008±0.001±0.001
0.170	0.181±0.025±0.019	0.041±0.006±0.003	0.017±0.003±0.002	0.006±0.001±0.001
0.190	0.152±0.024±0.008	0.027±0.005±0.001	0.011±0.003±0.001	0.004±0.001±0.001
0.210	0.126±0.022±0.024	0.019±0.004±0.004	0.006±0.001±0.002	
0.230	0.084±0.017±0.008	0.012±0.003±0.002	0.004±0.001±0.001	
0.250	0.060±0.013±0.014	0.009±0.002±0.002	0.003±0.001±0.001	
0.270	0.057±0.013±0.008	0.006±0.001±0.001	0.001±0.000±0.000	
0.290	0.028±0.009±0.007	0.003±0.001±0.002	0.001±0.000±0.000	
0.310	0.023±0.006±0.010	0.005±0.002±0.002	0.002±0.001±0.001	
0.330	0.008±0.003±0.005			
0.350	0.003±0.001±0.010			
0.370	0.004±0.002±0.010			
0.390	0.003±0.002±0.006			

Table 25. Differential distribution for energy flow correlation for $a = 0.5$ and $\delta = 60°$.

JHEP10(2011)143

ε	$(1/\sigma)\cdot(\mathrm{d}\sigma/\mathrm{d}\varepsilon)$			
	$(\nu=10)$	$(\nu=25)$	$(\nu=35)$	$(\nu=50)$
	$\sqrt{s}=91.2$ GeV			
0.0075	39.381±0.041±0.608	32.943±0.035±0.551	29.633±0.032±0.522	25.631±0.028±0.485
0.0225	9.036±0.019±0.273	6.689±0.015±0.220	5.652±0.013±0.190	4.529±0.011±0.153
0.0375	2.841±0.010±0.136	1.830±0.007±0.106	1.435±0.006±0.093	1.044±0.004±0.079
0.0525	1.410±0.007±0.038	0.841±0.005±0.027	0.633±0.004±0.023	0.438±0.003±0.018
0.0675	0.796±0.005±0.029	0.455±0.003±0.017	0.334±0.003±0.013	0.225±0.002±0.010
0.0825	0.501±0.004±0.023	0.278±0.003±0.012	0.201±0.002±0.009	0.132±0.001±0.007
0.0975	0.313±0.003±0.018	0.166±0.002±0.009	0.118±0.001±0.007	0.075±0.001±0.005
0.1125	0.200±0.003±0.015	0.107±0.002±0.006	0.075±0.001±0.004	0.048±0.001±0.003
0.1275	0.123±0.002±0.012	0.065±0.001±0.006	0.046±0.001±0.004	0.029±0.001±0.002
0.1425	0.072±0.002±0.008	0.037±0.001±0.004	0.025±0.001±0.003	0.015±0.000±0.002
0.1575	0.039±0.001±0.004	0.021±0.001±0.001	0.015±0.000±0.001	0.009±0.000±0.001
0.1725	0.020±0.001±0.002	0.010±0.001±0.001	0.007±0.000±0.001	0.004±0.000±0.001
0.1875	0.019±0.001±0.002	0.005±0.000±0.001	0.003±0.000±0.001	0.002±0.000±0.001
	$\langle\sqrt{s}\rangle=197.0$ GeV			
0.005	59.130±0.720±1.570	51.561±0.637±1.439	47.662±0.597±1.381	42.847±0.548±1.310
0.015	10.562±0.311±0.557	7.780±0.231±0.478	6.616±0.201±0.433	5.376±0.169±0.380
0.025	3.999±0.197±0.231	2.670±0.132±0.153	2.158±0.109±0.124	1.646±0.086±0.096
0.035	2.208±0.149±0.100	1.428±0.095±0.064	1.140±0.077±0.053	0.860±0.061±0.042
0.045	1.521±0.127±0.126	0.969±0.079±0.073	0.771±0.064±0.059	0.580±0.050±0.046
0.055	1.191±0.111±0.057	0.701±0.068±0.029	0.541±0.056±0.022	0.399±0.044±0.019
0.065	0.843±0.094±0.062	0.527±0.060±0.034	0.415±0.049±0.028	0.312±0.039±0.023
0.075	0.810±0.095±0.053	0.482±0.057±0.035	0.362±0.044±0.030	0.250±0.032±0.025
0.085	0.494±0.068±0.058	0.289±0.041±0.043	0.217±0.032±0.037	0.152±0.025±0.029
0.095	0.490±0.073±0.064	0.294±0.045±0.031	0.220±0.035±0.023	0.151±0.026±0.017
0.105	0.469±0.075±0.051	0.270±0.044±0.022	0.202±0.034±0.015	0.141±0.025±0.011
0.115	0.322±0.057±0.048	0.208±0.037±0.016	0.163±0.030±0.010	0.117±0.023±0.007
0.125	0.214±0.049±0.041	0.144±0.034±0.019	0.115±0.028±0.012	0.087±0.021±0.007
0.135	0.127±0.034±0.050	0.090±0.024±0.020	0.074±0.020±0.012	0.056±0.016±0.006
0.145	0.119±0.033±0.033	0.073±0.022±0.016	0.056±0.018±0.011	0.040±0.013±0.007
0.155	0.076±0.022±0.032	0.049±0.015±0.016	0.037±0.012±0.011	0.025±0.009±0.008
0.165	0.063±0.020±0.023	0.037±0.013±0.010	0.027±0.010±0.007	0.018±0.008±0.005
0.175	0.052±0.018±0.023	0.034±0.013±0.010	0.026±0.010±0.007	0.018±0.007±0.004
0.185	0.019±0.011±0.008	0.011±0.006±0.005	0.008±0.005±0.004	0.005±0.003±0.003
0.195	0.005±0.005±0.010	0.002±0.002±0.006	0.001±0.001±0.004	

Table 26. Differential distribution for energy flow correlation for $a=-1.0$ and $\delta=75°$.

JHEP10(2011)143

ε	$(1/\sigma)\cdot(\mathrm{d}\sigma/\mathrm{d}\varepsilon)$			
	$(\nu=10)$	$(\nu=25)$	$(\nu=35)$	$(\nu=50)$
	$\sqrt{s}=91.2$ GeV			
0.0075	36.676±0.038±0.562	28.238±0.031±0.475	24.250±0.027±0.438	19.735±0.023±0.395
0.0225	8.095±0.017±0.255	5.367±0.012±0.185	4.285±0.010±0.150	3.199±0.008±0.111
0.0375	2.450±0.009±0.125	1.370±0.005±0.090	0.999±0.004±0.076	0.664±0.003±0.060
0.0525	1.195±0.006±0.033	0.608±0.003±0.021	0.423±0.003±0.017	0.265±0.002±0.013
0.0675	0.665±0.005±0.025	0.320±0.002±0.013	0.216±0.002±0.009	0.131±0.001±0.007
0.0825	0.416±0.004±0.018	0.191±0.002±0.009	0.126±0.001±0.007	0.073±0.001±0.005
0.0975	0.256±0.003±0.015	0.112±0.001±0.007	0.072±0.001±0.004	0.041±0.001±0.003
0.1125	0.164±0.002±0.012	0.071±0.001±0.004	0.045±0.001±0.003	0.025±0.000±0.002
0.1275	0.100±0.002±0.010	0.043±0.001±0.004	0.027±0.001±0.002	0.015±0.000±0.001
0.1425	0.057±0.001±0.007	0.023±0.001±0.003	0.014±0.000±0.002	0.007±0.000±0.001
0.1575	0.032±0.001±0.003	0.013±0.000±0.001	0.008±0.000±0.001	
0.1725	0.016±0.001±0.002	0.007±0.000±0.001	0.004±0.000±0.001	
0.1875	0.007±0.000±0.002	0.003±0.000±0.001		
	$\langle\sqrt{s}\rangle=197.0$ GeV			
0.005	56.032±0.684±1.599	46.186±0.581±1.420	41.439±0.534±1.342	35.845±0.477±1.245
0.015	9.546±0.278±0.543	6.396±0.194±0.423	5.199±0.164±0.368	3.996±0.133±0.307
0.025	3.459±0.169±0.239	2.082±0.105±0.123	1.603±0.084±0.094	1.151±0.064±0.069
0.035	1.929±0.128±0.096	1.124±0.076±0.051	0.855±0.060±0.041	0.608±0.046±0.032
0.045	1.290±0.105±0.123	0.742±0.062±0.064	0.564±0.048±0.050	0.400±0.036±0.037
0.055	1.001±0.092±0.046	0.524±0.054±0.022	0.385±0.043±0.019	0.266±0.033±0.020
0.065	0.711±0.079±0.060	0.395±0.046±0.029	0.295±0.037±0.022	0.208±0.029±0.015
0.075	0.670±0.078±0.054	0.331±0.040±0.018	0.227±0.029±0.011	0.141±0.020±0.006
0.085	0.451±0.059±0.049	0.214±0.030±0.038	0.148±0.023±0.032	0.096±0.017±0.023
0.095	0.442±0.067±0.065	0.225±0.036±0.027	0.155±0.026±0.019	0.095±0.018±0.012
0.105	0.389±0.058±0.039	0.190±0.031±0.012	0.132±0.023±0.009	0.086±0.017±0.007
0.115	0.272±0.055±0.039	0.147±0.029±0.018	0.105±0.021±0.012	0.067±0.014±0.008
0.125	0.174±0.040±0.046	0.099±0.024±0.017	0.073±0.018±0.009	0.049±0.012±0.004
0.135	0.129±0.034±0.023	0.078±0.021±0.007	0.058±0.016±0.005	0.039±0.011±0.004
0.145	0.092±0.024±0.024	0.047±0.014±0.008	0.034±0.011±0.005	0.022±0.009±0.003
0.155	0.070±0.021±0.025	0.036±0.011±0.009	0.023±0.008±0.006	0.013±0.005±0.003
0.165	0.051±0.016±0.019	0.024±0.009±0.007	0.015±0.006±0.005	0.009±0.004±0.003
0.175	0.038±0.014±0.016	0.019±0.007±0.005	0.012±0.005±0.002	0.006±0.003±0.002
0.185	0.016±0.009±0.009	0.007±0.004±0.005	0.004±0.003±0.004	0.002±0.001±0.002
0.195	0.004±0.004±0.008	0.001±0.001±0.003		

Table 27. Differential distribution for energy flow correlation for $a=-0.5$ and $\delta=75^\circ$.

JHEP10(2011)143

ε	$(1/\sigma)\cdot(\mathrm{d}\sigma/\mathrm{d}\varepsilon)$			
	$(\nu=10)$	$(\nu=25)$	$(\nu=35)$	$(\nu=50)$
	$\sqrt{s}=91.2$ GeV			
0.0075	31.982±0.034±0.466	21.042±0.024±0.359	16.535±0.019±0.329	11.954±0.015±0.303
0.0225	6.691±0.015±0.229	3.670±0.009±0.144	2.652±0.007±0.109	1.741±0.005±0.074
0.0375	1.920±0.007±0.111	0.850±0.004±0.071	0.549±0.002±0.055	0.313±0.002±0.040
0.0525	0.910±0.005±0.028	0.358±0.002±0.016	0.218±0.001±0.011	0.115±0.001±0.008
0.0675	0.497±0.003±0.018	0.180±0.002±0.008	0.105±0.001±0.006	0.053±0.001±0.004
0.0825	0.307±0.003±0.014	0.104±0.001±0.006	0.059±0.001±0.004	0.028±0.000±0.003
0.0975	0.186±0.002±0.010	0.059±0.001±0.003	0.032±0.001±0.002	0.015±0.000±0.001
0.1125	0.118±0.002±0.008	0.036±0.001±0.002	0.019±0.000±0.001	0.008±0.000±0.001
0.1275	0.071±0.001±0.007	0.021±0.000±0.002	0.011±0.000±0.001	0.005±0.000±0.001
0.1425	0.040±0.001±0.005	0.011±0.000±0.001	0.005±0.000±0.001	
0.1575	0.022±0.001±0.001			
0.1725	0.011±0.001±0.001			
0.1875	0.005±0.000±0.001			
	$\langle\sqrt{s}\rangle=197.0$ GeV			
0.005	50.431±0.622±1.383	37.425±0.491±1.160	31.785±0.435±1.064	25.672±0.372±0.944
0.015	7.981±0.233±0.469	4.623±0.148±0.329	3.495±0.119±0.270	2.450±0.090±0.208
0.025	2.822±0.137±0.164	1.445±0.077±0.073	1.023±0.058±0.051	0.660±0.040±0.035
0.035	1.548±0.102±0.071	0.756±0.054±0.038	0.528±0.041±0.029	0.337±0.029±0.020
0.045	1.038±0.082±0.084	0.505±0.043±0.046	0.355±0.033±0.035	0.229±0.024±0.024
0.055	0.767±0.073±0.048	0.333±0.037±0.014	0.227±0.029±0.011	0.144±0.021±0.009
0.065	0.596±0.066±0.052	0.269±0.033±0.025	0.184±0.025±0.016	0.117±0.019±0.010
0.075	0.490±0.056±0.028	0.190±0.024±0.013	0.116±0.017±0.011	0.063±0.011±0.009
0.085	0.311±0.043±0.050	0.113±0.018±0.027	0.069±0.012±0.019	0.038±0.008±0.012
0.095	0.320±0.048±0.039	0.117±0.020±0.016	0.068±0.013±0.011	0.034±0.008±0.007
0.105	0.260±0.039±0.016	0.095±0.017±0.003	0.058±0.012±0.003	0.032±0.007±0.002
0.115	0.216±0.042±0.037	0.087±0.017±0.010	0.053±0.011±0.005	0.028±0.006±0.002
0.125	0.128±0.028±0.046	0.054±0.012±0.015	0.033±0.008±0.008	0.018±0.005±0.004
0.135	0.087±0.025±0.022	0.036±0.010±0.005	0.021±0.006±0.002	0.010±0.003±0.001
0.145	0.070±0.018±0.016	0.025±0.008±0.005	0.015±0.005±0.003	0.008±0.003±0.002
0.155	0.053±0.016±0.017	0.019±0.007±0.004	0.011±0.004±0.002	0.005±0.002±0.001
0.165	0.041±0.014±0.010	0.013±0.005±0.003	0.007±0.003±0.001	0.003±0.001±0.001
0.175	0.029±0.011±0.009	0.010±0.004±0.002	0.005±0.002±0.001	0.002±0.001±0.001
0.185	0.012±0.007±0.009	0.004±0.002±0.004	0.002±0.001±0.003	0.001±0.000±0.000
0.195	0.002±0.002±0.004	0.000±0.000±0.000	0.000±0.000±0.000	0.000±0.000±0.000

Table 28. Differential distribution for energy flow correlation for $a = 0.0$ and $\delta = 75°$.

JHEP10(2011)143

ε	$(1/\sigma)\cdot(\mathrm{d}\sigma/\mathrm{d}\varepsilon)$			
	$(\nu = 10)$	$(\nu = 25)$	$(\nu = 35)$	$(\nu = 50)$
	$\sqrt{s} = 91.2$ GeV			
0.0075	23.742±0.026±0.365	11.132±0.014±0.268	7.212±0.009±0.230	4.014±0.006±0.183
0.0225	4.574±0.010±0.185	1.710±0.005±0.088	1.003±0.003±0.058	0.501±0.002±0.034
0.0375	1.212±0.005±0.081	0.339±0.002±0.037	0.171±0.001±0.024	0.070±0.000±0.013
0.0525	0.547±0.003±0.019	0.129±0.001±0.007	0.059±0.000±0.004	0.022±0.000±0.002
0.0675	0.290±0.002±0.011	0.061±0.001±0.004	0.026±0.000±0.002	0.009±0.000±0.001
0.0825	0.174±0.002±0.009	0.032±0.000±0.003	0.013±0.000±0.002	0.004±0.000±0.001
0.0975	0.102±0.001±0.006	0.017±0.000±0.001	0.006±0.000±0.001	
0.1125	0.065±0.001±0.004	0.010±0.000±0.001		
0.1275	0.038±0.001±0.004	0.005±0.000±0.001		
0.1425	0.021±0.001±0.003			
0.1575	0.012±0.000±0.001			
0.1725	0.006±0.000±0.001			
0.1875	0.002±0.000±0.001			
	$\langle\sqrt{s}\rangle = 197.0$ GeV			
0.005	40.150±0.509±1.077	23.383±0.331±0.836	17.407±0.263±0.732	11.839±0.197±0.611
0.015	5.745±0.174±0.364	2.483±0.089±0.201	1.603±0.063±0.146	0.911±0.041±0.095
0.025	1.979±0.098±0.082	0.727±0.043±0.033	0.434±0.028±0.023	0.223±0.017±0.014
0.035	1.031±0.069±0.049	0.355±0.028±0.020	0.204±0.018±0.012	0.100±0.010±0.006
0.045	0.704±0.056±0.055	0.241±0.023±0.019	0.139±0.015±0.011	0.068±0.009±0.005
0.055	0.470±0.048±0.023	0.146±0.020±0.014	0.083±0.013±0.011	0.041±0.008±0.007
0.065	0.356±0.041±0.027	0.116±0.017±0.010	0.066±0.011±0.006	0.032±0.007±0.003
0.075	0.308±0.036±0.020	0.070±0.010±0.006	0.032±0.006±0.004	0.012±0.003±0.003
0.085	0.211±0.029±0.019	0.046±0.009±0.008	0.022±0.005±0.004	0.009±0.002±0.002
0.095	0.193±0.029±0.032	0.041±0.008±0.009	0.018±0.004±0.005	0.006±0.002±0.002
0.105	0.194±0.030±0.020	0.039±0.007±0.002	0.017±0.004±0.001	0.006±0.002±0.000
0.115	0.122±0.022±0.013	0.028±0.006±0.002	0.012±0.003±0.001	0.004±0.001±0.001
0.125	0.084±0.018±0.024	0.020±0.005±0.004	0.009±0.002±0.002	0.003±0.001±0.001
0.135	0.054±0.014±0.008	0.011±0.003±0.001	0.004±0.001±0.001	0.001±0.000±0.000
0.145	0.051±0.015±0.010	0.013±0.006±0.003	0.007±0.004±0.002	0.004±0.003±0.001
0.155	0.028±0.009±0.008	0.005±0.002±0.001		
0.165	0.021±0.007±0.008	0.003±0.002±0.001		
0.175	0.019±0.006±0.006	0.002±0.001±0.001		
0.185	0.006±0.003±0.004			
0.195	0.001±0.001±0.003			

Table 29. Differential distribution for energy flow correlation for $a = 0.5$ and $\delta = 75°$.

JHEP10(2011)143

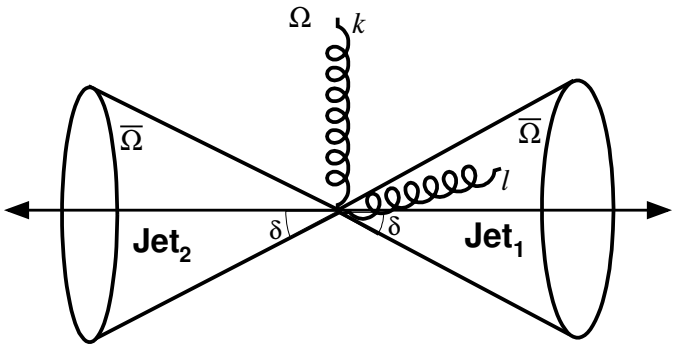

Figure 1. A soft gluon with momentum k $(= \varepsilon \cdot Q)$ is radiated into region Ω by an energetic gluon with momentum l radiated in $\bar{\Omega}$, giving a next-to-leading order contribution to the energy flow distributions.

JHEP10(2011)143

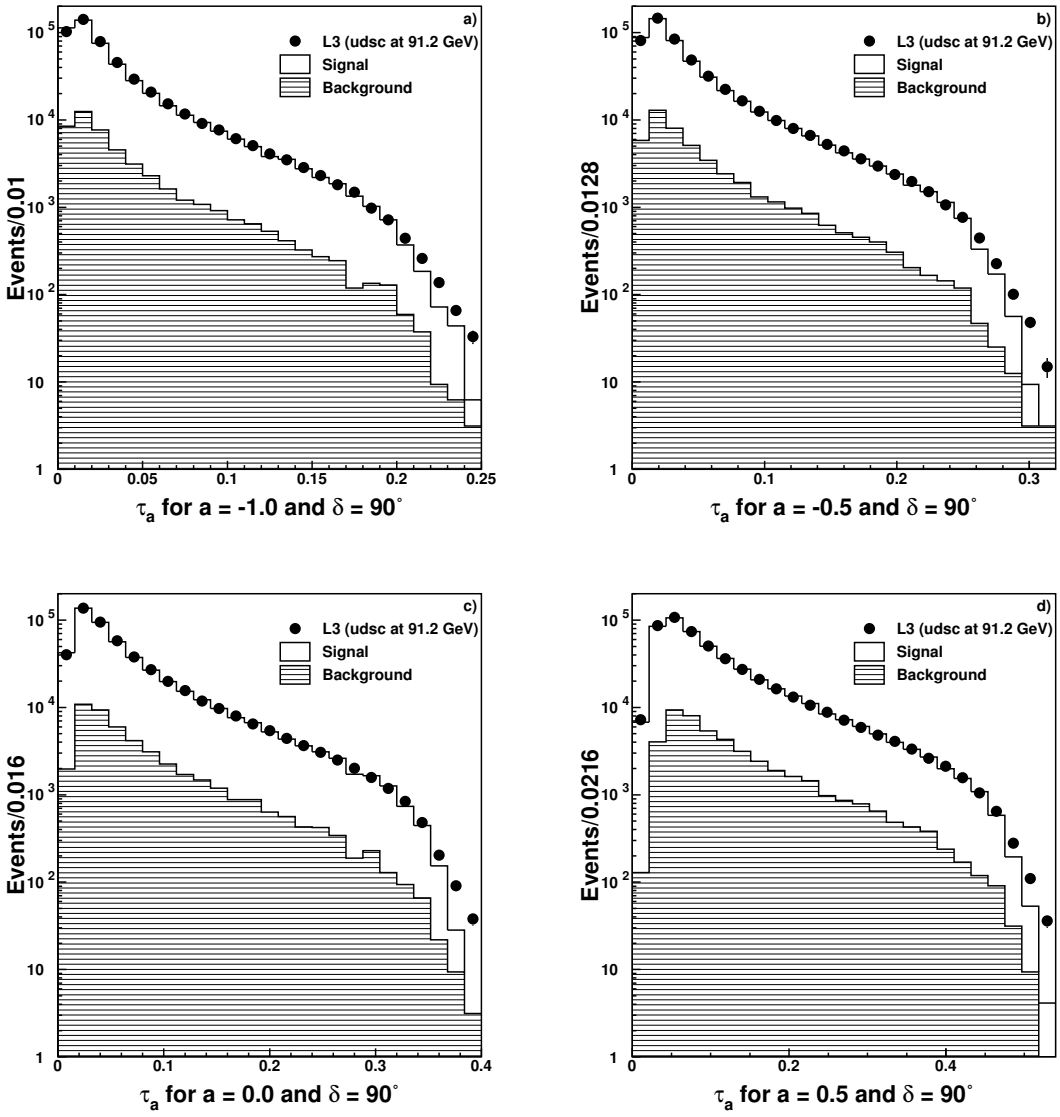

Figure 2. Measured inclusive event shape distributions at $\sqrt{s} = 91.2$ GeV for data sample enriched in light flavour (udsc) for $a = -1.0$ (a), -0.5 (b), 0.0 (c), 0.5 (d). These distributions are compared with expectation from JETSET parton shower Monte Carlo program. The shaded areas refer to different backgrounds

JHEP10(2011)143

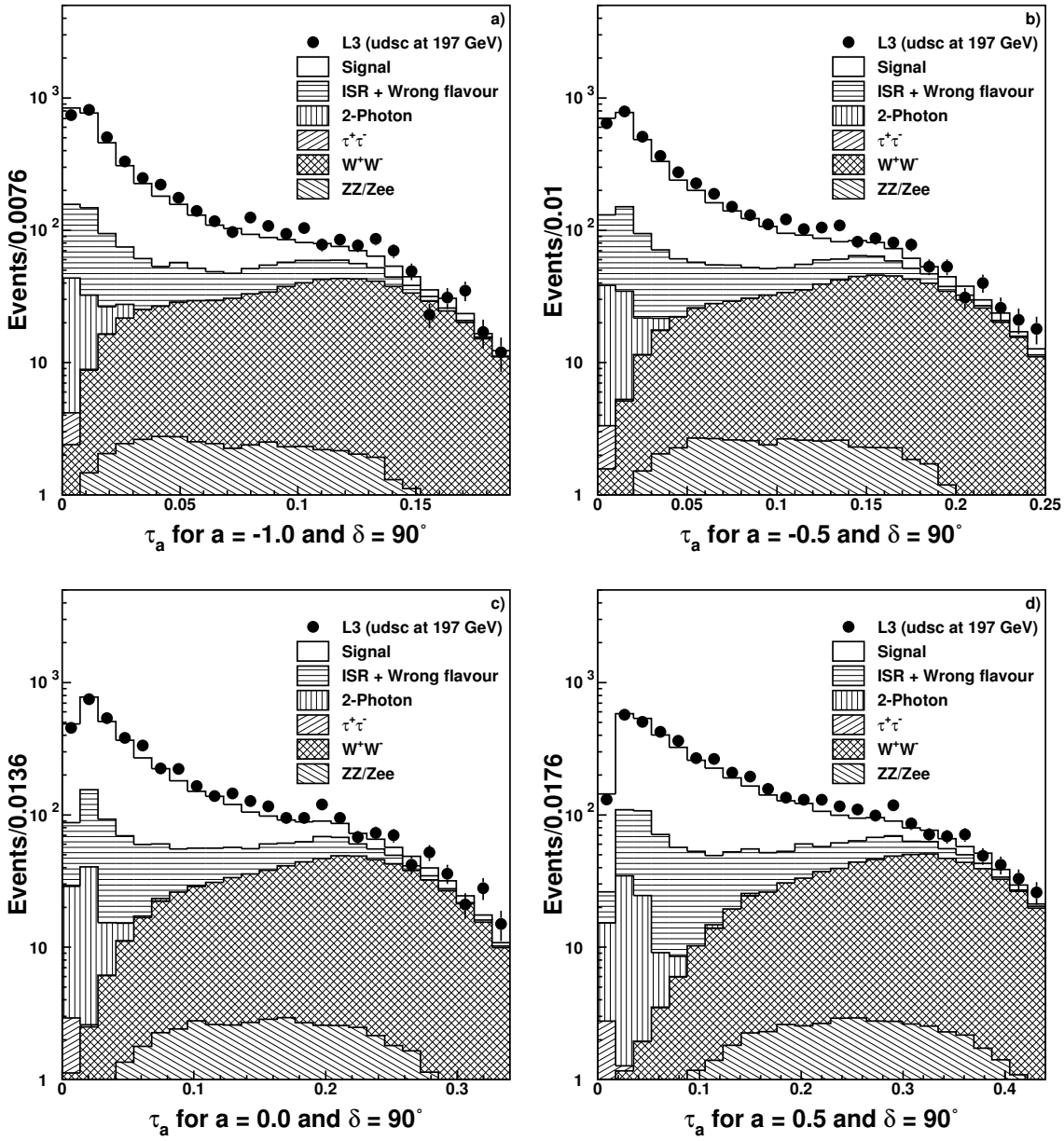

Figure 3. Measured inclusive event shape distributions at $\langle\sqrt{s}\rangle = 197.0$ GeV for data sample enriched in light flavour (udsc) for $a = -1.0$ (a), -0.5 (b), 0.0 (c), 0.5 (d). These distributions are compared with expectation from JETSET parton shower Monte Carlo program. The shaded areas refer to different backgrounds

JHEP10(2011)143

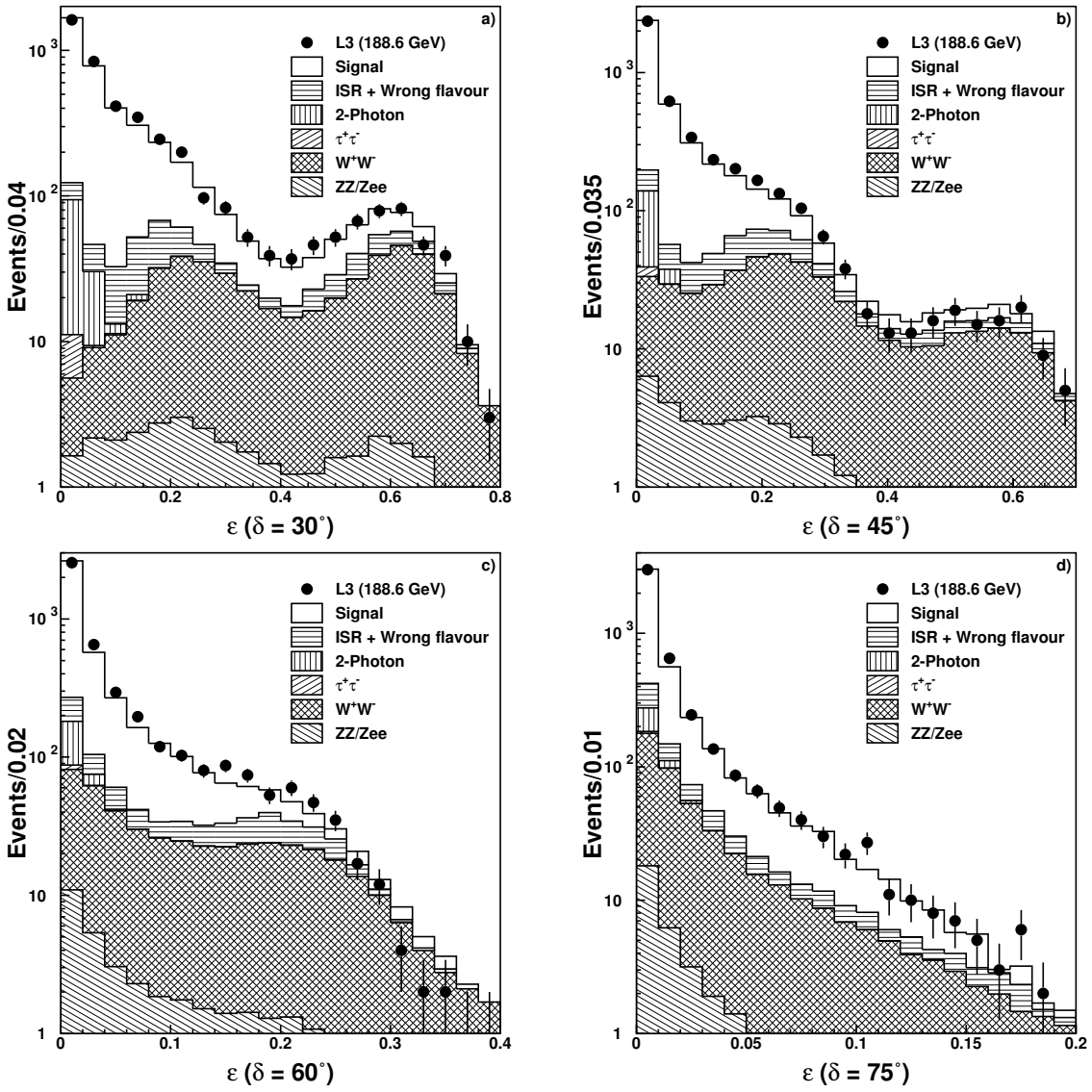

Figure 4. Measured inclusive distributions of ε at $\sqrt{s} = 188.6$ GeV for the overall data sample for $\delta = 30°$ (a), 45° (b), 60° (c), 75° (d). These distributions are compared with expectation from JETSET parton shower Monte Carlo program. The shaded areas refer to different backgrounds

JHEP10(2011)143

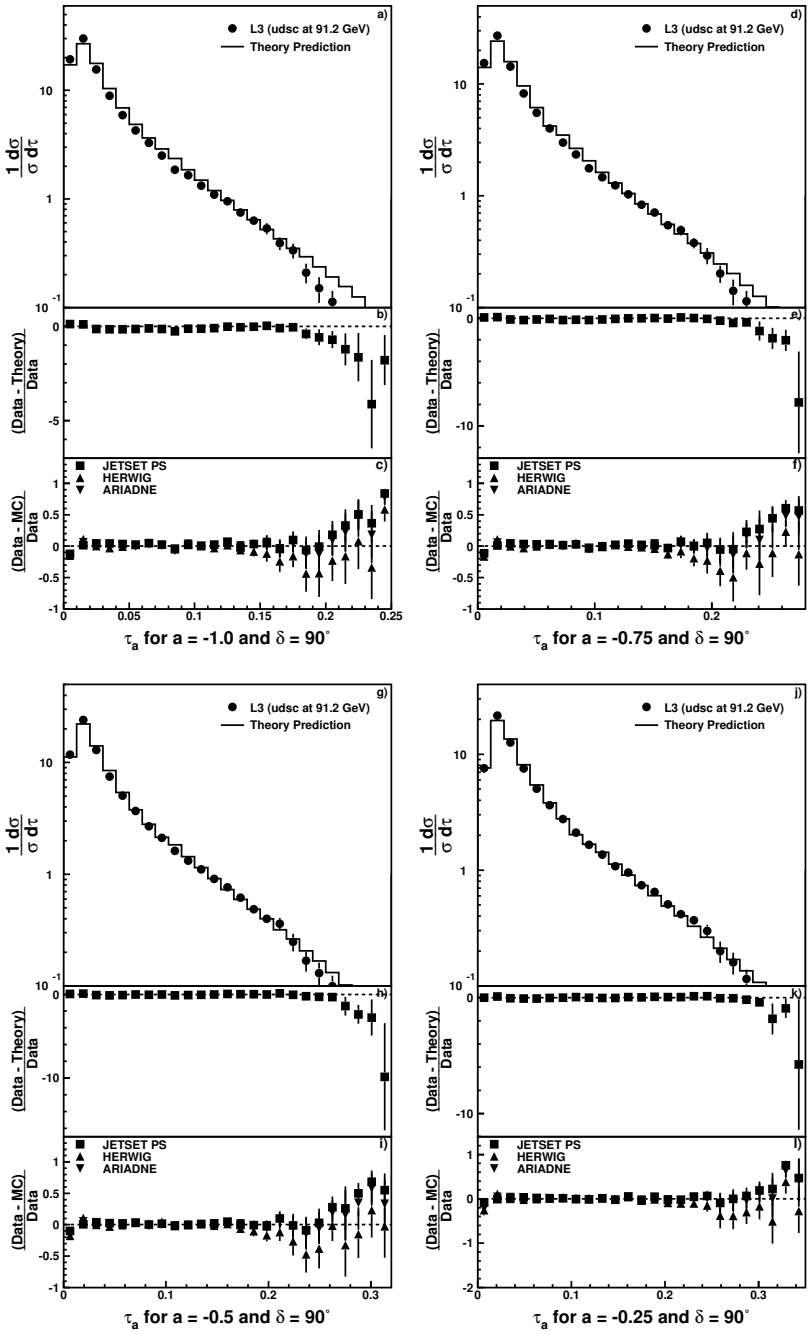

Figure 5. Corrected inclusive event shape distributions at $\sqrt{s} = 91.2$ GeV for udsc-flavour data samples for $a = -1.0$ (a), -0.75 (d), -0.5 (g), -0.25 (j). These distributions are compared with predictions from the scaling hypothesis. The fractional differences are shown for $a = -1.0$ (b), -0.75 (e), -0.5 (h), -0.25 (k). Comparisons with predictions from several QCD motivated Monte Carlo programs are shown as fractional differences for $a = -1.0$ (c), -0.75 (f), -0.5 (i), -0.25 (l). The data points shown here are also tabulated in tables 4, 5, 6, 7.

JHEP10(2011)143

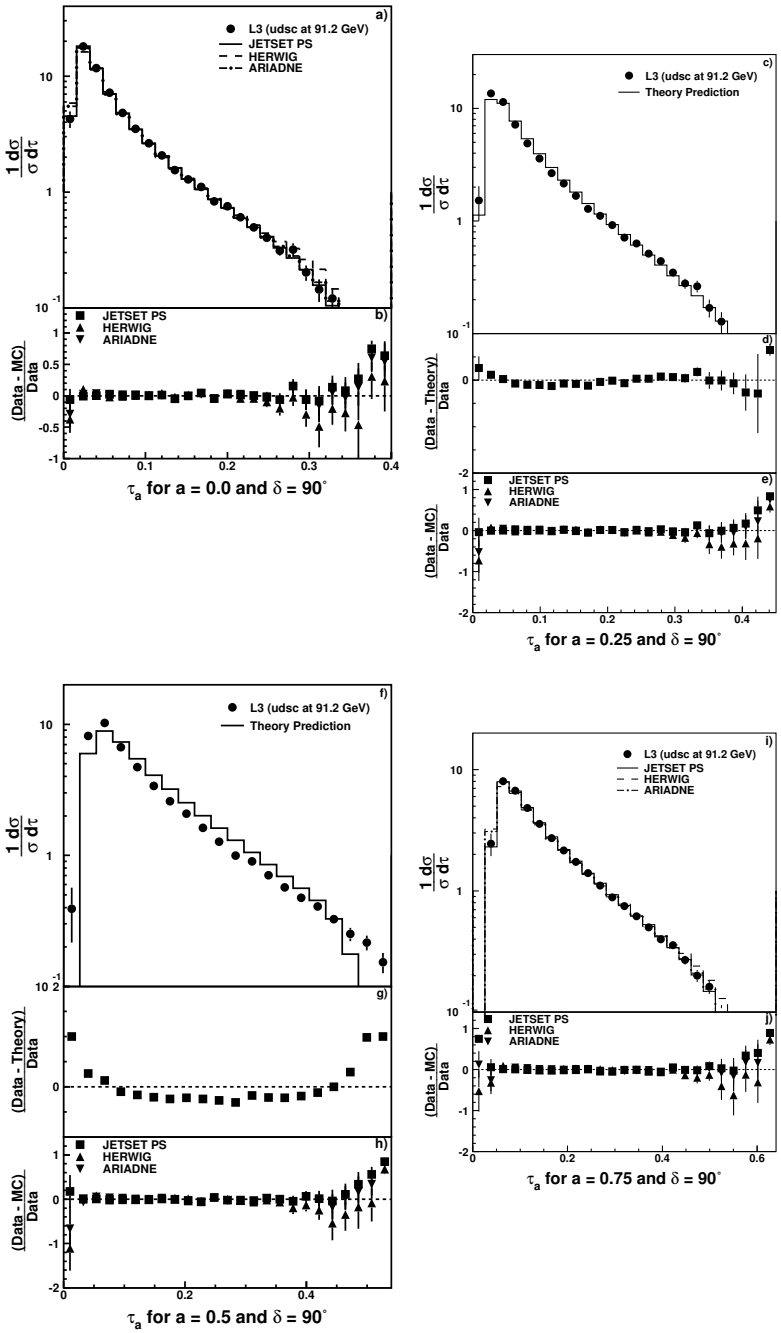

Figure 6. Corrected inclusive event shape distributions at $\sqrt{s} = 91.2$ GeV for udsc-flavour data samples for $a = 0.0$ (a), 0.25 (c), 0.5 (f), 0.75 (i). The distributions for $a = 0.25$ and 0.5 are compared with predictions from the scaling hypothesis, while those for $a = 0.0$ and 0.75 are compared with predictions from several QCD motivated Monte Carlo programs. The fractional differences for the scaling hypothesis are shown for $a = 0.25$ (d), 0.5 (g) while the fractional differences with respect to the Monte Carlo programs are shown for $a = 0.0$ (b), 0.25 (e), 0.5 (h), 0.75 (j). The data points shown here are also tabulated in tables 8, 9, 10, 11.

JHEP10(2011)143

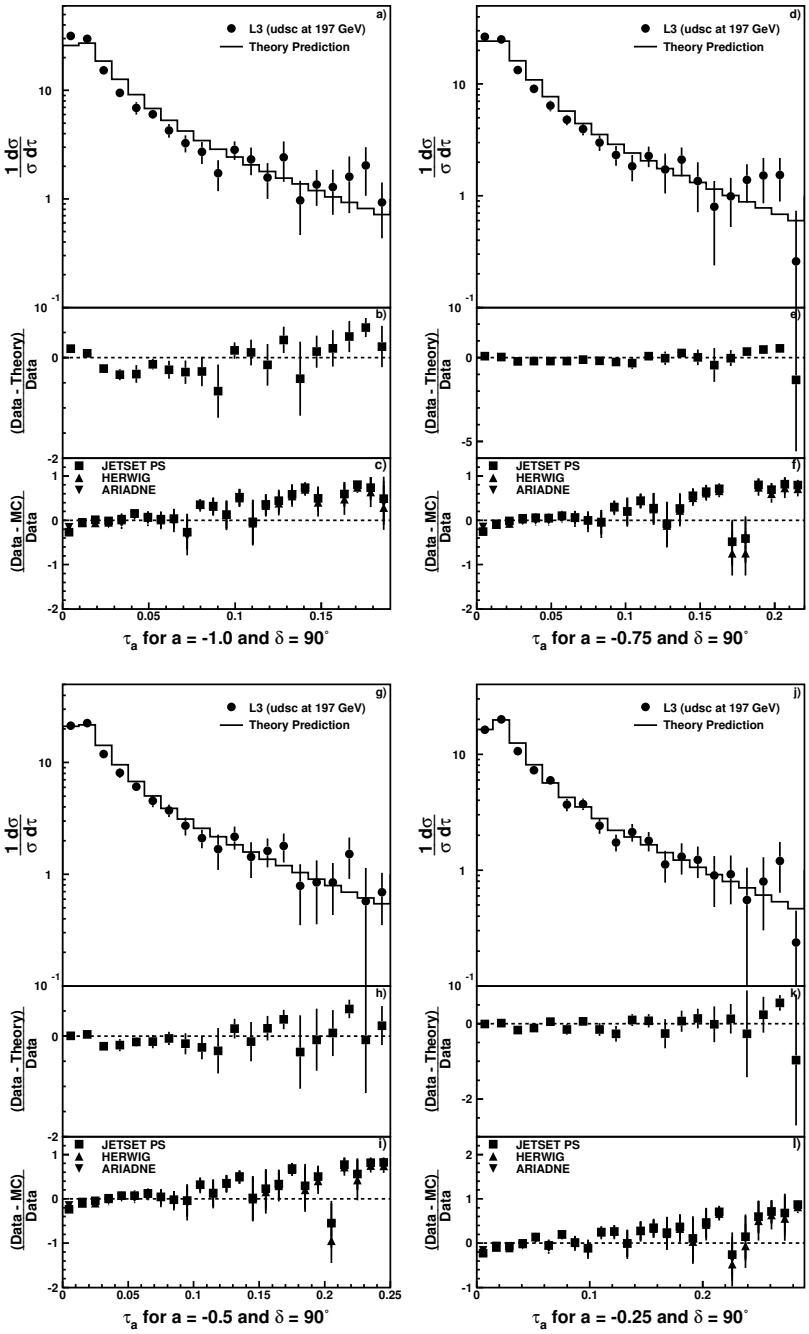

Figure 7. Corrected inclusive event shape distributions at $\langle\sqrt{s}\rangle = 197.0$ GeV for udsc-flavour data samples for $a = -1.0$ (a), -0.75 (d), -0.5 (g), -0.25 (j). These distributions are compared with predictions from the scaling hypothesis. The fractional differences are shown for $a = -1.0$ (b), -0.75 (e), -0.5 (h), -0.25 (k). Comparisons with predictions from several QCD motivated Monte Carlo programs are shown as fractional differences for $a = -1.0$ (c), -0.75 (f), -0.5 (i), -0.25 (l). The data points shown here are also tabulated in tables 4, 5, 6, 7.

JHEP10(2011)143

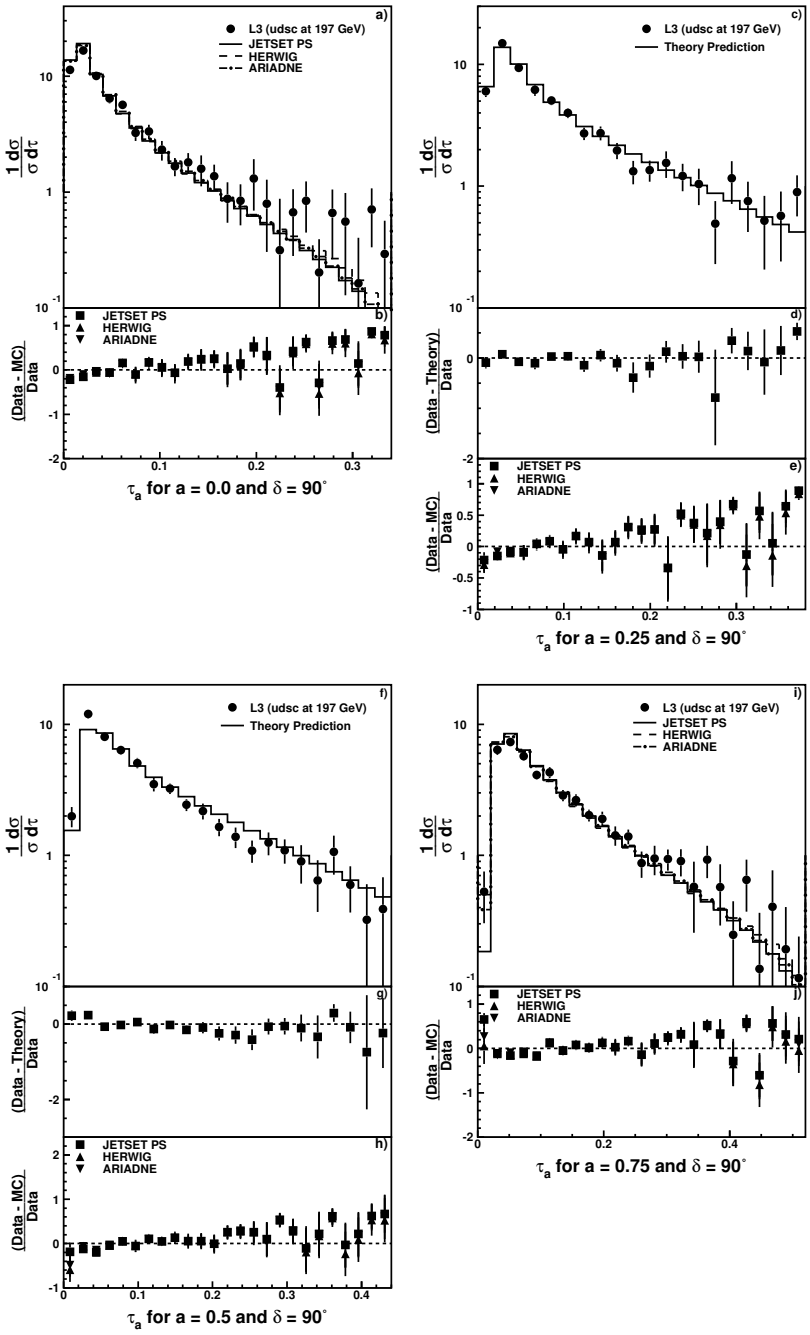

Figure 8. Corrected inclusive event shape distributions at $\langle\sqrt{s}\rangle = 197.0$ GeV for udsc-flavour data samples for $a = 0.0$ (a), 0.25 (c), 0.5 (f), 0.75 (i). The distributions for $a = 0.25$ and 0.5 are compared with predictions from the scaling hypothesis, while those for $a = 0.0$ and 0.75 are compared with predictions from several QCD motivated Monte Carlo programs. The fractional differences for the scaling hypothesis are shown for $a = 0.25$ (d), 0.5 (g) while the fractional differences with respect to the Monte Carlo programs are shown for $a = 0.0$ (b), 0.25 (e), 0.5 (h), 0.75 (j). The data points shown here are also tabulated in tables 8, 9, 10, 11.

JHEP10(2011)143

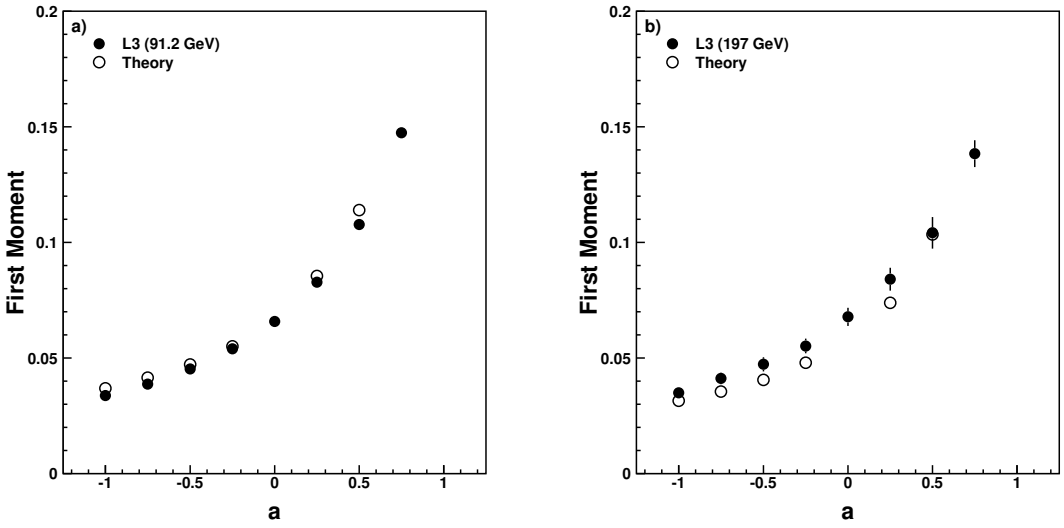

Figure 9. First moments of the inclusive event shape distributions for different values of a at (a) $\sqrt{s} = 91.2$ GeV and (b) $\langle\sqrt{s}\rangle = 197.0$ GeV for udsc-flavour data samples compared to theoretical predictions. The comparison is not possible for $a = 0$ as these data are used to estimate the non-perturbative part of the shape distribution.

JHEP10(2011)143

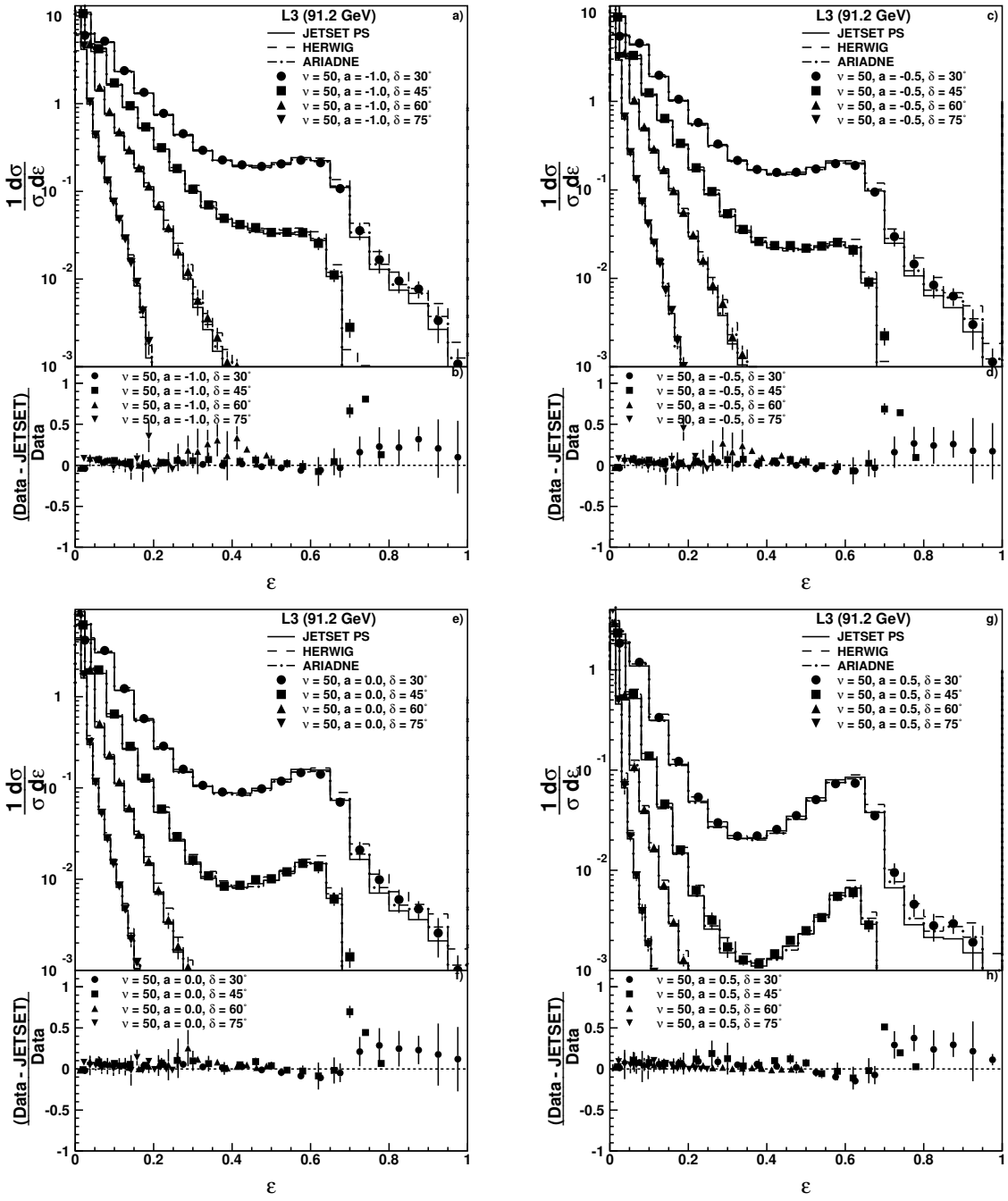

Figure 10. Corrected distributions of energy flow correlation at $\sqrt{s} = 91.2$ GeV; $\nu = 50$, $a = -1.0$ (a), -0.5 (c), 0.0 (e), 0.5 (g) compared to various QCD Monte Carlo programs. The fractional differences are shown for $a = -1.0$ (b), -0.5 (d), 0.0 (f), 0.5 (h).

JHEP10(2011)143

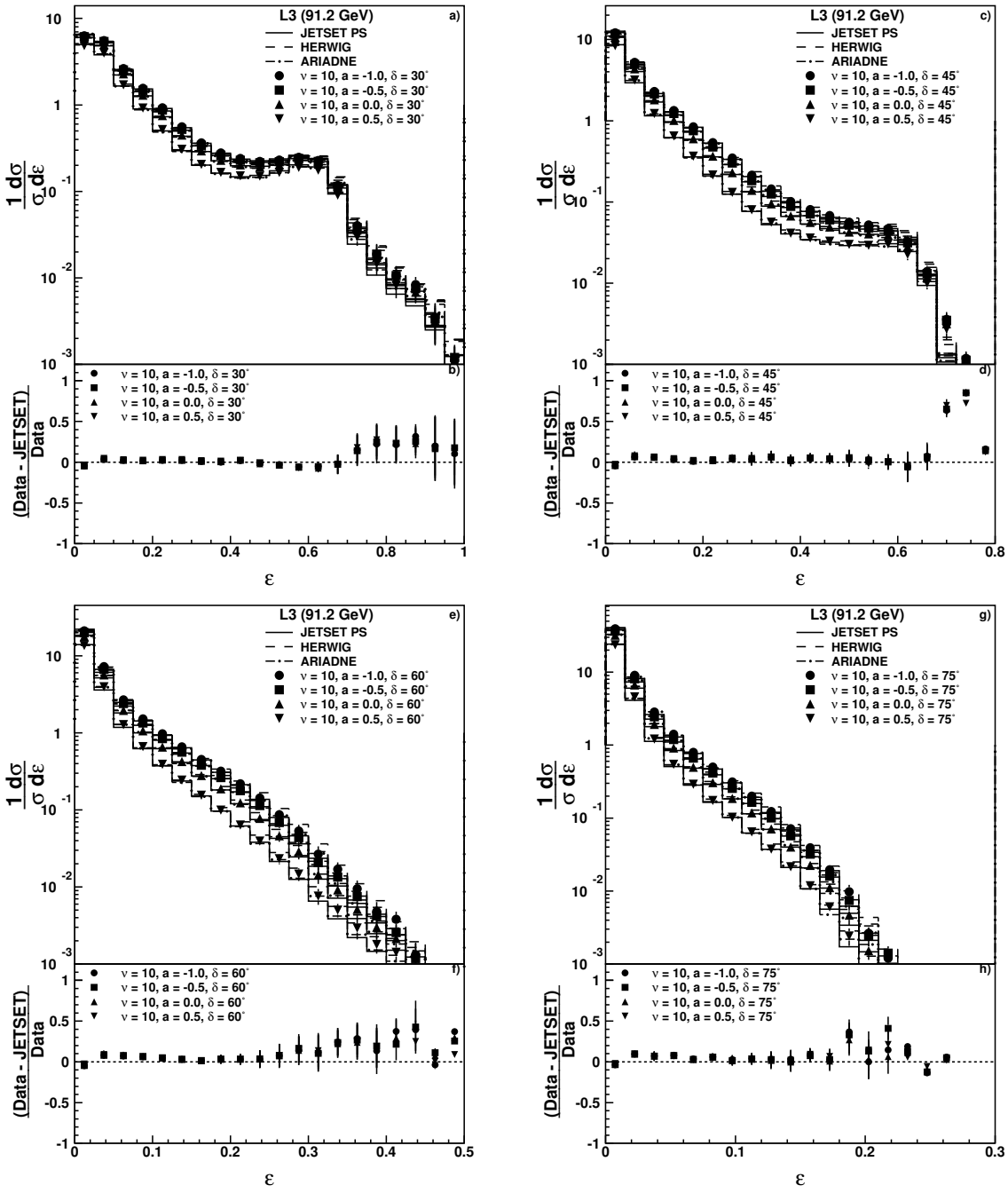

Figure 11. Variation of the energy flow correlation at $\sqrt{s} = 91.2$ GeV for $\delta = 30°$ (a), 45° (c), 60° (e) and 75° (g) for $\nu = 10$ compared to various QCD Monte Carlo programs. The fractional differences are shown for $\delta = 30°$ (b), 45° (d), 60° (f) and 75° (h).

JHEP10(2011)143

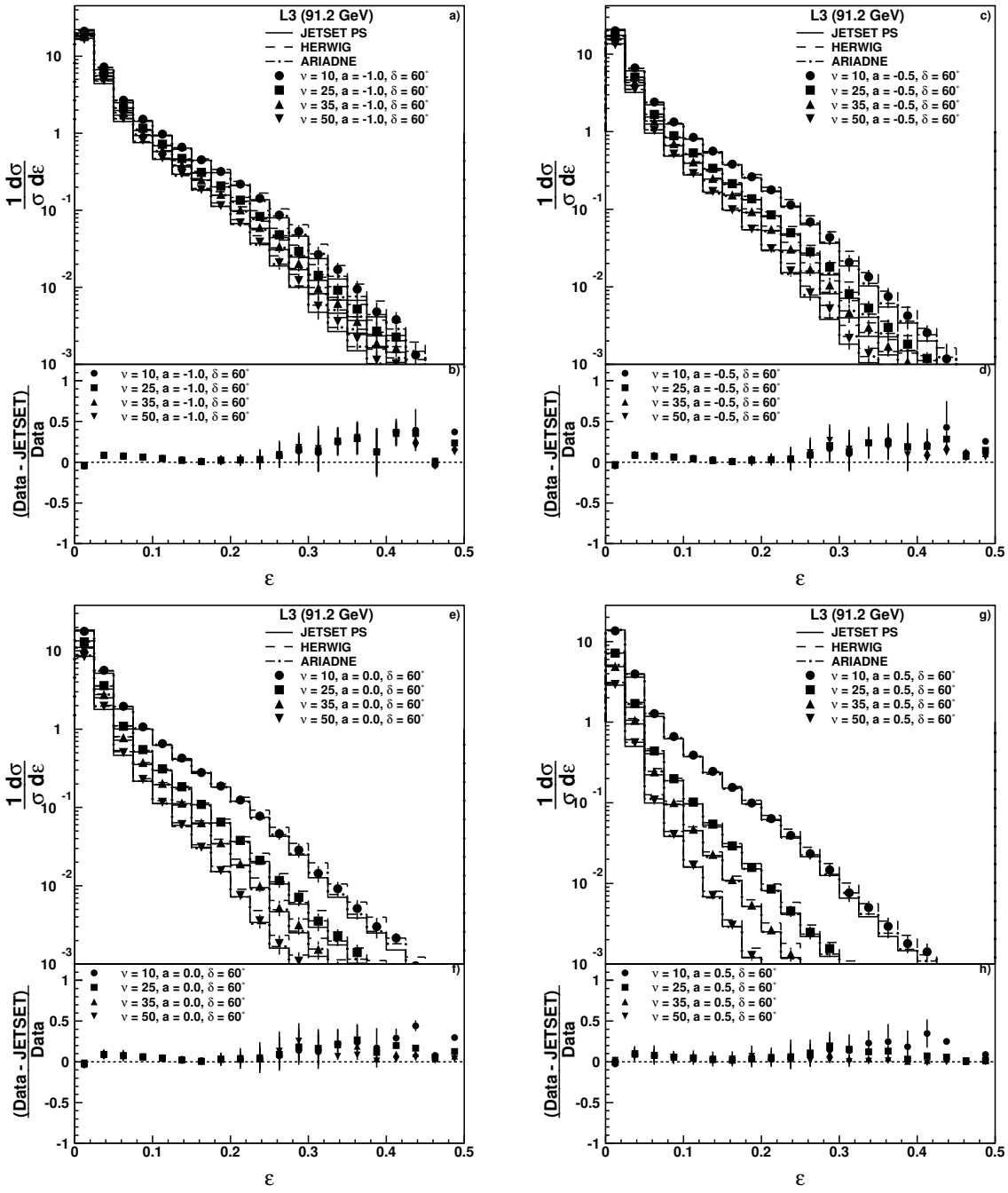

Figure 12. Variation in ν of the energy flow correlation at $\sqrt{s} = 91.2$ GeV for $\delta = 60°$ $a = -1.0$ (a), -0.5 (c), 0.0 (e) and 0.5 (g) compared to various QCD Monte Carlo programs. The fractional differences are shown for $a = -1.0$ (b), -0.5 (d), 0.0 (f), 0.5 (h).

JHEP10(2011)143

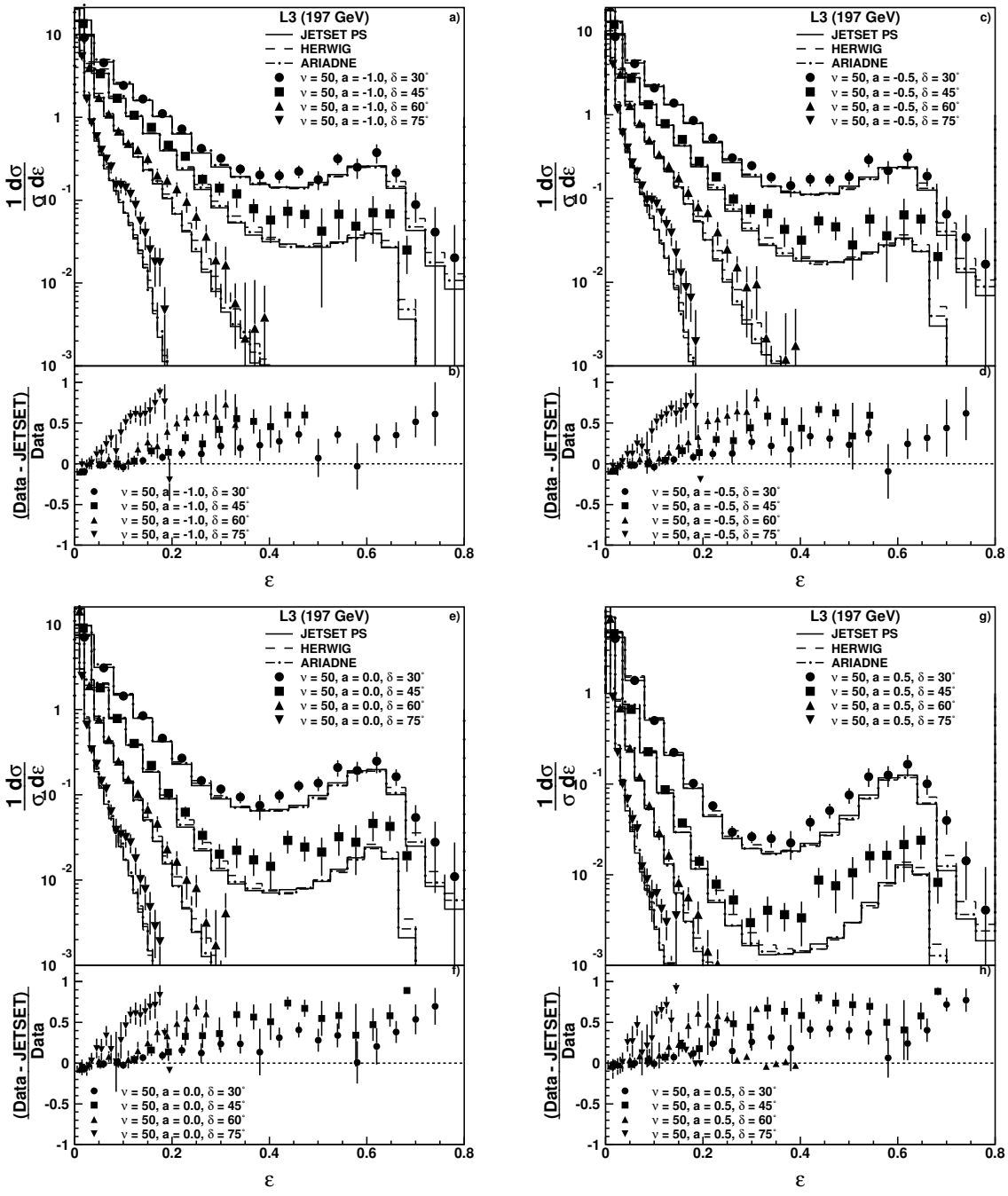

Figure 13. Corrected distributions of energy flow correlation at $\langle\sqrt{s}\rangle = 197.0$ GeV; $\nu = 50$, $a = -1.0$ (a), -0.5 (c), 0.0 (e) and 0.5 (g) compared to various QCD Monte Carlo programs. The fractional differences are shown for $a = -1.0$ (b), -0.5 (d), 0.0 (f), 0.5 (h).

JHEP10(2011)143

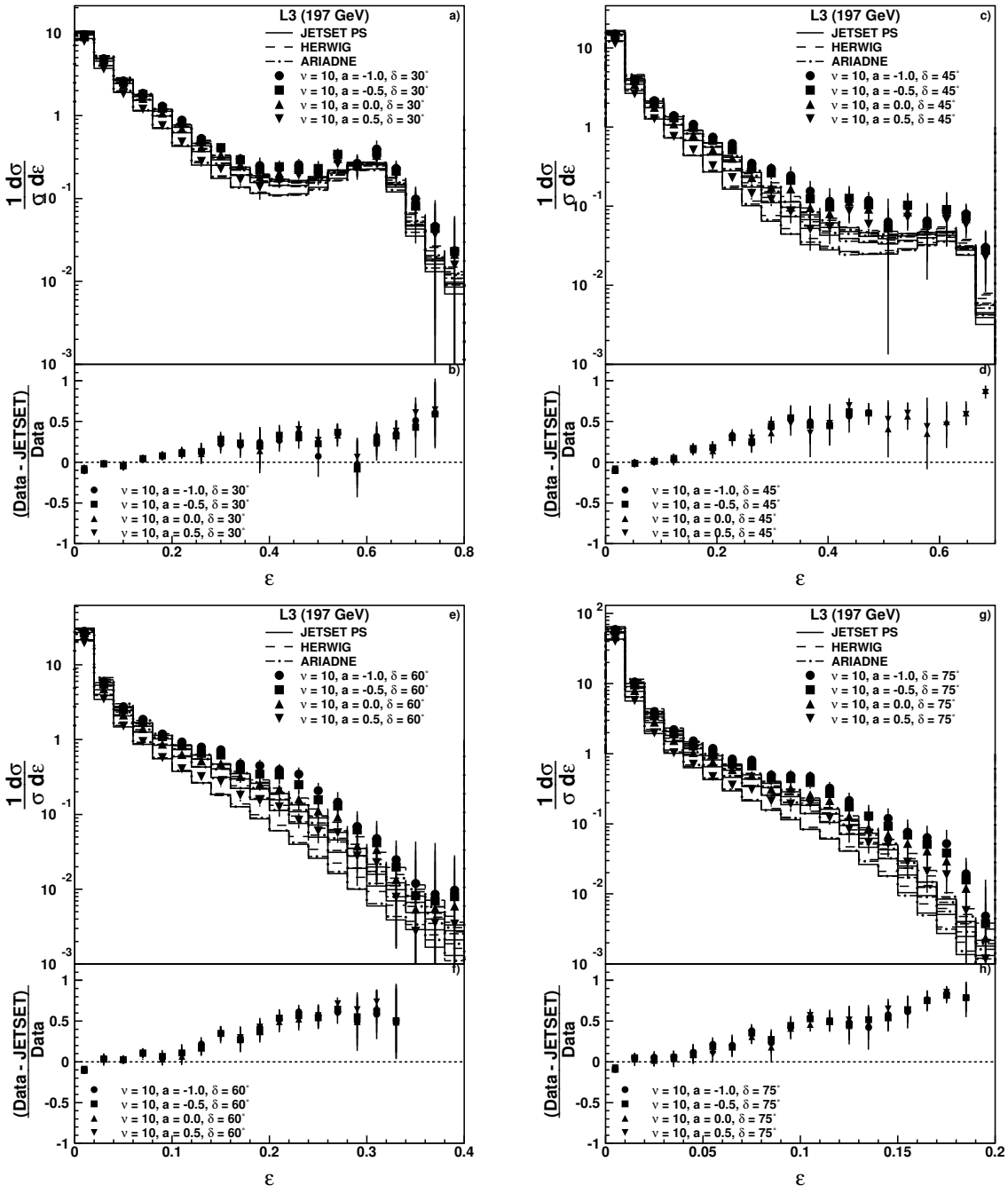

Figure 14. Variation of the energy flow correlation at $\langle\sqrt{s}\rangle = 197.0$ GeV for $\delta = 30°$ (a), 45° (c), 60° (e) and 75° (g) for $\nu = 10$ compared to various QCD Monte Carlo programs. The fractional differences are shown for $\delta = 30°$ (b), 45° (d), 60° (f) and 75° (h).

JHEP10(2011)143

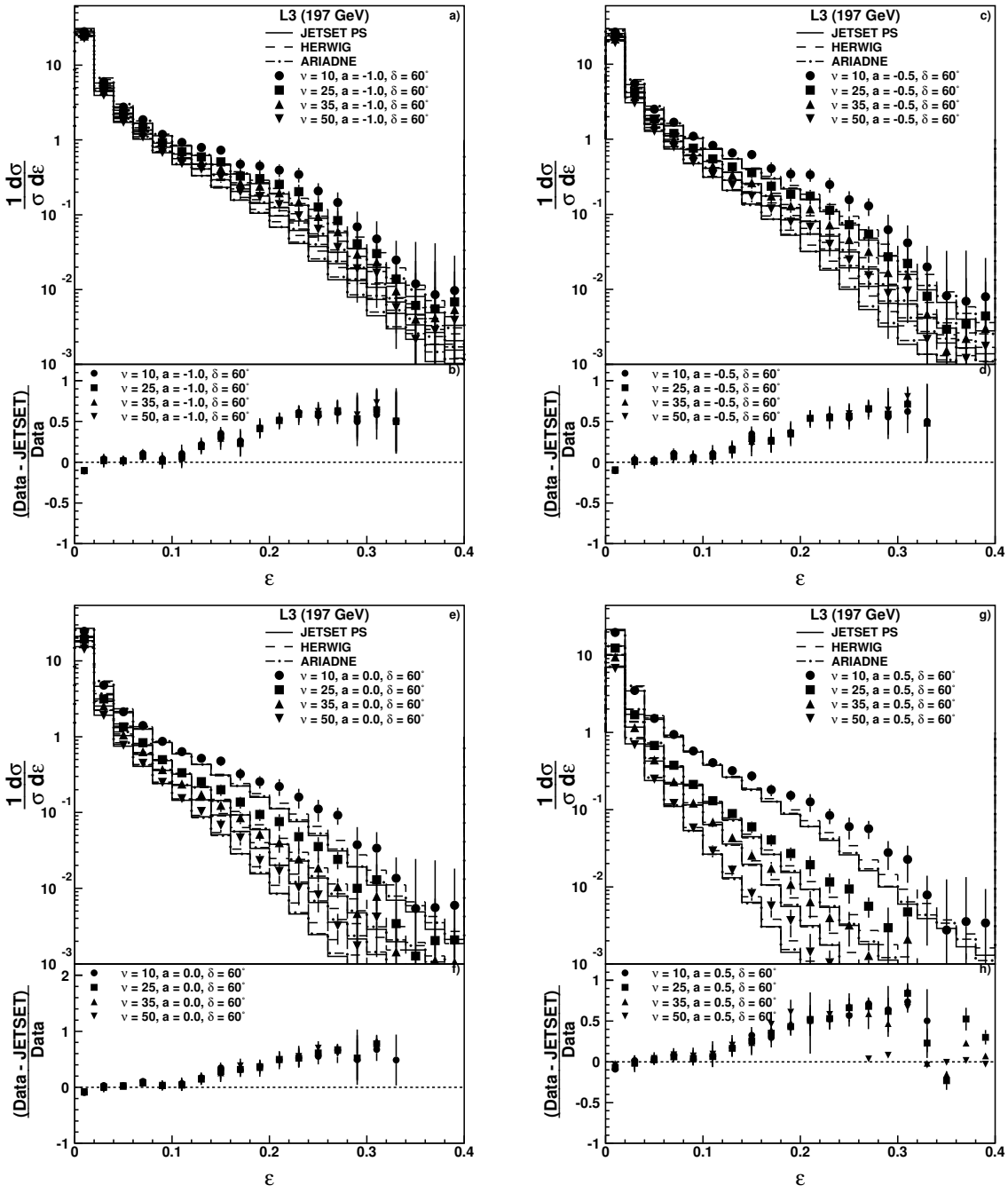

Figure 15. Variation in ν of the energy flow correlation at $\langle\sqrt{s}\rangle = 197.0$ GeV for $\delta = 60°$ $a = -1.0$ (a), $= -0.5$ (c), $= 0.0$ (e), $= 0.5$ (g) compared to various QCD Monte Carlo programs. The fractional differences are shown for $a = -1.0$ (b), -0.5 (d), 0.0 (f), 0.5 (h).

JHEP10(2011)143

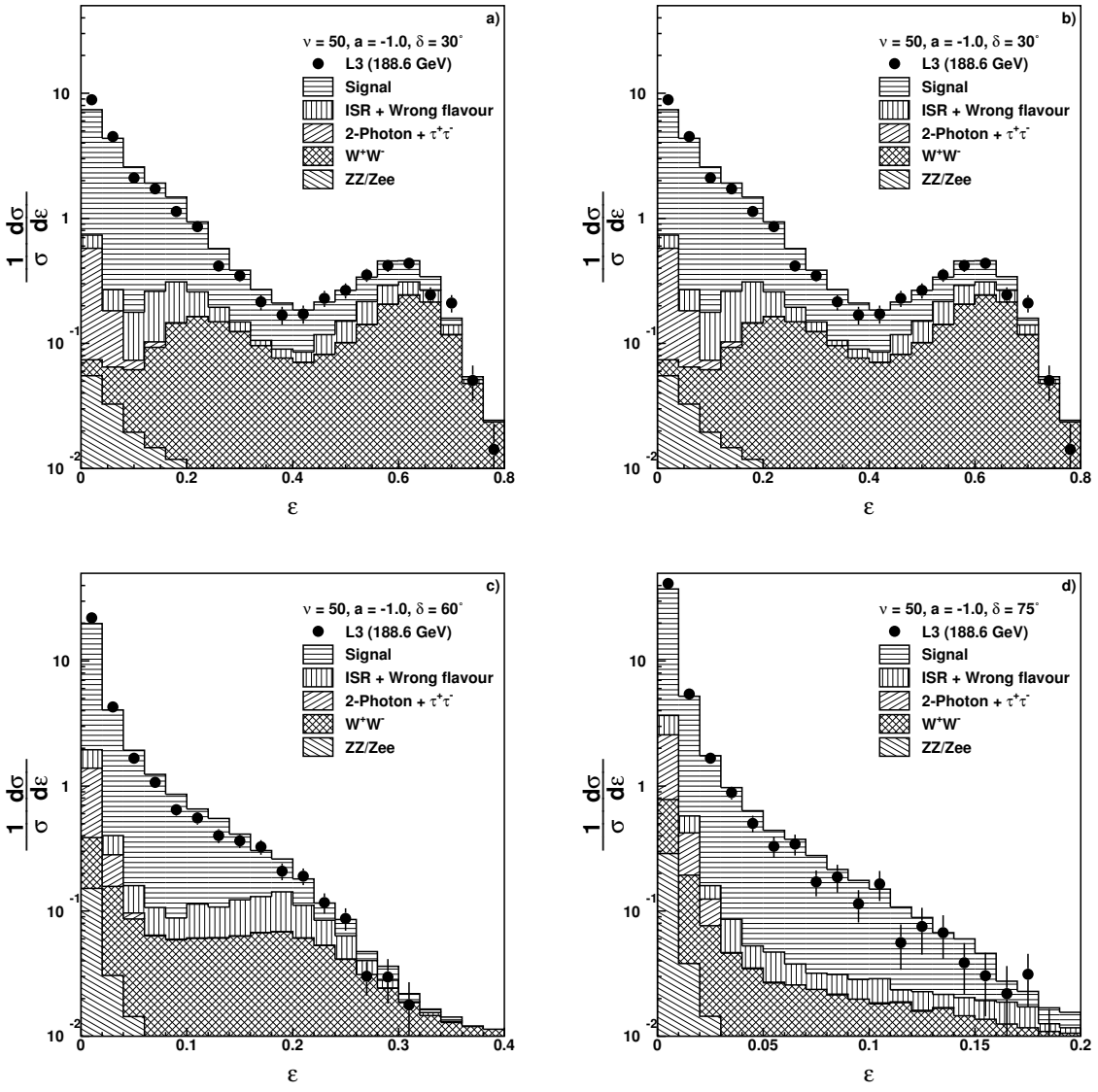

Figure 16. Energy flow correlation measured at $\sqrt{s} = 188.6$ GeV together with contributions from signal and background processes for $\nu = 50$, $a = -1.0$ and four different values of δ: (a) 30°, (b) 45°, (b) 60°, (b) 75°.

JHEP10(2011)143